Severely Fading MIMO Channels

Seung-Ho Choi

A thesis submitted in partial fulfilment
of the requirements for the degree of
Master of Engineering
in
Electrical and Computer Engineering
at the
University of Canterbury,
Christchurch, New Zealand.

March 2007

ABSTRACT

In most wireless communications research, the channel models considered experience less severe fading than the classic Rayleigh fading case. In this thesis, however, we investigate MIMO channels where the fading is more severe. In these environments, we show that the coefficient of variation of the channel amplitudes is a good predictor of the link mutual information, for a variety of models. We propose a novel channel model for severely fading channels based on the complex multivariate t distribution. For this model, we are able to compute exact results for the ergodic mutual information and approximations to the outage probabilities for the mutual information. Applications of this work include wireless sensors, RF tagging, land-mobile, indoor-mobile, ground-penetrating radar, and ionospheric radio links. Finally, we point out that the methodology can also be extended to evaluate the mutual information of a cellular MIMO link and the performance of various MIMO receivers in a cellular scenario. In these cellular applications, the channel itself is not severely fading but the multivariate t distribution can be applied to model the effects of intercellular interference.

ACKNOWLEDGEMENTS

My Masters study at Canterbury University has been a journey of discovery and professional growth. Having arrived where I am today, I owe thanks to many people.

First of all, I would like to express my deepest gratitude to my supervisor, Assoc. Prof. Peter J. Smith, for his guidance, support, encouragement and patience with me throughout my thesis. Without his encouragement, this thesis would never have been written.

Secondly, I am specially indebted to a number of people that have helped me along the path to this completed thesis. In particular, thanks to Alan Wright, Chun-Hong Yoon, Wallace Kuo, William Lee, Judy Zhou, Sanitta Thongpang and Samara Alzaidi.

Finally, I would like to thank my family, my parents and my sisters for their love, patience, continuous encouragement and moral support.

Seung-Ho Choi

University of Canterbury

March 2007

ABBREVIATIONS

ACI	Adjacent Channel Interference
AF	Amount of Fading
AoA	Angle of Arrival
AWGN	Additive White Gaussian Noise
BER	Bit Error Rate
BPSK	Binary Phase Shift Keying
BS	Base Station
cdf	Cumulative Density Function
CCI	Co-Channel Interference
CMT	Complex Multivariate t
CV	Coefficient of Variation
dB	Decibel
FCC	Federal Communications Commission
i.i.d.	Independent and Identically distributed
ISI	Inter-symbol Interference
LD	Linear Detection
LOS	Line of Sight
mgf	Moment Generating Function
MA	Multiple Access

MI	Mutual Information
MIMO	Multiple Input Multiple Output
MISO	Multiple Input Single Output
MMSE	Minimum Mean Squared Error
MSE	Mean Squared Error
NLOS	Non Line of Sight
OCI	Other Cell Interference
pdf	Probability Density Function
QoS	Quality of Service
S-V	Saleh-Valenzuela
SFC	Severely Fading Channel
SI	Spatial Interference
SIMO	Single Input Multiple Output
SINR	Signal to Interference plus Noise Ratio
SISO	Single Input Single Output
SNR	Signal to Noise Ratio
UWB	Ultra WideBand
WLAN	Wireless Local Area Networks
WPAN	Wireless Personal Area Networks
ZF	Zero Forcing

NOTATION

$\mathbf{r}$	the received signal vector
$\mathbf{s}$	the transmitted signal vector
n_T	the number of transmit antennas
n_R	the number of receive antennas
$\mathbf{n}$	the AWGN vector
$\mathbf{H}$	MIMO channel matrix
h_{rs}	the channel coefficients between receive antenna r and transmit antenna s
θ_{rs}	i.i.d. uniform phase
A_{rs}	i.i.d. amplitude
$N(\cdot)$	the Gaussian random variable
$f(\cdot)$	the probability density function
$\mathbf{H}_{\text{LOS}}$	LOS component of $\mathbf{H}$
$\mathbf{H}_{\text{NLOS}}$	NLOS component of $\mathbf{H}$
y^2	the average power of the LOS components
I_0	the modified Bessel function of the first kind of zeroth order
K	the Ricean K fading parameter
$\Gamma(\cdot)$	the Gamma function
m	the Nakagami-m fading parameter
$E[\cdot]$	statistical expectation

$Var[\cdot]$	variance
β	the Weibull fading parameter
Ω	the average power of the received signal
ξ	$10/\ln 10$
μ	mean
σ	standard deviation
$\mathcal{I}$	mutual information
ρ	the average SNR at any receive antenna
h	the normalized channel gain
h_r	the channel gain for receive antenna r
h_s	the channel gain for receive antenna s
P	transmit power constraint
$det(\cdot)$	the determinant of a matrix
$(^\dagger)$	the conjugate transpose
$\mathbf{I}_{N_R}$	the $n_R \times n_R$ identity matrix
$E(\mathcal{I})$	the ergodic mutual information
P_{out}	the outage probability
$Prob(\cdot)$	the probability
$\mathbf{W}$	the weight matrix at the receiver
$\tilde{\mathbf{r}}$	the estimated signal before quantizing
$Re(\cdot)$	the real part
$sgn(\cdot)$	the signum function
$\mathbf{W}_{ZF}$	ZF weight matrix
$\mathbf{W}_{MMSE}$	MMSE weight matrix

$\gamma(\cdot,\cdot)$	the incomplete gamma function
$I(\cdot,\cdot)$	the incomplete beta function
σ_n^2	the noise power at each antenna
$\mathbf{I}_{n_T}$	the $n_T \times n_T$ identity matrix
$\hat{\mathbf{s}}$	the estimated signals
p, q	beta - shape parameter
a, b	uniform - minimum and maximum boundary
ν	degree of freedom for the t distribution
r	degree of freedom for the CMT distribution
S^2	complex χ^2 distribution
λ_{CMT}	arbitrary non-zero eigenvalue of $\mathbf{H}_{\mathrm{CMT}}\mathbf{H}_{\mathrm{CMT}}^{\dagger}$
m	the minimum number of the transmit or receive antennas
n	the maximum number of the transmit or receive antennas
λ	arbitrary non-zero eigenvalue of the Wishart matrix
$\lceil\,\rceil$	the ceiling function
${}_2F_1(\cdot,\cdot,\cdot,\cdot)$	Gauss hypergeometric function
Γ	the SINR resulting from a noise and intercellular interference
$R(\cdot)$	the link reliability
γ	the average SNR
Γ_n	the power of the nth interferer

CONTENTS

LIST OF FIGURES

LIST OF TABLES

Chapter 1

INTRODUCTION

1.1 BACKGROUND

Over the millennia, humans have transmitted messages through the atmosphere using methods such as voice, sounds, and smoke signals, but these systems are limited to conveying simple messages over short distances. With the advent of telegraphy and telephony, long distance communication became possible for businesses that needed to transmit messages quickly and globally. These systems used electrical wires as the communication medium with great success. However, it was soon determined that the exclusive use of wires severely limited the deployment of the new communication systems. For instance, providing each home with a telephone cable is expensive and time consuming. Also replacing the wire infrastructure when it fails is even more costly. In late 2006, undersea fiber optic cables were damaged by a powerful earthquake off the southern tip of Taiwan, causing the largest recorded outage of telephone and internet service [1].

Over the last century, dramatic advances have been made in telecommunications. Radio technology has evolved remarkably since Guglielmo Marconi [2], first demonstrated the radio's ability to send a telegraph across the English channel in 1897. Since then, more information has became accessible via radio, television, internet, multimedia, and

mobile phones. As a result, there is an increase in demand for higher data rates and higher network capacities [3, 4]. The old wired systems seem to be ill-suited to meet these needs, while wireless systems have a potential to resolve the bottleneck of network capacity. In fact, the change is occurring today in telephony, where wireless (cellular) technology is partially replacing the old wired telephone network [4, 5]. Wireless networks have been increasingly used as a replacement for wires within homes, offices, and factories through the deployment of wireless local area networks (WLANs) [4]. Moreover, the evolving Bluetooth promises to replace troublesome appliance communication cords with invisible wireless connections within a personal workplace [4]. In short, wireless communications overcome the basic limitations as described above. This emerging technology will bring enormous benefits: lower costs, easier deployment, greater flexibility and better reliability. Moreover, it offers mobility to access the information anywhere at anytime [6, 7].

One of the most important properties of the atmosphere as a communication medium is the huge capacity of radio spectrum that enables the simple transmission telephone, television and radio channels. However, as demand increases with the growth of a system, even this radio spectrum can become saturated [8,9]. One approach to meet this demand is to increase the channel bandwidth over which radio signals are transmitted. However, this approach is not practical because frequency spectrum is expensive and the channel bandwidth is determined by regulatory standards. Other approaches to improve the capacity is to use more complex modulation schemes. This, however, increases the complexity of the radio system and, thus, the cost. This problem requires a better solution.

Recent research has shown that higher data rate and quality over wireless channels

could be achieved by exploiting the spatial diversity with multiple antennas at both the transmitting and receiving ends, which form a *multiple-input multiple-output* (MIMO) system [10–19]. Foschini [16] and Telatar [18] boosted interest in this area by predicting that a significant gain in capacity can be achieved by using MIMO systems. As the number of antennas at both the transmitter and the receiver gets larger, the capacity increases linearly with the minimum number of transmit and receive antennas [16, 18, 20], even if the fades between antenna pairs are correlated [21].

However, the information theory results [15] do not reflect the performance realized by actual MIMO systems, since they only provide a theoretical upper bound on achievable spectral efficiency [22]. Actual MIMO performance depends on the system architecture and the nature of the channel [12,23]. Several channel models have been used to describe random fading [3, 24, 25]. These include Rayleigh, Ricean, and Nakagami distributions. The Rayleigh distribution is commonly used to model the fading in strongly dispersive linear channels comprising homogeneous media, such as some urban wireless channels. Based on the Jakes model, this description assumes a large number of overlapping taps with uniformly distributed phases and angles-of-arrival (AoA). Results on the mutual information of Rayleigh-faded MIMO channels are widely available in research literature [26]. The Ricean distribution is another popular model for a range of line-of-sight (LOS) and non-line-of-sight (NLOS) channels. Results on non Gaussian channels are fewer, but some recent results can be found in [27, 28].

1.2 PROBLEM DEFINITION

It is well known that the Nakagami-m distribution can model the amplitude for cases when the fading is more severe than Rayleigh. These scenarios arise in a variety of applications: Radio frequency (RF) tagging [29], wireless sensors [30], UWB-MIMO [31]

and cellular-MIMO systems [32].

Despite the range of applications where severe fading may be encountered, relatively little attention has been given to such channels, with the exception of the Nakagami model. For severely fading MIMO channels, there is even less information available in the literature, partly due to the difficulty of performing any statistical analyses of random Nakagami matrices. Therefore, an appropriate channel model that accurately describes the severely fading channel (SFC), yet is simple enough to enable tractable analysis is needed.

In this thesis, MIMO channels are investigated where the fading is more severe than Rayleigh fading. A novel channel model is proposed for this scenario, which is simple, flexible, leads to closed form analysis, and is a direct extension of the Rayleigh model to the severe fading region. Here, fading severity is defined in terms of the probability of deep fading events. It does not concern the level crossing rate, the average fade duration, or Doppler effect. The propagation channel is assumed to be narrowband.

1.3 RESEARCH OBJECTIVES

The main objectives of this thesis are to:

- Investigate the effects of the fading severity on the ergodic mutual information in terms of the coefficient of variation.
- Derive an analytical formulae for the severely fading channels and compute the associated ergodic mutual information and approximate outage probabilities.
- Evaluate the mutual information of cellular MIMO and the performance of various MIMO receivers.

1.4 THESIS ORGANISATION

This section briefly outlines the content of each chapter in this thesis.

Chapter 2 presents an overview of the fundamentals of MIMO systems. It begins with a brief introduction of MIMO systems and then presents the MIMO system model that is followed in the rest of the thesis. Several channel models are introduced including Rayleigh, Ricean, Nakagami and Weibull fast fading and lognormal shadowing. The mutual information (MI) results for SISO to MIMO systems are also presented. Performance measures for MIMO systems are described including the ergodic MI, MI outage and the coefficient of variation (CV). It is shown that the CV of the channel amplitudes yields a good prediction of the MI. At the end of the chapter, linear detection (LD) in MIMO systems is discussed using the two different criteria of zero forcing (ZF) and minimum mean squared error (MMSE).

Chapter 3 introduces the severely fading channels in terms of the CV and discusses the potential applications, such as UWB-MIMO and cellular-MIMO systems. This chapter provides an insight into the MIMO channels where the fading is more severe than Rayleigh fading.

Chapter 4 shows the effects of the CV on the ergodic MI for a range of amplitude distributions. We investigate the sensitivity of the ergodic MI to the type of amplitude distribution and whether the CV is a good measure of the effect of the fading severity on the ergodic MI. Also we show the BER performance of MIMO systems using ZF and MMSE combining at the receiver.

Chapter 5 proposes using the complex multivariate t (CMT) distribution to model the channel amplitudes for a variety of channels. To verify this analytical formulae, we compute the associated ergodic mutual information and approximate outage probabil-

ities.

In Chapter 6, this CMT model is easily extended to evaluate the MI of cellular MIMO and the performance of various MIMO receivers. For these scenarios, the complex multivariate t distribution is used to model the inter-cell interference. This chapter shows that the CMT model can be applied to cellular MIMO systems and allows a closed form evaluation of both MI and performance.

Finally, Chapter 7 draws conclusions and also provides some directions for future work.

Based on the work in this thesis, the conference paper titled, "Severely Fading MIMO Channels: Models and Mutual Information", was accepted for presentation at the IEEE International Conference on Communications 2007 (ICC'07) [33]. The paper will also appear in the Proceedings of the ICC. A full journal paper based on this work is in preparation.

Chapter 2

MULTIPLE-INPUT MULTIPLE OUTPUT SYSTEMS

The primary purpose of this chapter is to briefly review the principles of channel modeling and capacity of MIMO systems. This chapter is organized as follows. Section 2.1 introduces the basic concepts of MIMO systems. Section 2.2 presents the system model for MIMO systems. Section 2.3 describes the most commonly used channel models. Section 2.4 summarizes the MIMO capacity results from basic SISO to MIMO. Finally, Section 2.5 discusses the performance analysis of MIMO systems.

2.1 INTRODUCTION TO MIMO

The wireless channel poses several challenges as a medium for reliable communication. These include the limited availability of frequency spectrum and transmission problems caused by such factors as multipath, interference, path loss and shadowing. Mutipath arises from the fact that a transmitted signal travels through multiple paths before arriving at the receiver. Some of the multipath reflected signals arrive at different times and are subject to different attenuations than the others. When the reflections add destructively, a phenomenon known as "fading" appears. Also, interference arises as soon as more than one user attempts to transmit a signal on the same channel sets. The two major types of interference are "co-channel interference" (CCI) and "adjacent-channel interference" (ACI). CCI is caused by users in the same network (or cells) on

the same frequency, whereas ACI is caused by extraneous power from a signal in an adjacent channel. Other limiting factors are "path loss" and "shadowing". Path loss is caused by dissipation of the power radiated by the transmitter as well as the effects of the propagation channel. Path loss models generally assume that path loss is the same at a given transmit-receive distance. Shadowing is caused by obstacles between the transmitter and receiver that absorb power. When the obstacle absorbs all the power, the signal is blocked. In addition, there is an increasing demand for high data rates and better quality of service for wireless systems. Meeting these needs requires new techniques to increase spectral efficiency and to improve link reliability.

Recent research has shown that large gains in capacity and link quality can be achieved by exploiting the spatial diversity with multiple antennas at both transmitting and receiving ends, which forms a *Multiple-Input Multiple-Output* (MIMO) system [16–18]. MIMO systems offer a capacity that increases linearly with the number of antennas used without increasing bandwidth or power [16, 18]. A typical MIMO system with n_T antennas at the transmitter an n_R antennas at the receiver is shown in Figure 2.1.

A key feature of MIMO systems is the ability to turn the multipath fading into a benefit to increase the capacity. Usually, fading has been known as a problem of wireless communications. One solution to this problem uses the idea of "diversity". Diversity is achieved by transmitting multiple replicas of the signals in the hope that at least one of the replicas may survive over the channels. The most common diversity technique is called spatial diversity [34], whereby multiple antennas are spatially separated and the receiver is able to select the antenna with the best signals at any time. Other diversity techniques include polarization diversity, frequency diversity and time diversity [35]. Another way to improve the level strength of the desired received signal is "beamform-

ing". The latter refers to the concentration of energy towards certain directions in such a way that both the signal-to-noise ratio (SNR) and signal-to-interference-plus-noise ratio (SINR) increase. For example, the receiver array can form a radiation pattern where the main beams are directed towards the transmitter to obtain a higher received signal strength, while nulls are introduced in the directions of the interfering signals. MIMO systems can use both above mentioned methods to combat fading with an added advantage, thus increasing the diversity gain at both sides of the link, each of them with an antenna array.

However, the main idea in MIMO systems is "spatial multiplexing" [26] in which the transmitted data are split or multiplexed into several parallel streams and each stream is transmitted simultaneously across the channel by different transmitter antennas and through distinct paths. The signals received on the multiple receive antennas are thus a combination of the transmitted data streams. The idea is that since the receiver detects the same signal several times at different positions in space, at least one position should not be in a deep fading. Hence, when the correlation between received signals in different antennas is low, a substantial increase in the capacity will occur. To achieve this, a rich multipath propagation channel is required and as a result, the received signals at each receive antenna will be linearly independent of each other. Much subsequent work is focused on characterizing MIMO capacity under more realistic assumptions about the underlying channel model and the channel estimates available at the transmitter and receiver.

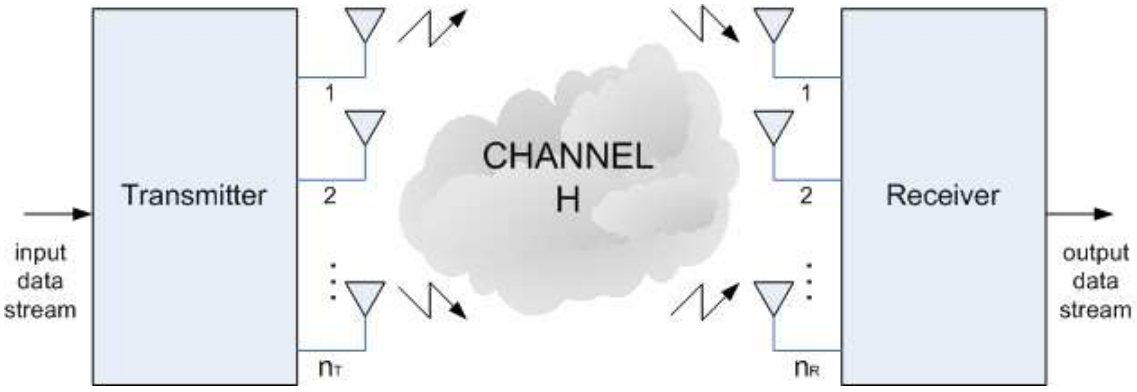

Figure 2.1 A MIMO system model

2.2 MIMO SYSTEM EQUATION

Consider a single user (n_T, n_R) MIMO system with n_T transmit and n_R receive antennas as illustrated in Figure 2.1. The system equation is given by [16, 18]

$$\mathbf{r} = \mathbf{H}\mathbf{s} + \mathbf{n} \tag{2.1}$$

where $\mathbf{r}$ is the $n_R \times 1$ received signal vector, $\mathbf{s}$ is the complex $n_T \times 1$ transmitted signal vector, $\mathbf{n}$ is an $n_R \times 1$ additive white complex Gaussian noise vector, and $\mathbf{H}$ is an $n_R \times n_T$ complex channel matrix, which can be represented as

$$\mathbf{H} = \begin{bmatrix} h_{11} & h_{12} & \cdots & h_{1n_T} \\ h_{21} & h_{22} & \cdots & h_{2n_T} \\ \vdots & \vdots & \ddots & \vdots \\ h_{n_R1} & h_{n_R2} & \cdots & h_{n_Rn_T} \end{bmatrix} \tag{2.2}$$

The entries, h_{rs}, $r = 1, 2, \cdots, n_R$ and $s = 1, 2, \cdots, n_T$, of $\mathbf{H}$ are the channel coefficients between receive antenna r and transmit antenna s.

In Chapters 2, 3 and 4, we consider the channel coefficients, $h_{rs} = (\mathbf{H})_{rs}$ to be of the form

$$h_{rs} = A_{rs} \exp(j\theta_{rs}) \tag{2.3}$$

where θ_{rs} are independent and identically distributed (i.i.d.) uniform phase variables over $[0, 2\pi]$ and the A_{rs} are i.i.d. amplitudes drawn from a range of distribution types. As is standard practice [16, 18], we normalize the amplitude distributions so that the mean power is unity, $E[A_{rs}^2] = 1$. This allows a fair comparison across distribution types.

2.3 MIMO CHANNEL MODELS

It is necessary to have detailed knowledge of the channel, in order to evaluate the performance of the MIMO systems. Considerable attention has been devoted to the statistical modeling of fading channels. In this section, we briefly review the classical models for the amplitude probability distribution including Rayleigh, Ricean, Nakagami and Weibull distributions. We also consider the classic log-normal model for the shadow fading.

2.3.1 Rayleigh Channel Model

The Rayleigh distribution is frequently used to model multipath fading with no direct line-of-sight (LOS) path (such as urban and suburban areas). The channel coefficients h_{rs} are defined as i.i.d. complex Gaussian random variables with zero mean and unit magnitude variance,

$$h_{rs} = N\left(0, \frac{1}{2}\right) + \jmath N\left(0, \frac{1}{2}\right) \tag{2.4}$$

where $N(\cdot)$ denotes the Gaussian random variable. In (2.4) and elsewhere, we use a slight abuse of notation and allow $N(0, \sigma^2)$ to represent an independent Gaussian variable with zero mean and variance σ^2.

In this case, the amplitude A_{rs} is Rayleigh distributed and the probability density

function (pdf) of A_{rs} is given by,

$$f_{A_{rs}}(x) = \frac{x}{\sigma^2} \exp\left(-\frac{x^2}{2\sigma^2}\right), \quad x \geq 0 \tag{2.5}$$

where $E[A_{rs}^2] = 2\sigma^2$ is the second order moment (average power).

The Rayleigh distribution is frequently referred to as fast-term or local-area fading. It typically agrees very well with experimental data for mobile systems, where no LOS path exists between the transmit and receive antennas. It also applies to the propagation of reflected and refracted path through the troposphere [36] and ionosphere [37] and to ship-to-ship [38] radio links.

2.3.2 Ricean Channel Model

The Ricean distribution is commonly modeled as a sum of two components: one is a line-of-sight component $\mathbf{H}_{\text{LOS}}$, and another is a non-line-of-sight component $\mathbf{H}_{\text{NLOS}}$ [39]. Hence, in the Ricean channel, $\mathbf{H}$ can be expressed as

$$\mathbf{H} = \mathbf{H}_{\text{LOS}} + \mathbf{H}_{\text{NLOS}} \tag{2.6}$$

where the random entries of $\mathbf{H}_{\text{NLOS}}$ are usually modeled as i.i.d. complex Gaussian random variables, i.e. a Rayleigh channel.

Here, the amplitude A_{rs} follows the distribution

$$f_{A_{rs}}(x) = \frac{x}{\sigma^2} \exp\left(-\frac{x^2 + y^2}{2\sigma^2}\right) I_0\left(\frac{xy}{\sigma^2}\right), \quad x \geq 0 \tag{2.7}$$

where y^2 is the average power of the LOS component, $2\sigma^2$ is the average power of the NLOS component and the function I_0 is the modified Bessel function of the first kind of zeroth order.

The Ricean pdf is often described by a Ricean K fading parameter, which is the ratio

of the power in the LOS component and the NLOS component. K is defined as

$$K = \frac{y^2}{2\sigma^2} \tag{2.8}$$

When $K = 0$ the Ricean channel has only a NLOS component, $\mathbf{H}_{\text{NLOS}}$, i.e. a pure Rayleigh channel. When $K \to +\infty$ the LOS component $\mathbf{H}_{\text{LOS}}$ is dominant, i.e. a pure LOS component channel. Hence, the Ricean channel can span the range from Rayleigh fading ($K = 0$) to no fading ($K \to +\infty$).

The Ricean distribution is typically observed in the first resolvable LOS paths of micro-cellular urban and suburban land-mobile [40], pico-cellular indoor [41] and factory [42] environments. It also applies to the dominant LOS path of satellite [43, 44] and ship-to-ship [38] radio links.

2.3.3 Nakagami Channel Model

In some cases, the channel information does not fit well into either of the previous channel models. Here, the Nakagami-m distribution may give an improved fit to the data. An advantage of the Nakagami distribution is that it can be reduced to the Rayleigh distribution and can also model fading conditions more severe or less severe than those in the Rayleigh case.

The Nakagami-m pdf is given by [45]

$$f_{A_{rs}}(x) = \frac{2}{\Gamma(m)} \left(\frac{m}{\Omega}\right)^m x^{2m-1} \exp\left(-\frac{mx^2}{\Omega}\right), \quad x \geq 0 \tag{2.9}$$

where $\Gamma(\cdot)$ is the gamma function, $\Omega = E[A_{rs}^2]$ is the average power and m is the Nakagami-m fading parameter, which is equal to

$$m = \frac{E[A_{rs}^2]^2}{Var[A_{rs}^2]} \tag{2.10}$$

where $E[\cdot]$ denotes statistical expectation and $Var[\cdot]$ denotes variance.

The Nakagami-m distribution covers a wide range of distributions, when $m = 1/2$ it is the truncated-Gaussian distribution, when $m = 1$ it is equal to the Rayleigh distribution and when $m \to +\infty$ it converges to a nonfading AWGN channel.

Furthermore, when $m \geq 1$, we can obtain a one-to-one mapping between the Nakagami m parameter and the Ricean K factor, allowing the Nakagami-m distribution to closely approximate the Ricean distribution. This mapping is given by [35]

$$m = \frac{(1 + K^2)^2}{1 + 2K^2}, \quad K \geq 0 \tag{2.11}$$

Finally, the Nakagami-m distribution often gives the best fit to land-mobile [46–48] and indoor mobile [49] multipath propagation, as well as scintillating ionospheric radio links [50–53].

2.3.4 Weibull Channel Model

The Weibull distribution has been applied in radar systems to model the dispersion of the received signal's level produced by some types of clutter [54, 55]. Recently, it has also been applied to model the fading phenomenon [56].

The Weibull distribution can also be regarded as an approximation to the generalized Nakagami distribution of the same order as the Nakagami-m distribution [56]. The pdf of the Weibull distribution is given by [57]

$$f_{A_{rs}}(x) = \frac{\beta}{\Omega} x^{\beta-1} \exp\left(-\frac{x^\beta}{\Omega}\right), \quad x \geq 0 \tag{2.12}$$

where β is the fading parameter and $\Omega = E[A_{rs}^2]$ is the average power. As the value of β increases, the severity of the fading decreases, while for the special case of $\beta = 2$, the Weibull distribution reduces to the Rayleigh distribution. Moreover, for the special

case of $\beta = 1$, it reduces to the well-known negative exponential distribution.

2.3.5 Lognormal Shadowing

In terrestrial and satellite cellular systems the link quality is also affected by the slow variation of the mean signal attenuation due to the shadowing from terrain, buildings and trees. Measurements have shown that the shadowing can be modeled by a lognormal distribution for various outdoor and indoor environments [58–62].

The pdf of the lognormal distribution is given by

$$f_{A_{rs}}(x) = \frac{\xi}{x\sigma\sqrt{2\pi}} \exp\left[-\frac{(10\log_{10} x - \mu)^2}{2\sigma^2}\right] \tag{2.13}$$

where $\xi = 10/\ln 10$, and μ (dB) and σ (dB) are the mean and standard deviation of $10\log_{10} A_{rs}$, respectively.

2.4 CAPACITY AND MUTUAL INFORMATION

In the work on MIMO systems the terms *capacity* and *mutual information* are sometimes used almost interchangeably. For example, Foschini and Gans [16] refer to the mutual information of a link as the capacity assuming equal power allocation across the transmit antennas. Since we do not consider any water-filling or other optimizations in this thesis, we prefer to use the term mutual information throughout.

In section 2.1, we mentioned that MIMO systems can offer substantial improvements over conventional systems in either quality of service (QoS) or transfer rate by exploiting spatial diversity. In this section, we summarize the bounds on mutual information (MI), which compare single-input single-output (SISO), single-input multiple-output (SIMO), multiple-input single-output (MISO) and multiple-input multiple output (MIMO) systems.

2.4.1 SISO Mutual Information

For a memoryless SISO system, the MI is given by [16]

$$\mathcal{I} = \log_2\left(1 + \rho|h|^2\right) \quad b/s/Hz \tag{2.14}$$

where h is the normalized complex gain of a fixed wireless channel or that of a particular realization of a random channel. ρ is the average SNR at any receive antenna.

2.4.2 SIMO Mutual Information

For a SIMO system with n_R receive antennas, the MI is given by [12]

$$\mathcal{I} = \log_2\left(1 + \rho\sum_{r=1}^{n_R}|h_r|^2\right) \quad b/s/Hz \tag{2.15}$$

where h_r is the gain for receive antenna r. Note that average MI increases logarithmically when we increase the number of receive antennas [26]. ρ is the SNR as before.

2.4.3 MISO Mutual Information

Similarly, if we want transmit diversity, where the transmitter does not have channel knowledge, we have a MISO system with n_T transmit antennas and the MI is given by [16]

$$\mathcal{I} = \log_2\left(1 + \frac{\rho}{n_T}\sum_{s=1}^{n_T}|h_s|^2\right) \quad b/s/Hz \tag{2.16}$$

where h_s is the gain for transmit antenna s. The SNR ρ is normalized by n_T to have a fixed total transmit power and the MISO system doesn't have the array gain offered by SIMO. Again, note that MI also increases logarithmically when we increase the number of transmit antennas [26].

2.4.4 MIMO Mutual Information

When the transmitted signal vector $\mathbf{s}$ is composed of n_T statistically independent equal power components each with a circularly symmetric complex Gaussian distribution, the MI under transmit power constraint P is given by [16, 18]

$$\mathcal{I} = \log_2 \left[\det \left(\mathbf{I}_{n_R} + \frac{\rho}{n_T} \mathbf{H}\mathbf{H}^{\dagger} \right) \right] \quad b/s/Hz \tag{2.17}$$

where $det(\cdot)$ denotes the determinant of a matrix, $(^{\dagger})$ denotes the conjugate transpose and $\mathbf{I}_{n_R}$ is the $n_R \times n_R$ identity matrix. Foschini [16] and Telatar [18] both demonstrated that the MIMO MI grows linearly with $min(n_T, n_R)$ rather than logarithmically as in (2.15) and (2.16).

2.5 PERFORMANCE ANALYSIS IN MIMO SYSTEMS

Several performance measures have been employed to characterize the behavior of MIMO channels. For a MIMO system, it is of interest to employ measures that can capture and quantify the improvement in system performance caused by the deployment of the antenna arrays.

In this thesis, we analyze the performance of MIMO systems with respect to ergodic MI, MI outage, the coefficient of variation (CV) and outages for SNR and SINR.

2.5.1 Ergodic Mutual Information

The "ergodic MI" of the MIMO channel is evaluated by averaging $\mathcal{I}$ with respect to the complex channel matrix $\mathbf{H}$ [63],

$$E(\mathcal{I}) = E \left\{ log_2 \left[\det \left(\mathbf{I}_{n_R} + \frac{\rho}{n_T} \mathbf{H}\mathbf{H}^{\dagger} \right) \right] \right\} \quad b/s/Hz \tag{2.18}$$

We note again that the MI in (2.18) is often described as the capacity for the scenario when the transmitter has no channel information.

2.5.2 Mutual Information Outage

Another performance measure that is commonly used is "MI outage". The MI outage of the MIMO channel is defined as the probability that the MI of the channel at any time is less than $\mathcal{I}_{out}$ and is given by [64]

$$P_{out} = Prob(\mathcal{I} < \mathcal{I}_{out}) \tag{2.19}$$

2.5.3 Coefficient of Variation

A simple way of quantifying the severity of fading is the "coefficient of variation" (CV) which can be obtained by using a measure directly related to the moments of the fading distribution itself. In terms of the pdf of the amplitude A_{rs}, the CV is defined by [65]

$$CV = \frac{\sqrt{Var(A_{rs})}}{E(A_{rs})} = \sqrt{\frac{1}{E(A_{rs})^2} - 1} \tag{2.20}$$

where $E[\cdot]$ denotes statistical expectation, $Var[\cdot]$ denotes variance and the amplitude A_{rs} is normalized to give $E[A_{rs}^2] = 1$.

Another measure of fading is the amount of fading (AF), which is defined as [66]

$$AF = CV^2 = \frac{Var(A_{rs})}{E(A_{rs})^2} \tag{2.21}$$

Clearly, CV and AF are closely related, and we will use the CV for the analysis in this thesis.

2.6 LINEAR DETECTION IN MIMO SYSTEMS

Since the received signal at the receiver is corrupted due to the multipath propagation and intersymbol interference (ISI), detection schemes are necessary to compensate for channel distortion in order to decrease the error rate in signal detection [3]. Thus, linear detection (LD) is considered using the two different criteria of "zero forcing" (ZF) and "minimum mean squared error" (MMSE). We restrict our attention to the case in which the transmitter has no knowledge of the channel information but the receiver has perfect knowledge of the channel.

In this thesis, we assume binary phase shift keying (BPSK) modulation and consider the bit error rate (BER) as the performance measure of these systems. Furthermore, the results obtained later in the thesis can be extended to a wider range of modulations, including PSK, QAM, etc. The approach is the same as that of Chapter 6. We take established results for the BER in Rayleigh fading and average over the scaling variable.

The linear detector is generally the simplest to implement. For the BPSK case, the estimated signals $\hat{\mathbf{s}}$ can be obtained from its knowledge of the received signals $\mathbf{r}$ and the weight matrix $\mathbf{W}$ as

$$\hat{\mathbf{s}} = sgn[Re(\tilde{\mathbf{r}})] = sgn[Re(\mathbf{Wr})] \tag{2.22}$$

where $\tilde{\mathbf{r}} = \mathbf{Wr}$ is the estimated signal before quantizing and the weight matrix $\mathbf{W}$ is determined by the particular linear detection scheme, i.e. ZF, MMSE, and the estimated channel. The function $Re(\cdot)$ denotes the real part and the function $sgn(\cdot)$ is

the signum function defined as

$$sgn(x) = \begin{cases} 1, & x > 0 \\ 0, & x = 0 \\ -1, & x < 0 \end{cases} \tag{2.23}$$

2.6.1 Zero Forcing

First we consider the ZF receiver. ZF is relatively simple to design because it ignores the effect of the channel noise $\mathbf{n}$. However, it may lead to considerable noise enhancement. The weight matrix $\mathbf{W}_{\mathrm{ZF}}$ for ZF is given by

$$\mathbf{W}_{\mathrm{ZF}} = (\mathbf{H}^{\dagger}\mathbf{H})^{-1}\mathbf{H}^{\dagger} \tag{2.24}$$

where superscript (†) denotes Hermitian transposition (i.e. the combination of complex conjugation and ordinary matrix transposition). Note that the ZF receiver is only possible when $n_R \geq n_T$ so suffers from some limitations.

For a ZF receiver, the estimated signals $\hat{\mathbf{s}}$ can be expressed as

$$\begin{aligned} \hat{\mathbf{s}} &= sgn[Re(\mathbf{W}_{\mathrm{ZF}}\,\mathbf{r})] \\ &= sgn[Re((\mathbf{H}^{\dagger}\mathbf{H})^{-1}\mathbf{H}^{\dagger}(\mathbf{H}\mathbf{s}+\mathbf{n}))] \\ &= sgn[Re(\mathbf{s}+(\mathbf{H}^{\dagger}\mathbf{H})^{-1}\mathbf{H}^{\dagger}\mathbf{n})] \\ &= sgn[Re(\mathbf{s}+\tilde{\mathbf{n}})] \end{aligned} \tag{2.25}$$

where $\tilde{\mathbf{n}} = (\mathbf{H}^{\dagger}\mathbf{H})^{-1}\mathbf{H}^{\dagger}\mathbf{n}$.

2.6.2 Minimum Mean Square Error

In contrast to the ZF receiver, the MMSE approach minimizes the expected mean squared error between the transmitted symbol and the symbol detected at the receiver,

thereby providing a better balance between ISI mitigation and noise enhancement.

In MMSE, the goal is to design the weight matrix $\mathbf{W}_{\text{MMSE}}$ so as to minimize the mean squared error (MSE) between $\mathbf{s}$ and its estimate $\tilde{\mathbf{r}}$ and can be written as,

$$\begin{aligned} \mathbf{W}_{\text{MMSE}} &= \arg\min_{\mathbf{W}} E[|\tilde{\mathbf{r}} - \mathbf{s}|^2] \\ &= (\sigma_n^2 \mathbf{I}_{n_T} + \mathbf{H}^\dagger \mathbf{H})^{-1} \mathbf{H}^\dagger \end{aligned} \tag{2.26}$$

where σ_n^2 is the noise power at each antenna and $\mathbf{I}_{n_T}$ is the $n_T \times n_T$ identity matrix. Therefore, the estimated signal vector $\hat{\mathbf{s}}$ is given by

$$\begin{aligned} \hat{\mathbf{s}} &= sgn[Re(\mathbf{W}_{\text{MMSE}}\, \mathbf{r})] \\ &= sgn[Re((\sigma_n^2 \mathbf{I}_{n_T} + \mathbf{H}^\dagger \mathbf{H})^{-1} \mathbf{H}^\dagger (\mathbf{H}\mathbf{s} + \mathbf{n}))] \end{aligned} \tag{2.27}$$

In (2.26) and (2.27), it is assumed that the symbols, s_i have unit power. It is well-known that the MMSE detection reduces the performance degradation of ZF detection caused by not taking into account the possible noise inflation. Therefore, the MMSE receiver tend to have a better BER performance than the ZF receiver [67].

Chapter 3

SEVERELY FADING CHANNELS

In this chapter, we provide an insight into the MIMO channels where the fading is more severe than Rayleigh fading. We describe severe fading (SF) in terms of the coefficient of variation (CV) using Rayleigh, Nakagami and lognormal channel models and discuss the potential applications, such as UWB-MIMO and cellular-MIMO systems.

3.1 INTRODUCTION TO SEVERELY FADING CHANNELS

Typical wireless systems experience multipath propagation which causes signal fading at the receiver. Considerable attention has been devoted to the statistical modeling of these effects. Several models have been used in the literature, for example, the Rayleigh, Ricean, and lognormal distributions described in [46–48].

However, it is well-known that these channel models do not accurately represent the real fading environment in all cases. Recent research has questioned the validity of these models for cases when the fading is more severe than Rayleigh [68–71]. Therefore, more realistic channel models, such as the Nakagami-m model, have been widely used to describe the multipath environment.

The Nakagami-m distribution is known as a versatile fading model since it can model a wide range of fading conditions by adjusting its fading parameter [45]. The fading parameter, m, describes the severity of the fading. The smaller the value of m, the

more severe the fading. In fact, Nakagami-m distributions with large values of m are similar to lognormal distributions [31].

In addition, the lognormal distribution is often used to model shadow fading [72, 73] and plays a key role in many UWB models [74, 75]. Unlike the previous models, results for the lognormal distribution are relatively sparse in the literature. The reason is that it is not possible to obtain an exact and simple closed-form expression for the moment generating function (mgf) of the combined output SNR. For example, average BER evaluation using the mgf-based approach will not provide analytical results. However, performance measures that depend only on the moments can often be obtained in closed form.

A large amount of the research on MIMO systems is based on a rich scattering environment, which provides an ideal transmission scenario for MIMO implementation. In reality, however, it is true that less ideal scenarios may arise in a variety of applications. For example, measurements reported in [29] were considerably more severe than Rayleigh for an RF tagging applications. Other areas where severe fading models are useful include wireless sensors [30], land-mobile, indoor-mobile and ionospheric radio links [76]. Moreover, new research areas such as UWB-MIMO [31, 77] and cellular-MIMO [32, 78] also seem to suffer from the severe fading.

3.2 THE CV OF SEVERELY FADING CHANNELS

As described in Section 2.5.3, the fading severity of a channel model can be measured by the coefficient of variation (CV) of the amplitudes, A. Note that we assume the amplitude, A is normalized to have unit power, $E[A^2] = 1$. We shall now consider the CVs of the classical models including Rayleigh, Nakagami and lognormal.

In the baseline case of a rich scattering environment, A has a Rayleigh distribution with CV given by

$$\text{CV} = \sqrt{\frac{4}{\pi} - 1} \approx 0.5227 \tag{3.1}$$

Hence, SFC can be defined as a particular channel model where the CV is greater than the CV of the Rayleigh case, i.e. $CV > 0.5227$.

The CV of the Nakagami-m distribution is given by

$$\text{CV} = \sqrt{\frac{\Gamma(m)^2 m}{\Gamma(m+1/2)^2} - 1} \tag{3.2}$$

Hence, as m varies, the Nakagami-m distribution spans a wide range of CV values. In particular, when $m \to \infty$, the CV approaches 0 which corresponds to the case of no fading. When $m = 1$, the CV corresponds to the Rayleigh model. When $m \to 0$, the CV approaches $+\infty$ giving severe fading.

Lastly, the CV of the lognormal distribution is given by

$$\text{CV} = \sqrt{\exp(\sigma^2 - 1)} \tag{3.3}$$

where σ (dB) is the standard deviation. In practice, typical values of σ can be arbitrarily high, e.g. 4.3-13.3 dB [4] and 6-12 dB [72]. Hence the CV of the lognormal is usually well into the severe fading region.

Note that although the CV of the Rayleigh distribution is known, the CVs of the other distributions are not reported in the literature for the power normalized case. Hence, (3.2), (3.3) and the CVs reported in Table 4.3 were derived from first principles. Since the calculations are straightforward, although a little tedious, they are omitted.

3.3 UWB-MIMO APPLICATIONS

Recently, ultra-wideband (UWB) communication has attracted great interest for applications in short-range radio links operating at high data rate and overlaying with other existing wireless systems [79–84]. This is due to the potential advantages of UWB such as high data rates, inherent robustness to multi-path fading, flexibility of operation, low power consumption, low cost of implementation, and excellent range resolution capabilities [77].

In particular, substantial attention to this technology has been paid in the standardization process of the IEEE 802.15 Wireless Personal Area Networks (WPAN) proposal. UWB is defined as any radio transmission that occupies a bandwidth of more than 20% of its center frequency, or nominally more than 500 MHz [77]. In February 2001, the Federal Communications Commission (FCC) issued a Report and Order that UWB radio transmission can legally operate in the range from 3.1 GHz to 10.6 GHz, at a transmit power of -41.3 dBm/MHz [85]. UWB offers attractive solutions for applications including radar, imaging, sensor networks and positioning systems [86]. Recent results indicate that UWB has a potential to offer a capacity much higher than the current narrowband systems for short-range wireless applications.

Currently, UWB technology can achieve data rates ranging from 55 to 480 Mbits/s over distances up to 10m [31]. As described in Section 2.1, MIMO systems are well known for their potential in improving system performance in fading environments. Thus, MIMO schemes can be employed in UWB systems to achieve the very high data rate requirement for future short-range wireless applications. In fact, the GHz center frequency of UWB radio relaxes the requirements on the spacing between antenna array elements [31]. To date, existing research on MIMO systems has focused mostly on

narrowband systems, while research on UWB-MIMO systems is still largely unexplored. Thus, this is currently emerging as a promising research area.

Several indoor channel models has been proposed for UWB including the tap-delay line Nakagami fading model [74], the Saleh-Valenzuela (S-V) model [87], and the Δ-K model [62]. The IEEE 802.15.3 Working Group for Wireless Personal Area Networks (WPAN) [85] investigated these models and decided to use a modified S-V model for the UWB channel model in the standard. The amplitude statistics in the original S-V model were based on the Rayleigh distribution. However, measurements in UWB indoor channels indicated that the amplitudes do not follow a Rayleigh distribution. This led to a S-V model using a lognormal or a Nakagami distribution rather than the original Rayleigh distribution. Hence, one of the UWB standard models has lognormal fading, which gives a severe fading channel.

3.4 CELLULAR-MIMO APPLICATIONS

With the advent of cellular telephony, wireless communication has come to the forefront, the main goal of which is to allow a user to move freely within a service area, while at the same time being able to communicate with any telephone subscriber in the world.

Cellular systems offer very high capacity with a limited spectrum allocation by limiting the coverage of each base station (BS) to a small geographic area called a “cell”. Hence, the same radio channels may be reused by another BS located some distance away. The design process of allocating channels for all of the cellular BSs within a system is called “frequency reuse” [88]. When the user moves into a different cell while a conversation is in progress, a switching technique, called a “handoff”, transfers the call to a new channel associated with the new BS.

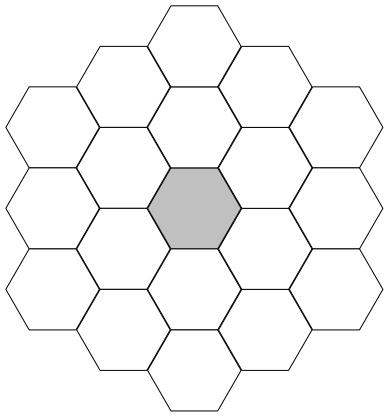

Figure 3.1 Cell layout

In cellular systems, the cells are modeled with a hexagon pattern, as shown in Figure 3.1, and each cell has a BS located at the center of the cell. The hexagonal pattern is conceptual, but it has been widely adopted since the hexagon shape allows easy analysis of a cellular system.

Multiple access (MA) is a set of techniques that enable multiple users to share a limited radio spectrum efficiently. There are four basic forms of MA for sharing the spectrum [24],

- FDMA - Frequency-Division Multiple Access refers to sharing the spectrum by assigning specific frequency channels to specific users.
- TDMA - Time-Division Multiple Access refers to allowing all users access to all of the available spectrum, but users are assigned specific time intervals during which they can access it.
- CDMA - Code-Division Multiple Access is a form of spread spectrum modulation in which users are allowed to use the available spectrum, but their signal must be spread with a specific code to distinguish it from other signals.
- SDMA - Space-Division Multiple Access refers to sharing the spectrum between

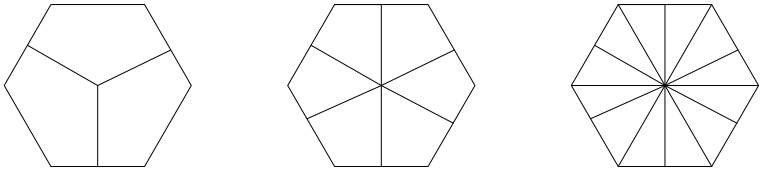

Figure 3.2 Cell sectorization

the users by exploiting the spatial distribution of user terminals through the use of directional antennas that minimize the interference between the terminals. One remarkably property of SDMA is that SDMA ca easily enhance channel capacity by a joint application with other MA techniques, such as FDMA, TDMA and CDMA.

While SDMA relies on the use of smart antennas, the simplest technique is "sectorization", whereby an antenna is dedicated for each "sector". To form sectors, a physical antenna reflector is designed to shape the antenna gain pattern. The sector size can be decreased as long as the antenna beamwidth is larger than the channel angle spread. The angle spread depends on a number of factors including carrier frequency, bandwidth and antenna heights. However, in typical fixed wireless applications, it is usually less than 20 degrees. Therefore, it is reasonable to assume that the cell could be divided into 12 sectors of 30 degrees each using 12 antennas. Alternatively with 12 antennas, one could create 6 sectors with 2 antennas per sectors or 3 sectors with 4 antennas per sectors. Each cell is divided into $S = 3$, 6, or 12 equal sectors shown in Figure 3.2. Full details of the cell sectorization and frequency reuse plans are discussed in Chapter 6.

Despite the benefits of MIMO, the application of MIMO techniques in a cellular system has received much less attention than the single-user scenario, which is well-summarized in [12]. However, with MIMO research entering a maturing stage, MIMO is of great interest to 3G cellular providers and MIMO is being widely considered for cdma2000 (3GPP2) and WCDMA (3GPP), especially for the high data rate modes such as EV-

DV, EV-DO and HSDPA.

A few notable studies [89, 90] have shown in cellular applications that the other-cell interference (OCI) severely degrades the overall capacity of MIMO systems. The main cause is that the MIMO receiver cannot suppress the OCI, while also suppressing the spatial interference (SI) introduced by the multiple transmit antennas.

Chapter 4

A COMPARISON OF SEVERELY FADING CHANNEL MODELS

In Chapter 3, we discussed the basic idea of a severely fading channel and applications of the severely fading scenario. Having defined the CV as a measure of the severity of the fading, now we investigate the sensitivity of MIMO system performance to the CV over a wide range of amplitude distributions.

We first derive the CV for the amplitude distributions discussed in Section 4.1. We then investigate whether the CV is a good measure of the effect of the fading severity on the ergodic MI and BER in Section 4.2.

4.1 A RANGE OF AMPLITUDE DISTRIBUTIONS

We consider a range of alternative distributions for the amplitudes including the lognormal, gamma, beta, uniform, truncated-t and truncated-Gaussian. Both the truncated distributions are truncated at zero to give positive amplitudes. The distributions are chosen to give a wide variation in the type of amplitude variable and to cover severe fading scenarios. Note that the selected models include short-tailed (Gaussian), long-tailed (lognormal), finite support (uniform) and infinite support (Nakagami) distributions. The Weibull distribution is another distribution that is worth consideration in a more comprehensive study, since it also covers the severe fading region.

In summary, there are considerable differences between the amplitude distributions considered in this work, covering a large variety of channel propagation conditions.

The parameters of the amplitude distributions, A, are shown in Table 4.1.

Table 4.1 The parameters of the amplitude distributions

A	**Parameters**
lognormal	$\sigma \geq 0$, standard deviation
$L[\mu, \sigma]$	$\mu = -\sigma^2$, mean
gamma	$r > 0$, shape parameter
$G[r, \theta]$	$\theta = \sqrt{r(r+1)}$, scale parameter
beta	$p > 0$, shape parameter
$B[p, q]$	$q > 0$, shape parameter
uniform	$0 \leq a < 1$, minimum boundary
$U[a, b]$	$b = \frac{-a \pm \sqrt{a^2 - 4(a^2-3)}}{2}$, maximum boundary
truncated-t	$2 < \nu < 42$, degree of freedom
$T_t[\nu, \theta]$	$\theta = \sqrt{\frac{\nu-2}{\nu}}$, scale parameter
Nakagami	$m > 0$, fading parameter
$N[m, \theta]$	$\theta = m$, scale parameter
truncated-Gaussian	$0 \leq \mu < 1$, mean
$N_t[\mu, \sigma]$	$\sigma = \sqrt{1 - \mu^2}$, standard deviation

The amplitude distributions considered here are all 2 parameter distributions. Distributions such as the uniform ($U[a, b]$) and beta ($B[p, q]$) have 2 parameters in their standard form. Others, such as the truncated-t, have only 1 parameter in their standard form but can be scaled by a constant to give an extra parameter. The 2 parameters are necessary since one is fixed by the normalization, $E[A^2] = 1$ and the remaining parameter is varied to give a range of CV values. Note that the restriction of one parameter by the condition, $E[A^2] = 1$, is given in Table 4.1. Hence, for example, a gamma distribution ($G[r, \theta]$) usually has unrestricted shape (r) and scale (θ) parameters, whereas

we require $\theta = \sqrt{r(r+1)}$ to give the unit power property.

This approach allows us to investigate the effect of CV on ergodic MI for a fixed type of normalized amplitude distribution. For example if A is uniform over $[a, b]$, for $0 < a < b$, then $0 < a < 1$ is required to satisfy the normalization condition and over this region it is simple to show that the resulting CV values are in the range $[0, 1/\sqrt{3}]$. Hence, for uniform amplitudes we are only able to consider the variation in ergodic MI over $0 < CV < 1/\sqrt{3}$. Several of the other distributions also have restrictions on the range of CV values that can be achieved.

In order to derive the CV, the expected values of the amplitude distributions, $E(A)$, are evaluated in Table 4.2.

Table 4.2 The expected values of the amplitude distributions

A	$E(A)$
lognormal	$\exp\left(\frac{\sigma^2}{2}\right)$
gamma	$\sqrt{\frac{r}{r+1}}$
beta	$\sqrt{\frac{p(p+q+1)}{(p+1)(p+q)}}$
uniform	$\frac{a+b}{2}$
truncated-t	$\frac{\sqrt{\nu-2}\,\Gamma\left(\frac{\nu-1}{2}\right)}{\sqrt{\pi}\,\Gamma\left(\frac{\nu}{2}\right)}$
Nakagami	$\frac{\Gamma\left(\frac{m+1}{2}\right)}{\sqrt{m}\Gamma(m)}$
truncated-Gaussian	$\frac{\sqrt{1-\mu^2}\,\sqrt{2}}{\pi}\,\exp\left(\frac{-\mu^2}{2(1-\mu^2)}\right) + \mu\left[1 - 2P\left(Z < \frac{-\mu}{\sqrt{1-\mu^2}}\right)\right]$

Finally, the CV values of the amplitude distributions are derived by using (2.20) and are shown in Table 4.3.

Table 4.3 CV values of the amplitude distributions

A	CV
lognormal	$\left[\exp(\sigma^2) - 1\right]^{1/2}$
gamma	$\left[\frac{1}{r}\right]^{1/2}$
beta	$\left[\frac{q}{p(p+q+1)}\right]^{1/2}, \quad 0 < \text{CV} < 1$
uniform	$\left[\frac{4}{(a+b)^2} - 1\right]^{1/2}, \quad 0 < \text{CV} \leq 1/\sqrt{3}$
truncated-t	$\left[\frac{\pi\Gamma(\nu/2)^2}{(\nu-2)\Gamma((\nu-1)/2)^2} - 1\right]^{1/2}$
Nakagami	$\left[\frac{m\Gamma(m)^2}{\Gamma(m+1/2)} - 1\right]^{1/2}$
truncated-Gaussian	$\left[1\Big/\left(\frac{\sqrt{1-\mu^2}\sqrt{2}}{\pi}\exp\left(\frac{-\mu^2}{2(1-\mu^2)}\right) + \mu\Big(1 - 2P\Big(Z < \frac{-\mu}{\sqrt{1-\mu^2}}\Big)\Big)\right)^2 - 1\right]^{1/2}$

4.2 SIMULATION RESULTS

The relationships between the CV, the amplitude distribution and ergodic MI and BER performance are illustrated in the following subsections.

4.2.1 Ergodic MI Results

For a range of amplitude distributions and a wide range of CV values the ergodic MI was simulated from using 1,000,000 replicates. Results for (2,2), (2,4), (4,2), (4,4) and (8,8) MIMO systems with a SNR of 0 dB, 6 dB and 18 dB are shown in Figures 4.1–4.15, respectively. Note that the legends in these figures refer to 't' and 'Gaussian', whereas truncated versions of these distributions were actually used. Figures 4.3, 4.9, 4.6 and 4.12 show that at high SNR the CV is an excellent predictor of the ergodic MI for system dimensions up to (4,4), which is not greatly affected by the precise amplitude distribution. Figures 4.1, 4.7, 4.4, 4.10 and 4.13 show that this

conclusion begins to break down at low SNR where the ergodic MI is more sensitive to the type of distribution. Four of the distributions considered can only give CV values less than 1. Hence the MI curves for these distributions are overlaid by the others and are difficult to see. As a reference point, the CV for Rayleigh channel is 0.5227. Clearly, for small CV values, all the amplitude distributions give very similar results. The top curve, which diverges from the others, corresponds to the beta distribution. This achieves the high CV values by becoming bimodal as shown in Figure 4.28. Hence the amplitude distribution is very different to physical reality and this case is an extreme example. The circle appearing on the y-axis of the Figures denotes zero CV, i.e. the case when the amplitude is exactly equal to one, $A = 1$.

In Figures 4.1 and 4.2, where the curves diverge, the short-tailed distributions (Nakagami and gamma) are similar and the long-tailed distributions (lognormal and truncated-t) are similar, Hence, at high SNR all the curves are similar, whereas at low SNR, distributions which are similar in nature show similar patterns. Clearly, at high CV values, the long-tailed distributions cause a more dramatic decrease in MIMO capacity. Considering the patterns in Figures 4.1–4.15, it is apparent that the longer tailed distributions (lognormal and truncated-t) usually have more of an effect in reducing capacity. The only scenario where this is not the case is for high SNR and a smaller system size (see Figures 4.3 and 4.6).

A comparison of (2,2), (4,4) and (8,8) systems has shown that the curves diverge markedly for larger systems, even in high SNR. Hence, for large MIMO systems, the ergodic MI is more sensitive to the type of distribution.

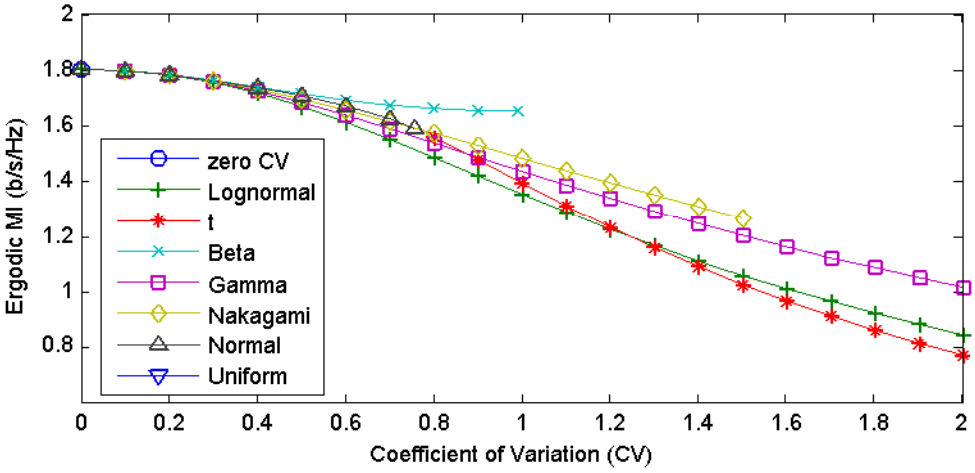

Figure 4.1 Ergodic MI vs CV in a (2,2) MIMO system with SNR = 0dB

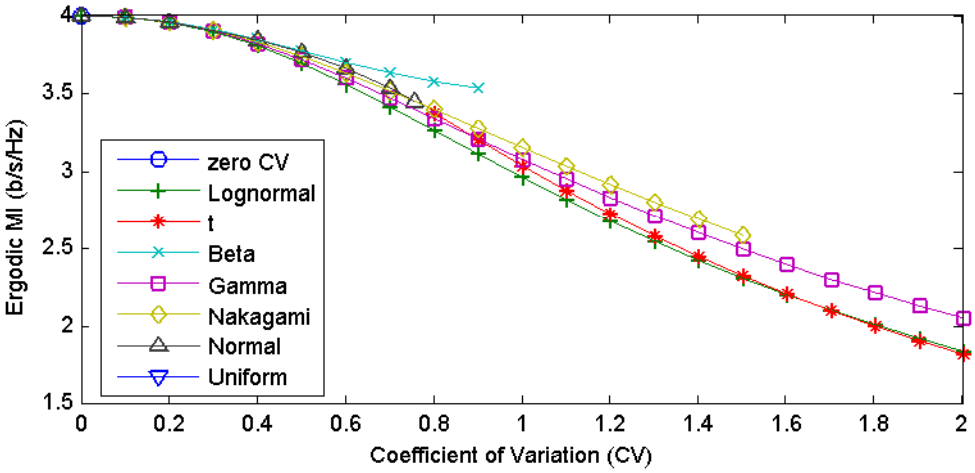

Figure 4.2 Ergodic MI vs CV in a (2,2) MIMO system with SNR = 6dB

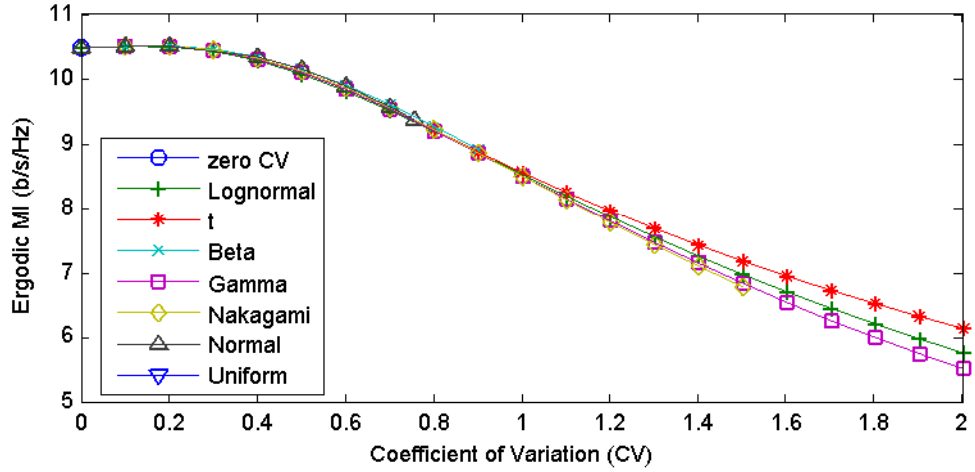

Figure 4.3 Ergodic MI vs CV in a (2,2) MIMO system with SNR = 18dB

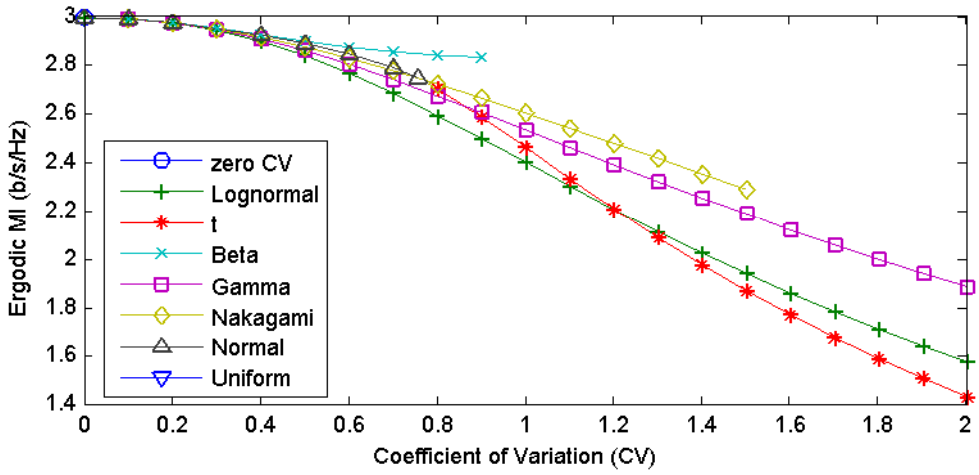

Figure 4.4 Ergodic MI vs CV in a (2,4) MIMO system with SNR = 0dB

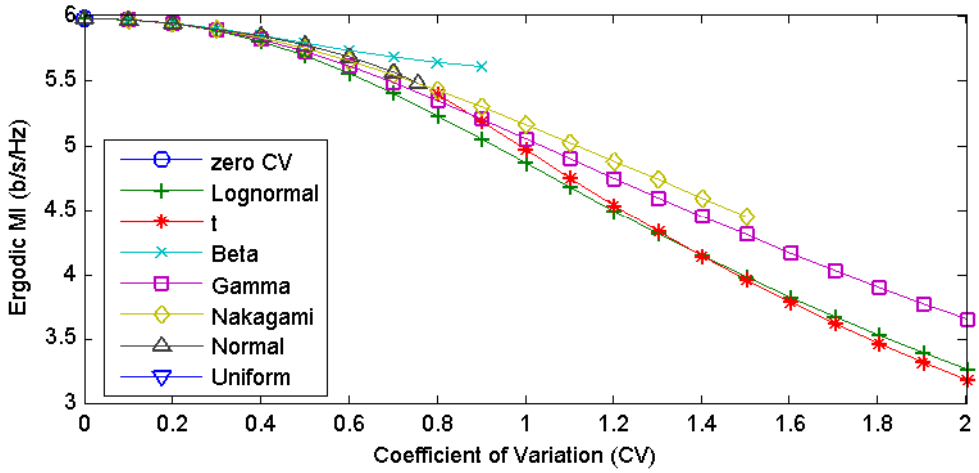

Figure 4.5 Ergodic MI vs CV in a (2,4) MIMO system with SNR = 6dB

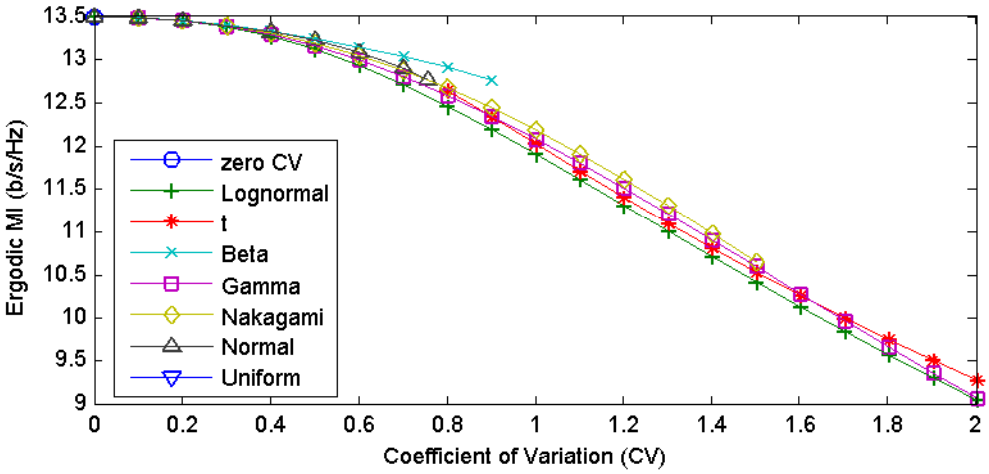

Figure 4.6 Ergodic MI vs CV in a (2,4) MIMO system with SNR = 18dB

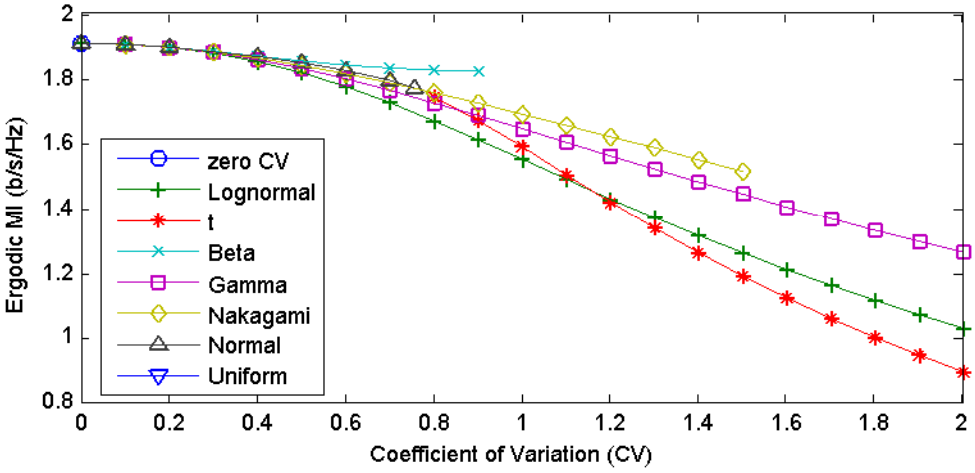

Figure 4.7 Ergodic MI vs CV in a (4,2) MIMO system with SNR = 0dB

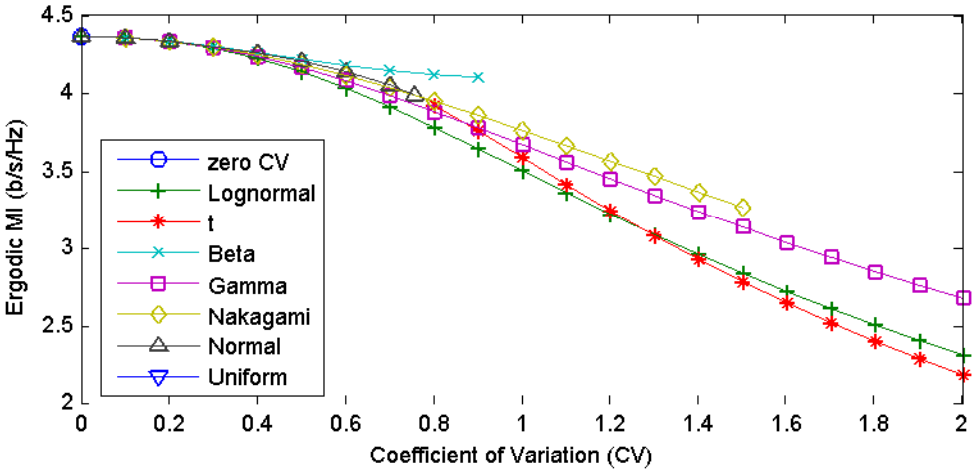

Figure 4.8 Ergodic MI vs CV in a (4,2) MIMO system with SNR = 6dB

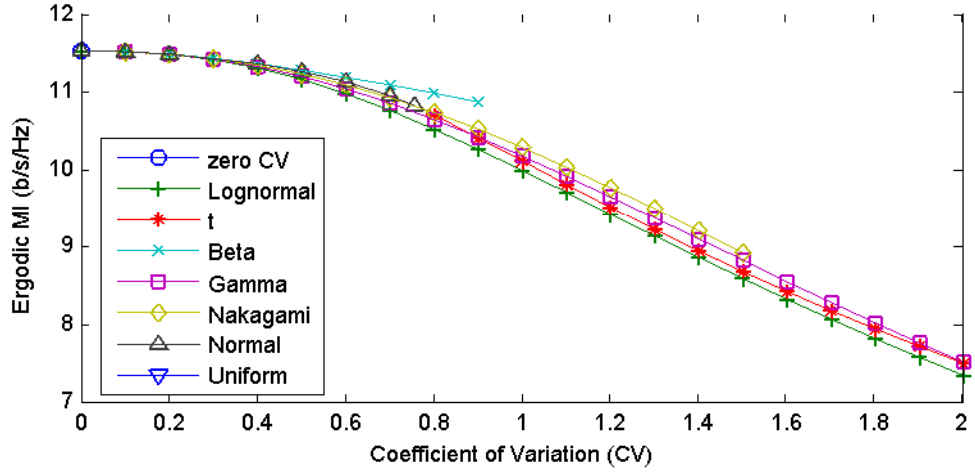

Figure 4.9 Ergodic MI vs CV in a (4,2) MIMO system with SNR = 18dB

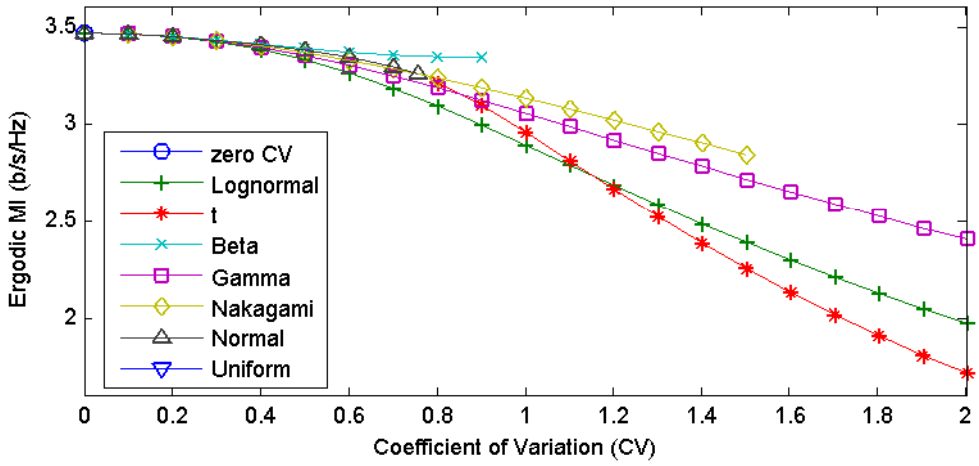

Figure 4.10 Ergodic MI vs CV in a (4,4) MIMO system with SNR = 0dB

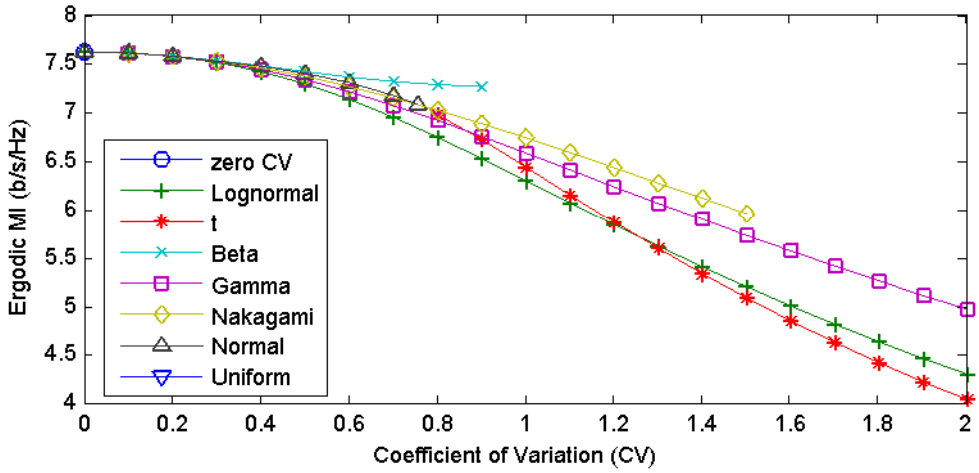

Figure 4.11 Ergodic MI vs CV in a (4,4) MIMO system with SNR = 6dB

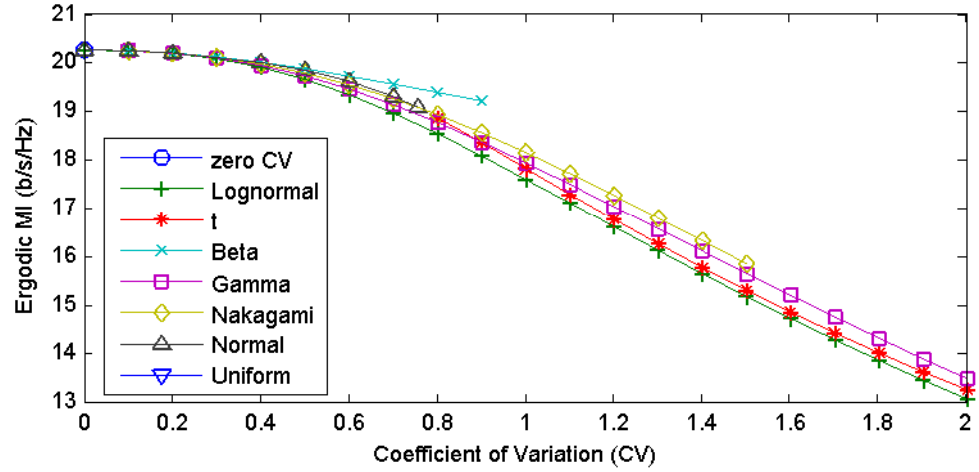

Figure 4.12 Ergodic MI vs CV in a (4,4) MIMO system with SNR = 18dB

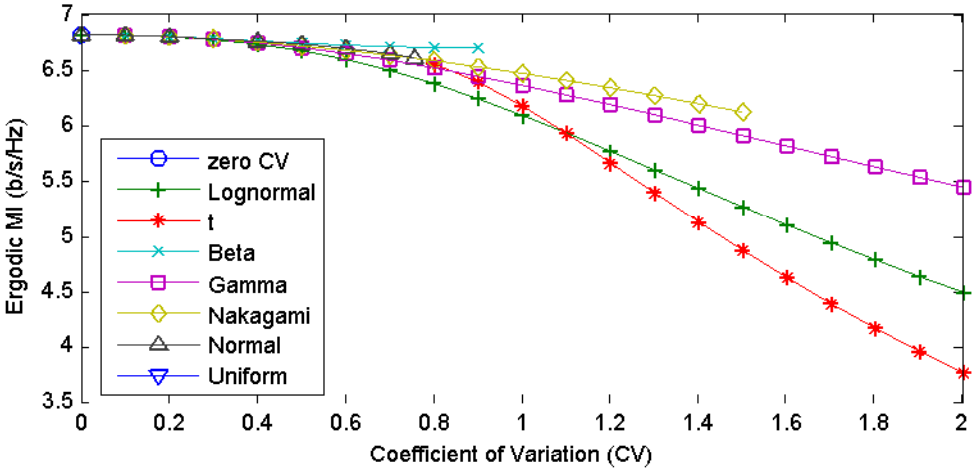

Figure 4.13 Ergodic MI vs CV in a (8,8) MIMO system with SNR = 0dB

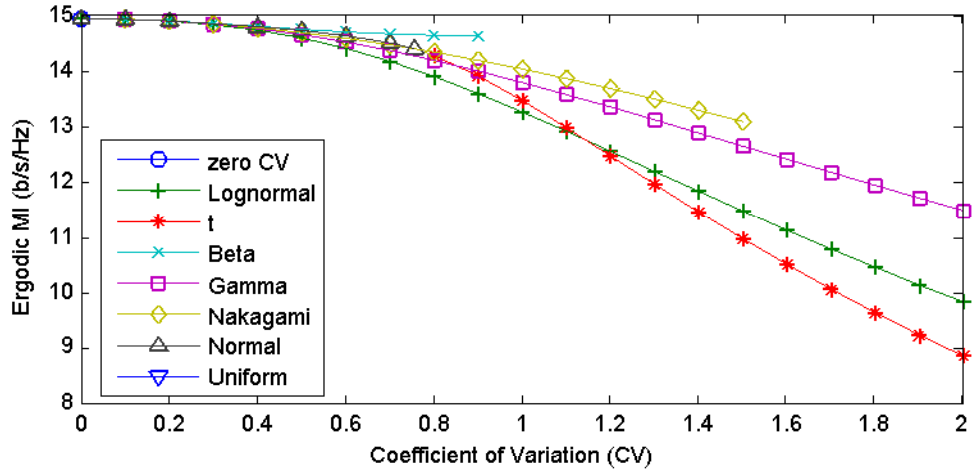

Figure 4.14 Ergodic MI vs CV in a (8,8) MIMO system with SNR = 6dB

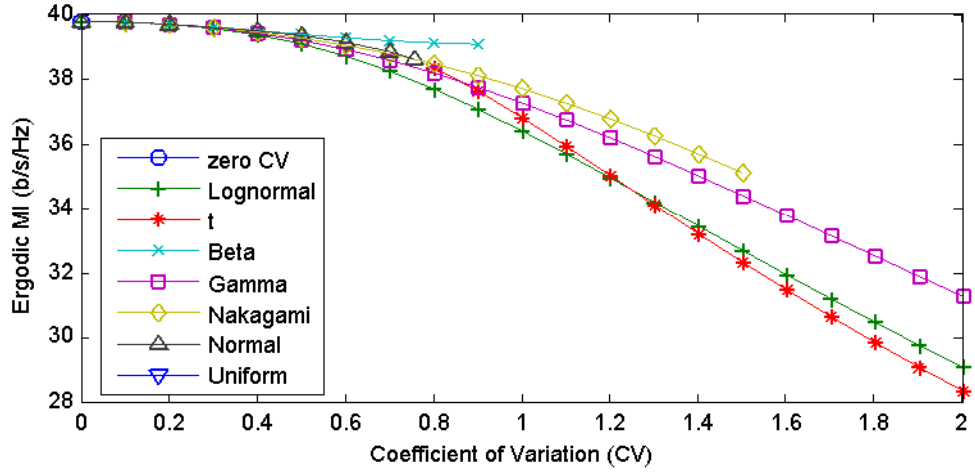

Figure 4.15 Ergodic MI vs CV in a (8,8) MIMO system with SNR = 18dB

4.2.2 BER Results

Now, we examine the results of the BER performance of MIMO systems using ZF and MMSE combining at the receiver. Figures 4.16–4.18 show the BER for the lognormal, t, and Nakagami cases in a (2,2) MIMO-ZF system with CV = 0.5, 1, 1.5. These results demonstrate that the BER performance of all cases are affected negatively by increasing CV. Figure 4.18 shows that the Nakagami model is particularly sensitive to the CV and suffers a very large degradation in BER performance when the CV is large. Note that in Figure 4.19, the BER for the lognormal case is very similar to the Nakagami case when CV is 0.5, whereas the t case becomes more similar to the lognormal as the CV increases (see Figures 4.20 and 4.21). Also, Figure 4.18 shows that the BER of the Nakagami case is very high at high CV values. This is due to the unusual shape the Nakagami case takes on for high CV values. Such a shape is physically unrealistic and so the other cases are more plausible in these regions.

To consider this effect, we consider Figure 4.29. Figure 4.29 shows the pdf of the Nakagami and lognormal amplitudes when the CV is 1.5. It suggests that the Nakagami distribution tends to have a very high probability of receiving small amplitudes, whereas the lognormal tends to a have a low probability. Therefore, the Nakagami leads to a very large degradation in BER performance when the CV is large.

We also consider the BER performance of (2,2) MIMO-MMSE systems as shown in Figures 4.22–4.27. As discussed in Section 2.6.2, the MMSE receiver tends to have better BER performance than ZF receiver. Interestingly, this superiority is more noticeable at low CV values. For high CV values (see Figures 4.21 and 4.27) the difference between MMSE and ZF is very small.

Figures 4.25–4.27 shows that the BER of the lognormal case is better than the t and

Nakagami cases. Also the difference in BER between the t and lognormal channel model gradually reduces as the CV increases.

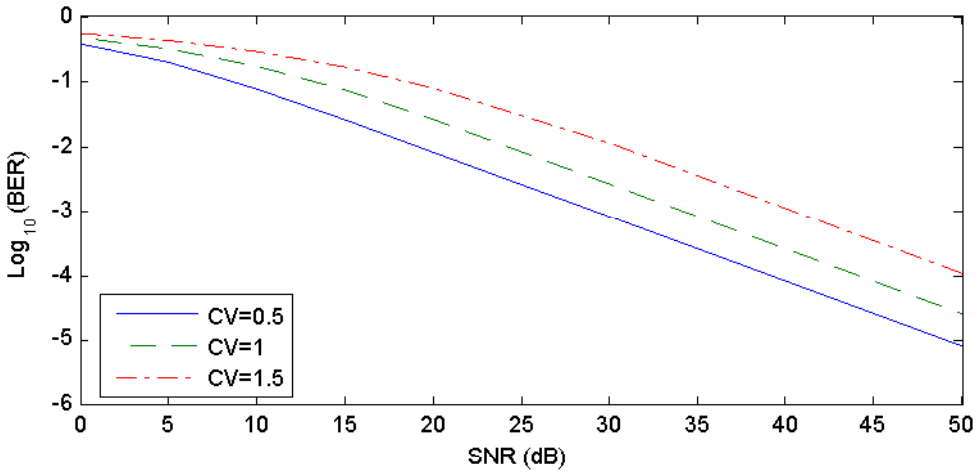

Figure 4.16 BER for the lognormal case in a (2,2) MIMO-ZF system with CV = 0.5, 1, 1.5

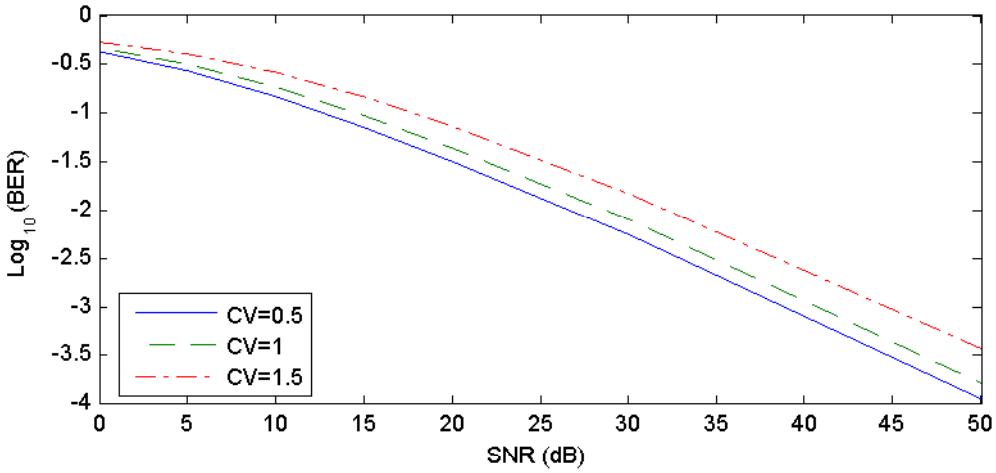

Figure 4.17 BER for the t case in a (2,2) MIMO-ZF system with CV = 0.5, 1, 1.5

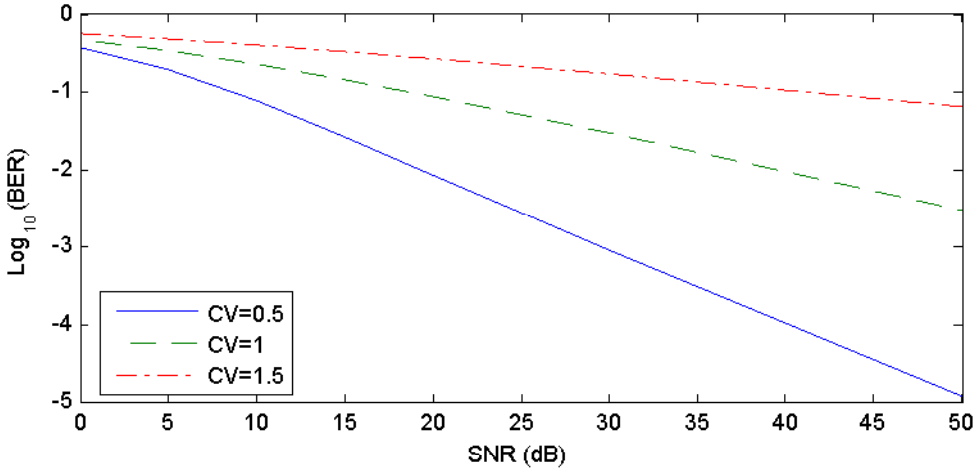

Figure 4.18 BER for a the Nakagami case in a (2,2) MIMO-ZF system with CV = 0.5, 1, 1.5

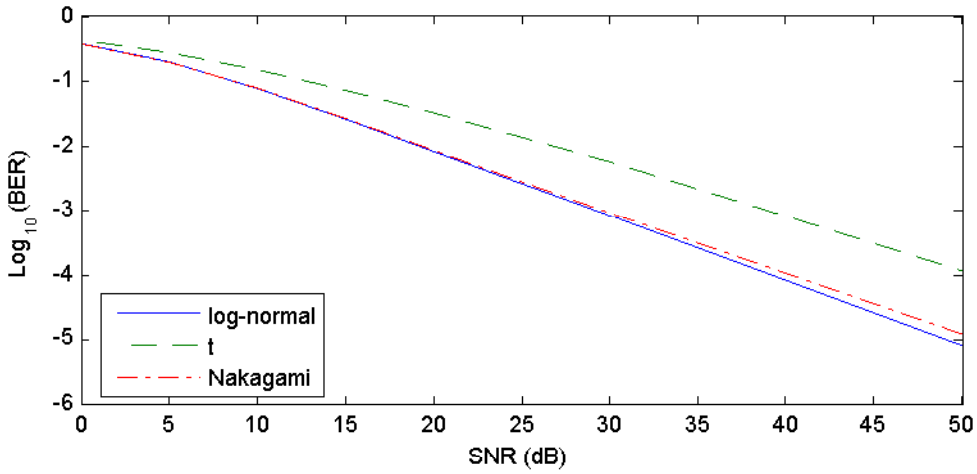

Figure 4.19 BER for lognormal, t, and Nakagami cases in a (2,2) MIMO-ZF system with CV = 0.5

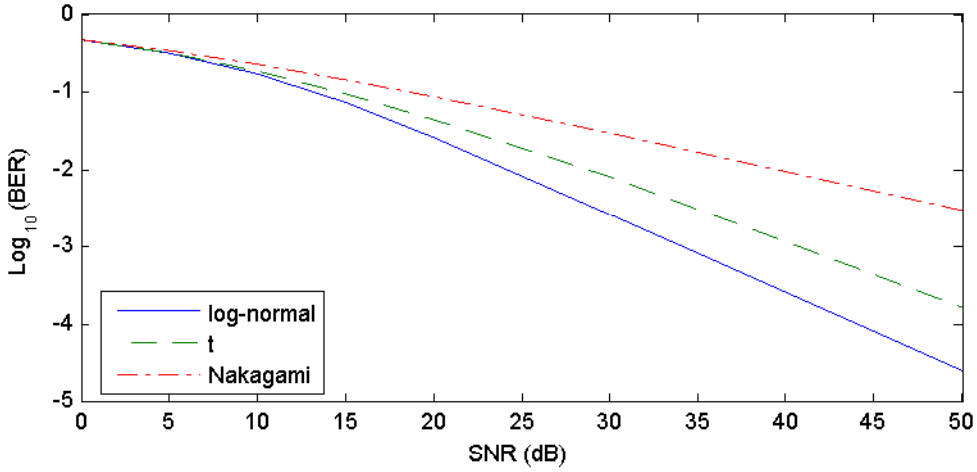

Figure 4.20 BER for lognormal, t, and Nakagami cases in a (2,2) MIMO-ZF system with CV = 1.0

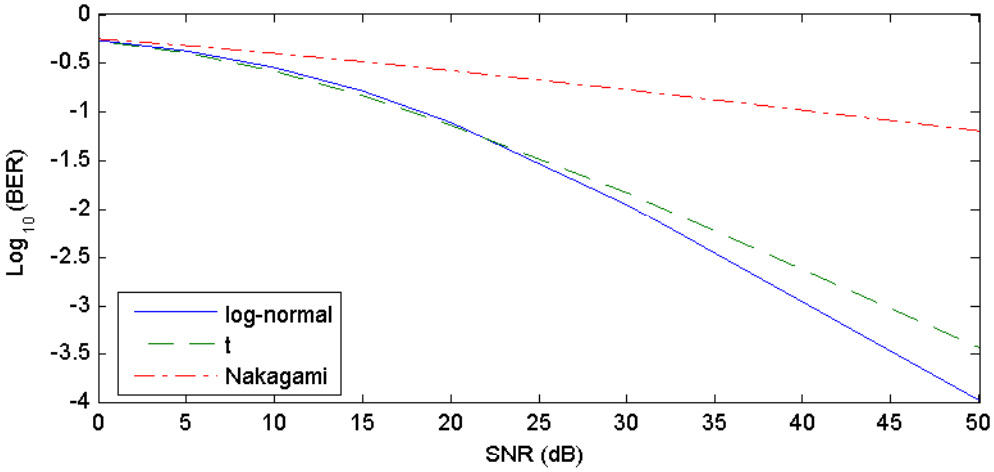

Figure 4.21 BER for lognormal, t, and Nakagami cases in a (2,2) MIMO-ZF system with CV = 1.5

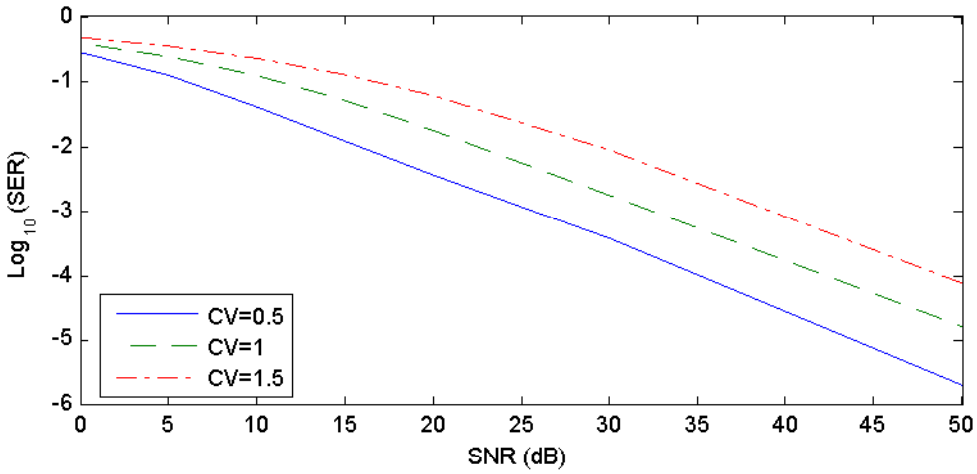

Figure 4.22 BER for the lognormal case in a (2,2) MIMO-MMSE system with CV = 0.5, 1, 1.5

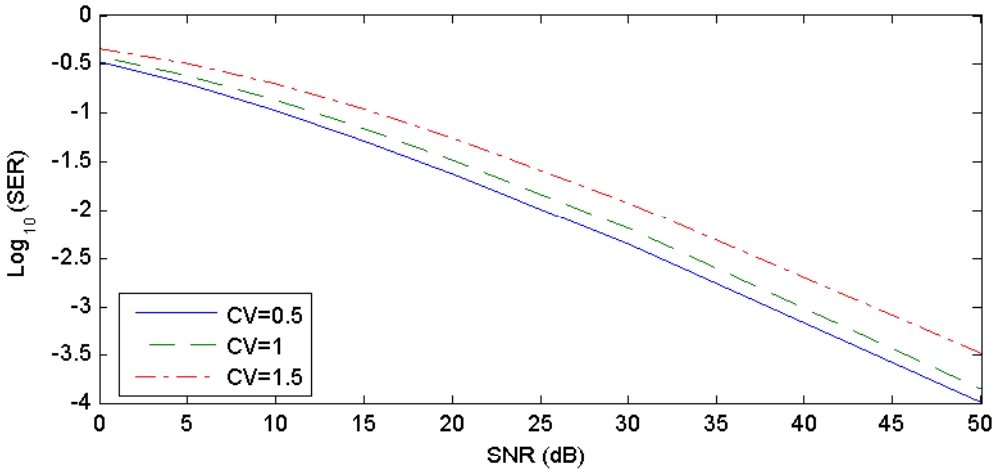

Figure 4.23 BER for the t case in a (2,2) MIMO-MMSE system with CV = 0.5, 1, 1.5

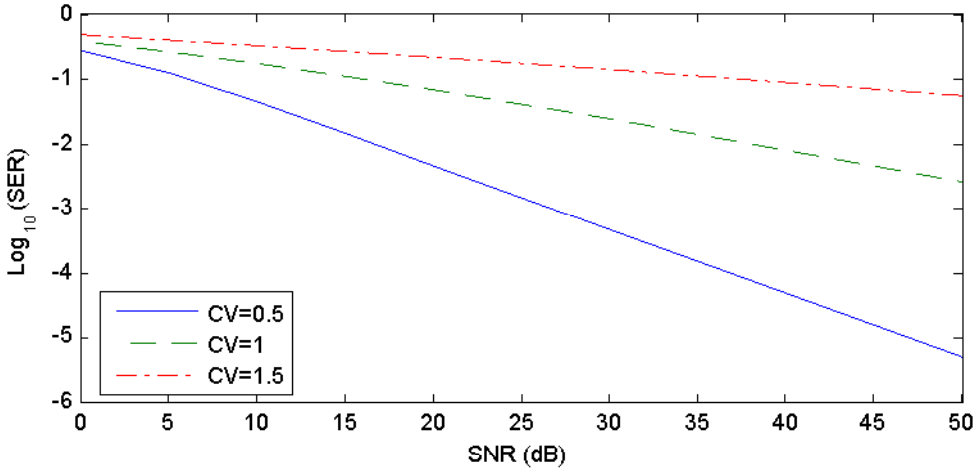

Figure 4.24 BER for the Nakagami case in a (2,2) MIMO-MMSE system with CV = 0.5, 1, 1.5

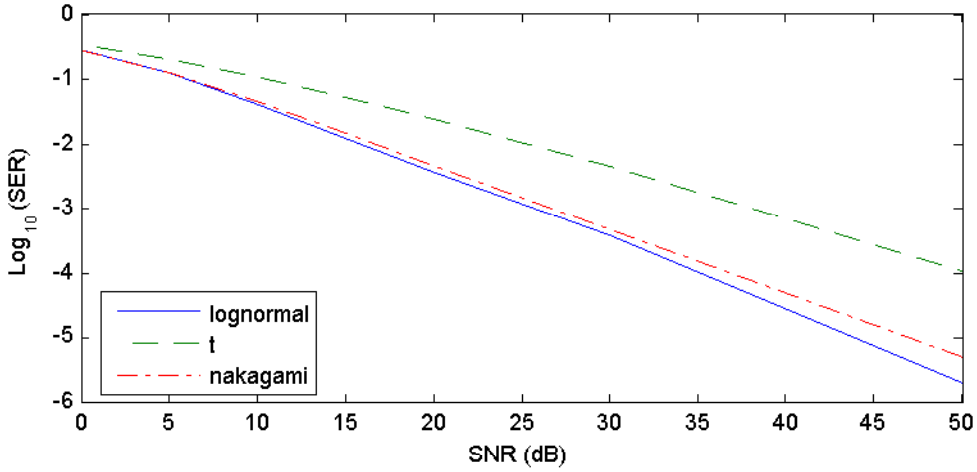

Figure 4.25 BER for the lognormal, t, and Nakagami cases in a (2,2) MIMO-MMSE system with CV = 0.5

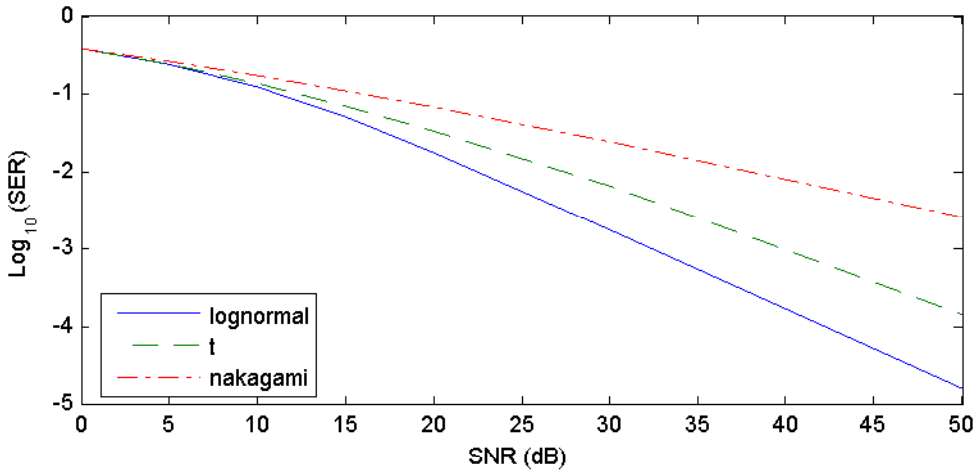

Figure 4.26 BER for the lognormal, t, and Nakagami cases in a (2,2) MIMO-MMSE system with CV = 1.0

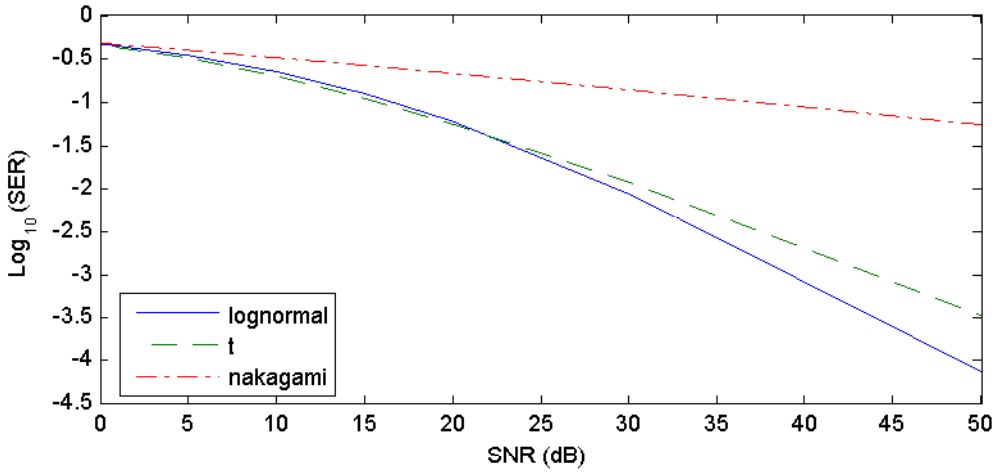

Figure 4.27 BER for the lognormal, t, and Nakagami cases in a (2,2) MIMO-MMSE system with CV = 1.5

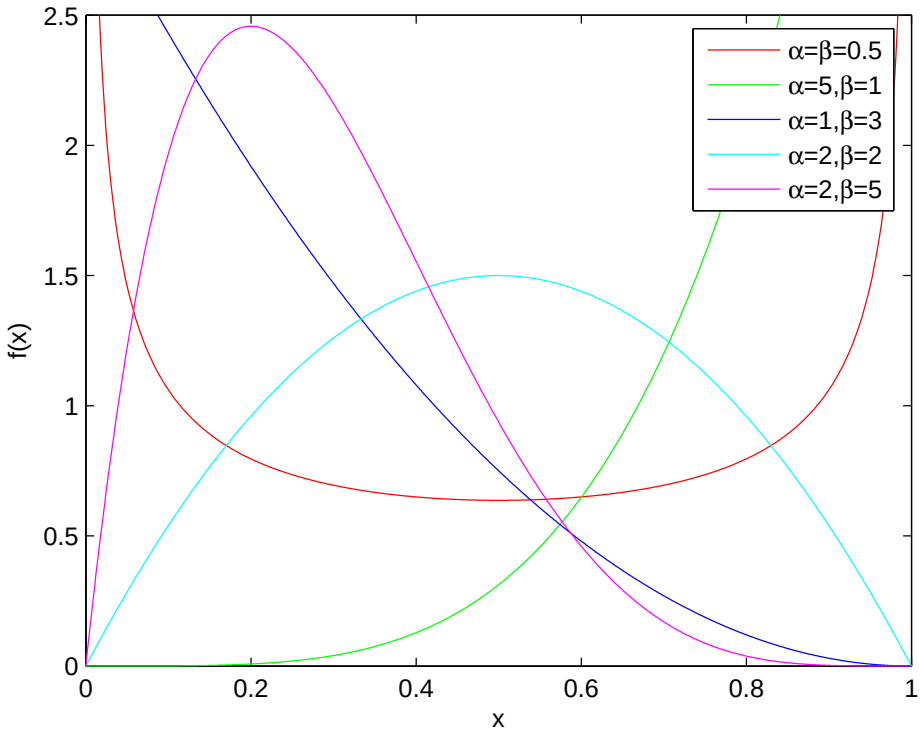

Figure 4.28 PDF of a beta distribution ($B[\alpha, \beta]$)

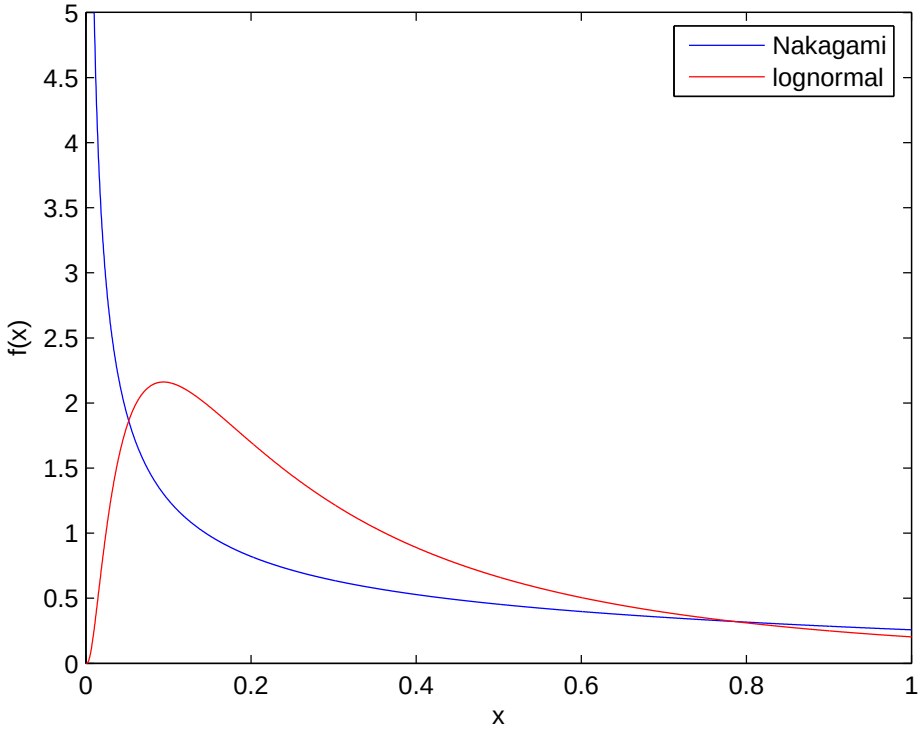

Figure 4.29 PDF of the Nakagami and lognormal distributions when CV = 1.5

Chapter 5

THE COMPLEX MULTIVARIATE T CHANNEL MODEL

In Chapter 4, the results motivated the development of a simple channel model which can cover the full range of severely fading channels, $\mathrm{CV} > \mathrm{CV}_{\mathrm{Rayleigh}}$, and act as an approximation to other severely fading channels with same CV. In the next section, we propose the complex multivariate t (CMT) model and show that it has the desired properties.

5.1 INTRODUCTION TO THE CMT MODEL

We are motivated by the desire to study severe fading in matrix channels to seek a model for the elements of the channel matrix which is simple, analytically tractable and covers the full range of cases in the region $\mathrm{CV} > \mathrm{CV}_{\mathrm{Rayleigh}}$. Such a model is the *complex multivariate t (CMT) distribution* [91, 92]. The CMT is one of the family of elliptical multivariate distributions [91] and hence a wide body of knowledge is available. Also, the CV of the amplitudes resulting from the use of the CMT satisfies the requirement that $\mathrm{CV}_{\mathrm{CMT}} > \mathrm{CV}_{\mathrm{Rayleigh}}$. Furthermore, the marginal distributions for any channel matrix element are complex t distributed and this includes the baseline case of complex Gaussian entries as a special case. Hence the CMT model generalizes the classical complex Gaussian matrix to the severe fading scenario.

The simplest description of the CMT channel matrix, $\mathbf{H}_{\mathrm{CMT}}$, is to express it as the

ratio of an iid complex Gaussian matrix, $\mathbf{H}$ and the square root of an independent scaled χ^2 variable [91, 92]. This formulation is:

$$\mathbf{H}_{\text{CMT}} = \frac{\mathbf{H}}{\sqrt{\frac{S^2}{r-1}}} \tag{5.1}$$

where S^2 has a complex χ^2 distribution with r degrees of freedom. The probability density function (pdf) of S^2 is given by

$$f_{S^2}(x) = x^{r-1}\frac{\exp(-x)}{\Gamma(r)} \tag{5.2}$$

where $r > 1$, $x > 0$ and $\Gamma(\cdot)$ is the gamma function. Note that the division of the i.i.d. matrix $\mathbf{H}$ by a single, common random variable results in dependent entries for $\mathbf{H}_{\text{CMT}}$. However, the independence of the $\mathbf{H}$ matrix preserves the uncorrelated nature of the entries. With this definition, the elements of $\mathbf{H}_{CMT}$ are uncorrelated, identically distributed, complex t variables with uniform phase over $[0, 2\pi]$. When $r \to \infty$ the model collapses to the baseline i.i.d. complex Gaussian matrix and the elements of $\mathbf{H}_{\text{CMT}}$ have amplitudes with CV equal to $\text{CV}_{\text{Rayleigh}}$. For finite r, the amplitudes are longer tailed than the Rayleigh case and give severe fading scenarios with a CV easily derived as

$$\text{CV}_{\text{CMT}} = \sqrt{\frac{\Gamma(r)^2}{\Gamma(r-1/2)^2\Gamma(3/2)^2(r-1)} - 1} \tag{5.3}$$

From (5.3) it can be seen that $\text{CV}_{\text{CMT}} \to \text{CV}_{\text{Rayleigh}}$ as $r \to \infty$ and $\text{CV}_{\text{CMT}} \to \infty$ as $r \to 1$.

Representations for $\mathbf{H}_{CMT}$, including the pdf, can be obtained from the viewpoint of multivariate statistical theory [91,92], but the representation in (5.1) is sufficient for our purposes and leads to a simple analytical method for computing both MI and system performance.

5.2 MUTUAL INFORMATION OF CMT

Consider the link model (2.1) with the CMT channel matrix $\mathbf{H}_{\mathrm{CMT}}$. We use the representation for the ergodic MI, $E(\mathcal{I})$, defined by [18]

$$E(\mathcal{I}) = E\left[m \log_2\left(1 + \frac{\rho}{n_T}\lambda_{\mathrm{CMT}}\right)\right] \tag{5.4}$$

where λ_{CMT} is an arbitrary non-zero eigenvalue of $\mathbf{H}_{\mathrm{CMT}}\mathbf{H}_{\mathrm{CMT}}^{\dagger}$ and $m = \min(n_R, n_T)$. Using (5.1) we can write (5.4) as

$$E(\mathcal{I}) = E\left[m \log_2\left(1 + \frac{\rho}{n_T}\frac{(r-1)\lambda}{S^2}\right)\right] \tag{5.5}$$

where λ is an arbitrary non-zero eigenvalue of the usual Wishart matrix $\mathbf{H}\mathbf{H}^{\dagger}$. The expectation in (5.5) is over both λ and S^2. Note that the effect of the CMT model is to leave the form of solution for an i.i.d. Rayleigh fading MIMO channel unchanged, but to replace the fixed SNR, ρ by a variable SNR, $\frac{\rho(r-1)}{S^2}$. This formulation allows us to derive the ergodic MI exactly as shown below.

$$\begin{aligned} E(\mathcal{I}) &= E\left[m \log_2\left(1 + \delta\frac{\lambda}{S^2}\right)\right] \\ &= \frac{m}{\log 2}\int_0^{\infty} \log(1 + \delta\, x)\, f_X(x)\, dx \end{aligned} \tag{5.6}$$

where δ is defined as $\frac{\rho(r-1)}{n_T}$ and $X = \frac{\lambda}{S^2}$ has density $f_X(x)$. We derive the density of X below.

Consider the pair of transformations $X = \frac{\lambda}{S^2}$, $Y = S^2$. Standard transformation theory gives:

$$f_{X,Y}(x, y) = f_{\lambda,S^2}(xy, y)\,|J| \tag{5.7}$$

where $J = \det\begin{bmatrix} y & x \\ 0 & 1 \end{bmatrix}$. Hence

$$\begin{aligned} f_{X,Y}(x,y) &= f_{\lambda}(xy)\, f_{S^2}(y)\, y \\ &= \sum_{j=n-m}^{n+m-2} \frac{c_j}{\Gamma(r)} x^j y^{r+j} e^{-(1+x)y}\, dy \end{aligned} \tag{5.8}$$

where we have used the pdf for λ given in [93] and $n = \max(n_R, n_T)$. Hence, $f_X(x)$ is evaluated as

$$\begin{aligned} f_X(x) &= \sum_{j=n-m}^{m+n-2} \left(\frac{c_j}{\Gamma(r)} x^j \right) \int_0^{\infty} y^{r+j} e^{-(1+x)y}\, dy \\ &= \sum_{j=n-m}^{n+m-2} \frac{c_j x^j}{\Gamma(r)} \frac{\Gamma(r+j+1)}{(1+x)^{r+j+1}} \end{aligned} \tag{5.9}$$

Substituting (5.9) in (5.6), $E(\mathcal{I})$ is written as

$$E(\mathcal{I}) = \frac{m}{\log 2} \sum_{j=n-m}^{n+m-2} \frac{c_j \Gamma(r+j+1)}{\Gamma(r)} \int_0^{\infty} \frac{\log(1+\delta\, x)\, x^j}{(1+x)^{r+j+1}}\, dx \tag{5.10}$$

where c_j is defined as [93]

$$c_j = \frac{1}{m} \sum_{l=\lceil \frac{i}{2} \rceil}^{m-1} \sum_{k=l}^{m-1} \frac{(-1)^{j+m-n} (2l)! \binom{2k-2l}{k-l} \binom{2n-2m+2l}{2l-j-m+n}}{2^{2k-j-m+n} l!(j+m-n)!(n-m+l)!} \tag{5.11}$$

and $i = j + m - n$ with $\lceil \rceil$ representing the ceiling function.

After evaluating the integral in (5.10), a closed-form expression for the MI of the CMT channel is derived as

$$\begin{aligned} E(\mathcal{I}) &= \frac{m}{\Gamma(r) \log 2} \sum_{j=n-m}^{n+m-2} c_j \Gamma(r+j+1) \times \\ &\quad \sum_{i=0}^{j} \binom{j}{i} (-1)^{j-i} \frac{1}{(r+j-i)^2} \times \\ &\quad {}_2F_1\left(1, r+j-i, r+j-i+1, -\frac{1}{\theta}\right) \end{aligned} \tag{5.12}$$

where θ is given by $\theta = \frac{\delta}{1-\delta}$ and ${}_2F_1$ is a Gauss hypergeometric function [94]. The

function ${}_2F_1$ is defined as

$$ {}_2F_1(a,b,c,z) = \sum_{j=0}^{\infty} \frac{(a)_j (b)_j z^j}{(c)_j j!}, \quad c \neq 0, -1, -2, \ldots \tag{5.13} $$

where $(a)_j$ is Pochhammer's symbol, which denotes the ascending factorial $a(a+1)(a+2)\ldots(a+j-1)$. Note that an ascending factorial can be represented as the ratio of two gamma functions, $(a)_j = \frac{\Gamma(a+j)}{\Gamma(a)}$. The series converges for $|z| < 1$ and diverges for $|z| > 1$; if $|z| = 1$, the series converges for $c - a - b > 0$.

In addition, when r is an integer, (5.12) can be further simplified since ${}_2F_1$ can be written in closed form [95], that is

$$ \begin{aligned} E(\mathcal{I}) &= \frac{m}{\Gamma(r)\log 2} \sum_{j=n-m}^{n+m-2} c_j \Gamma(r+j+1) \times \\ &\quad \sum_{i=0}^{j} \binom{j}{i} (-1)^{j-i} \frac{\theta}{r+j-i} \times \\ &\quad \left[(-1)^{r+j-i} \theta^{r+j-i-1} \log(\gamma) - \sum_{k=1}^{j+r-i-1} \frac{(-1)^k \theta^{k-1}}{r+j-i-k} \right] \end{aligned} \tag{5.14} $$

5.2.1 Mutual Information Results

In Figures 5.2–5.5, the ergodic MI is computed via (5.12) for (2,2), (3,3), (2,4) and (4,2) MIMO systems in a CMT channel with $r = 2$, 3, 40 and a range of SNR values. The analytical results are verified by simulation. The lines represent analytical results and the circles denote simulations. Larger differences are observed as the SNR increases and at SNR = 20 dB there is about a 13% drop in ergodic MI as r decreases from 40 (virtually a Rayleigh channel) to 2. In Figure 5.1, we show the effect that the CMT channel converges to a Rayleigh channel as $r \to \infty$. Here, for $r = 40$ the CMT results match the Rayleigh case almost perfectly. Figure 5.6 focuses on a (2,2) system with SNR=10 dB. The ergodic MI is shown to increase with r, i.e., as the CMT channel

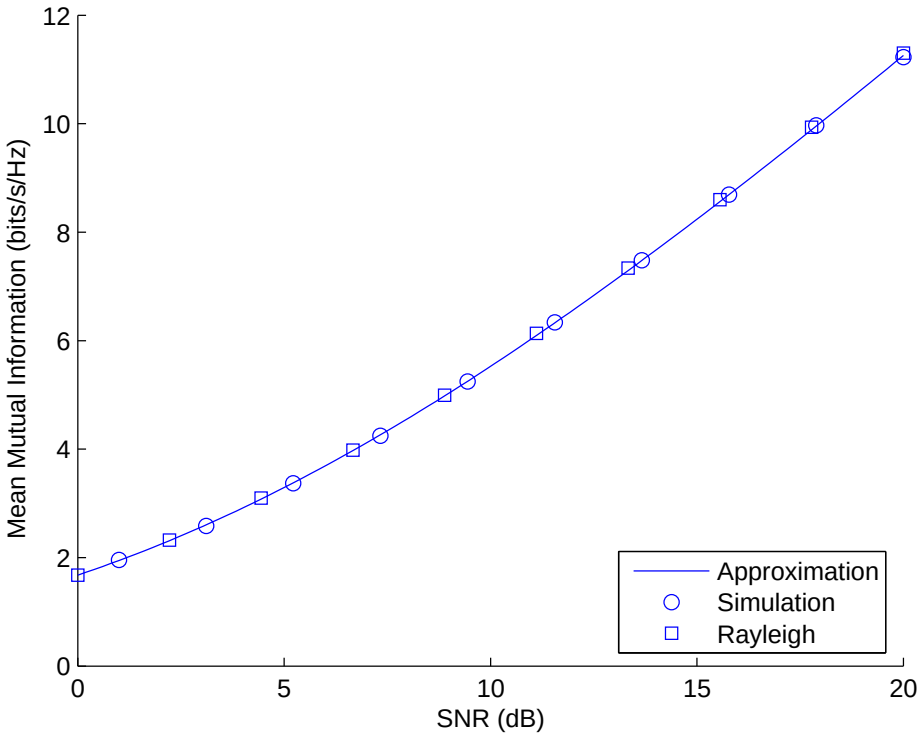

Figure 5.1 Ergodic MI vs SNR for a (2,2) MIMO system with the CMT and Rayleigh channel when $r = 40$

approaches a Rayleigh channel, which matches the results in Figures 4.1–4.15. Clearly, the severely fading channel needs to have a parameter, $r < 10$, before any noticeable effects occur. In Figure 5.7, the results of Figure 5.6 are presented again, but this time the x-axis is converted to measure the CV of the amplitude distribution rather than the severe fading parameter, r. This shows clearly the negative effect on ergodic MI of increasing the CV value for the CMT model.

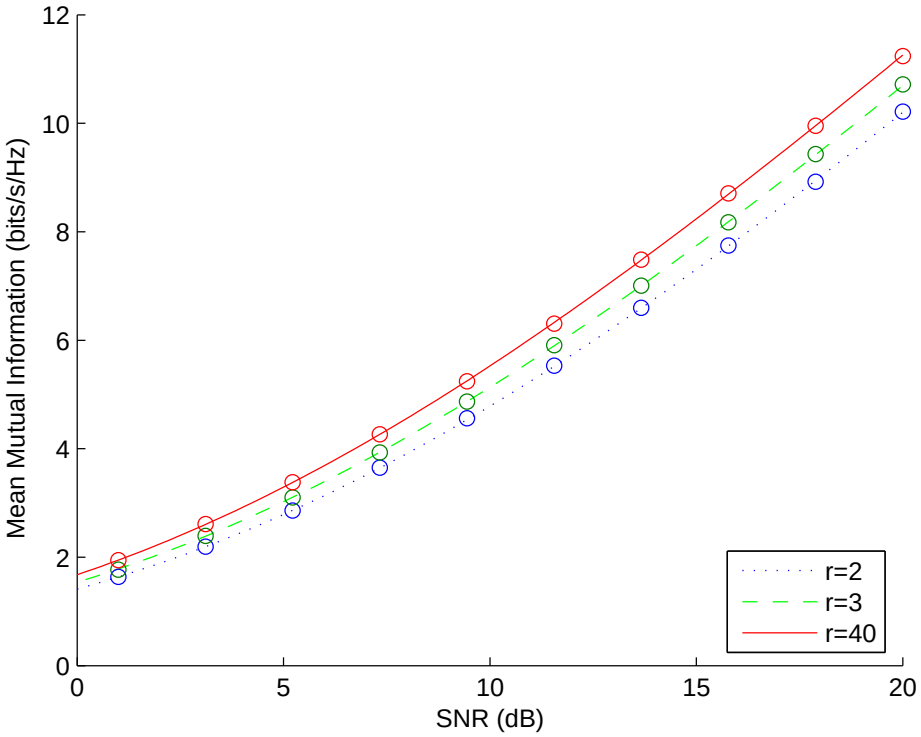

Figure 5.2 Ergodic MI vs SNR for a (2,2) MIMO system with the CMT channel and $r = 2, 3, 40$

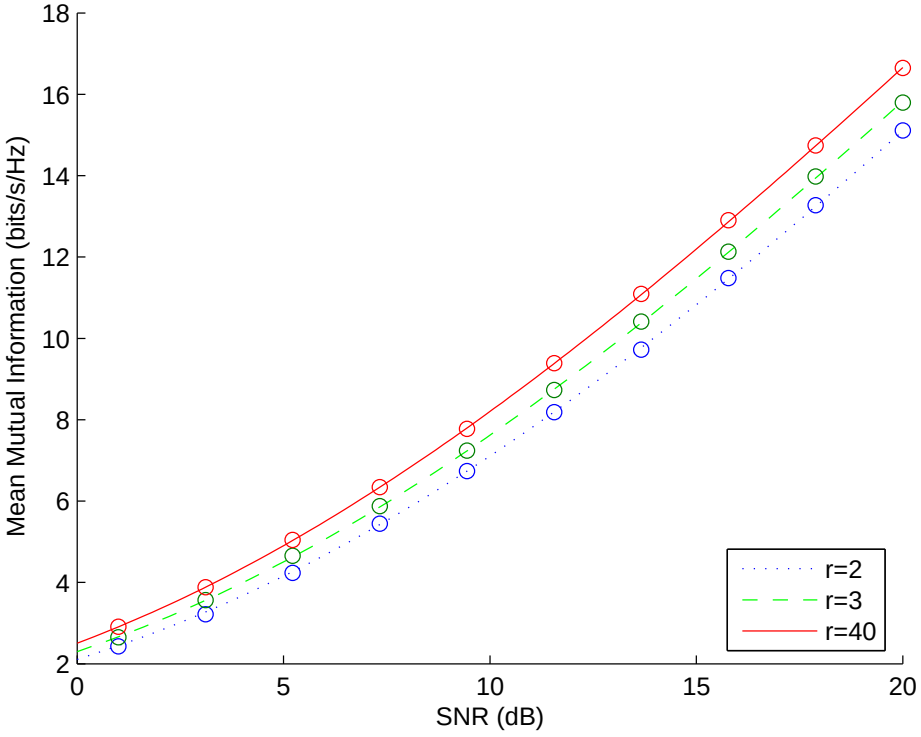

Figure 5.3 Ergodic MI vs SNR for a (3,3) MIMO system with the CMT channel and $r = 2, 3, 40$

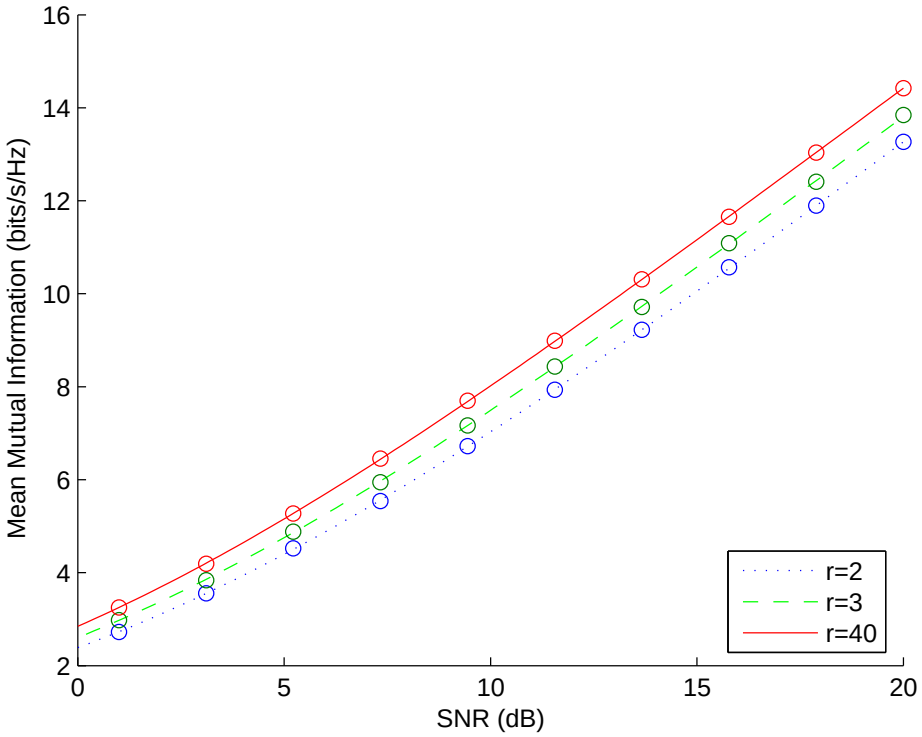

Figure 5.4 Ergodic MI vs SNR for a (2,4) MIMO system with the CMT channel and $r = 2, 3, 40$

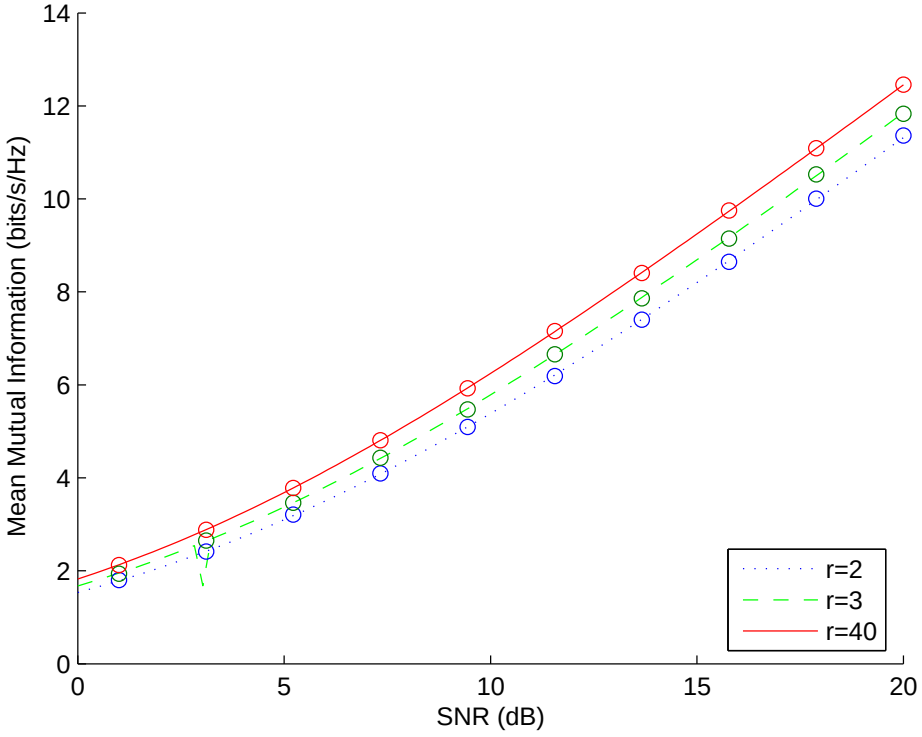

Figure 5.5 Ergodic MI vs SNR for a (4,2) MIMO system with the CMT channel and $r = 2, 3, 40$

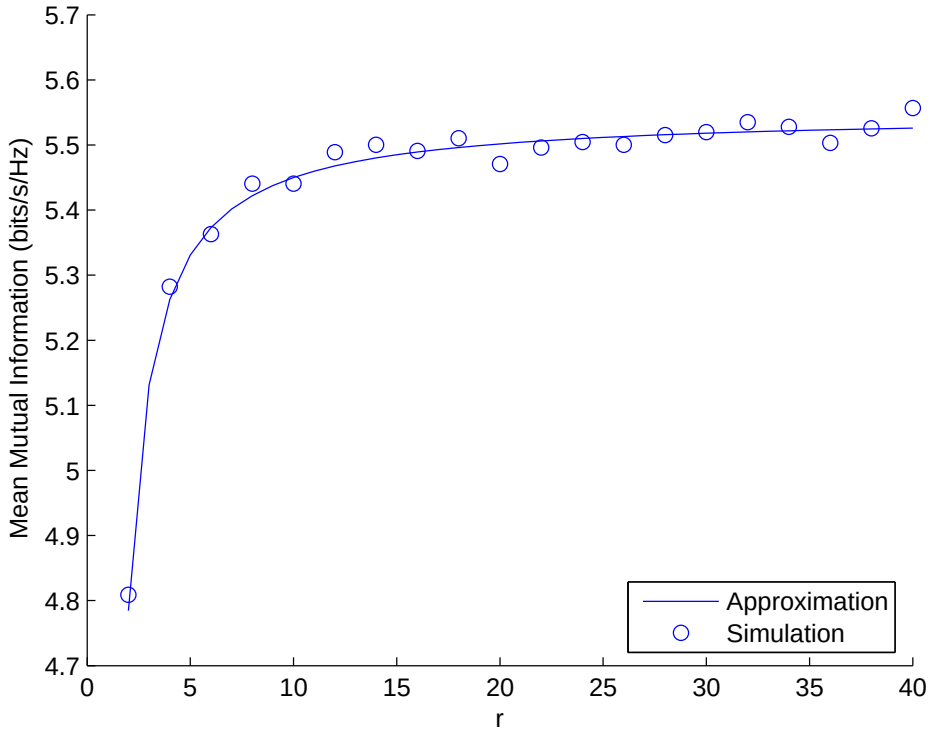

Figure 5.6 Ergodic MI vs r for a (2,2) MIMO system with the CMT channel and SNR = 10dB

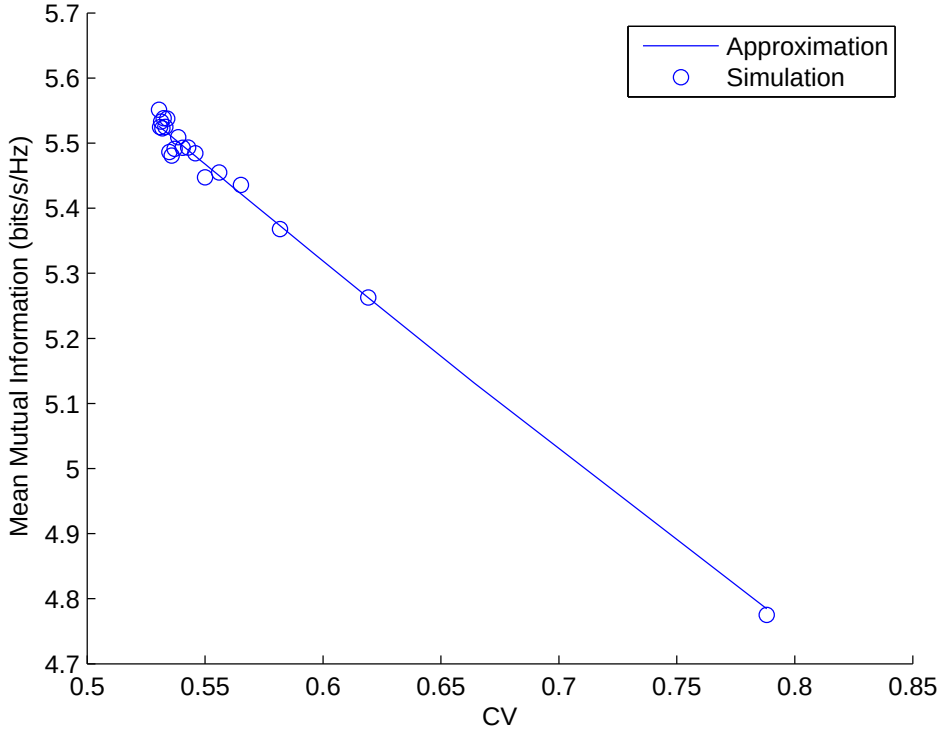

Figure 5.7 Ergodic MI vs CV for a (2,2) MIMO system with the CMT

5.3 MUTUAL INFORMATION OUTAGE OF CMT

For a fixed value of S^2, the MI is known to be well-approximated by a Gaussian random variable [64, 96]. Hence, we can approximate the MI outage of the CMT model by

$$P(\mathcal{I} < x) = \int_0^\infty \Phi\left(\frac{x - \mu_{\mathcal{I}}(y)}{\sigma_{\mathcal{I}}(y)}\right) f_{S^2}(y)dy \tag{5.15}$$

where $\mu_{\mathcal{I}}(y)$ and $\sigma_{\mathcal{I}}(y)$ are the mean and standard deviation of the MI respectively, for a fixed SNR denoted $P = \frac{\rho(r-1)}{y}$. In (5.15), the function Φ is the cumulative distribution function of the standard Gaussian distribution. It is possible to use the exact mean and variance results for $\mathcal{I}$ found in [18,96], but for simplicity we prefer to use the more compact asymptotic results [93,97], obtained for the case where $n_T \to \infty$ and $\frac{n_T}{n_R} \to \beta$. The variance result is

$$\sigma^2_{\mathcal{I}}(y) = -\log\left(1 - \frac{(1-\eta)^2}{\beta}\right) \tag{5.16}$$

where $\beta = \frac{n_T}{n_R}$, $\eta = 1 - \frac{F(\gamma,\beta)}{4\gamma}$, $\gamma = \frac{Pn_R}{n_T}$ and

$$F(\gamma,\beta) = \left[\sqrt{\gamma(1+\sqrt{\beta})^2+1} - \sqrt{\gamma(1-\sqrt{\beta})^2+1}\right]^2$$

The result for the mean is $\mu_{\mathcal{I}}(y) = mv$ where

$$v = \beta\log\left(1+\gamma-\frac{F(\gamma,\beta))}{4}\right) + \log\left(1+\gamma\beta-\frac{F(\gamma,\beta)}{4}\right) - \frac{\log_e}{4\gamma}F(\gamma,\beta) \tag{5.17}$$

5.3.1 MI Outage Results

In Figure 5.8, the cumulative distribution function (cdf) of the MI is computed via (5.15) for a (4,4) MIMO system in a CMT channel with $r = 2$ and SNR = 0, 10, 20 dB. The analytical approximation is shown by simulation to be very accurate for all SNR values. Similarly, at SNR = 0 dB, Figure 5.9 plots the cdfs of the MI for (2,2), (4,4), (6,6) and (8,8) systems in the CMT channel with $r = 2$. Figures 5.2– 5.9 demonstrate that the

CMT channel leads to compact, closed-form expressions for both the ergodic MI and outage probabilities. In addition, the CMT channel has a CV in the desired region, $\mathrm{CV}_{\mathrm{Rayleigh}} < \mathrm{CV}_{\mathrm{CMT}} < \infty$. Furthermore, as discussed in Chapter 6, the CMT model can lead to a range of analytical results, including performance analysis, in addition to the work on MI described in Chapter 5.

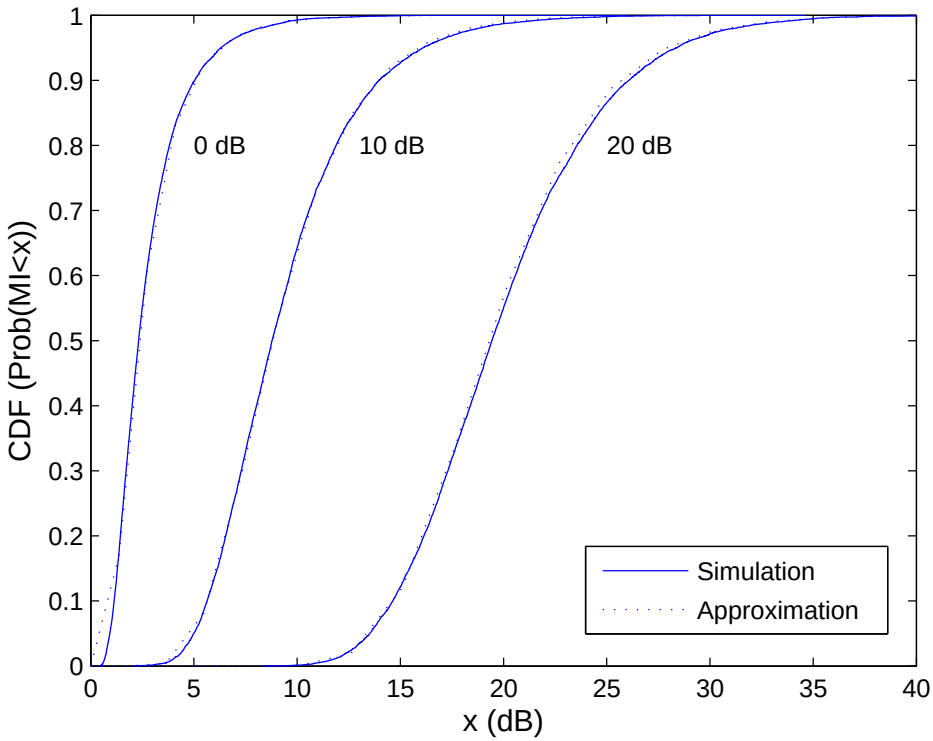

Figure 5.8 CDF of the MI for a (4,4) MIMO system in a CMT channel with $r = 2$ and SNR = 0, 10, 20dB

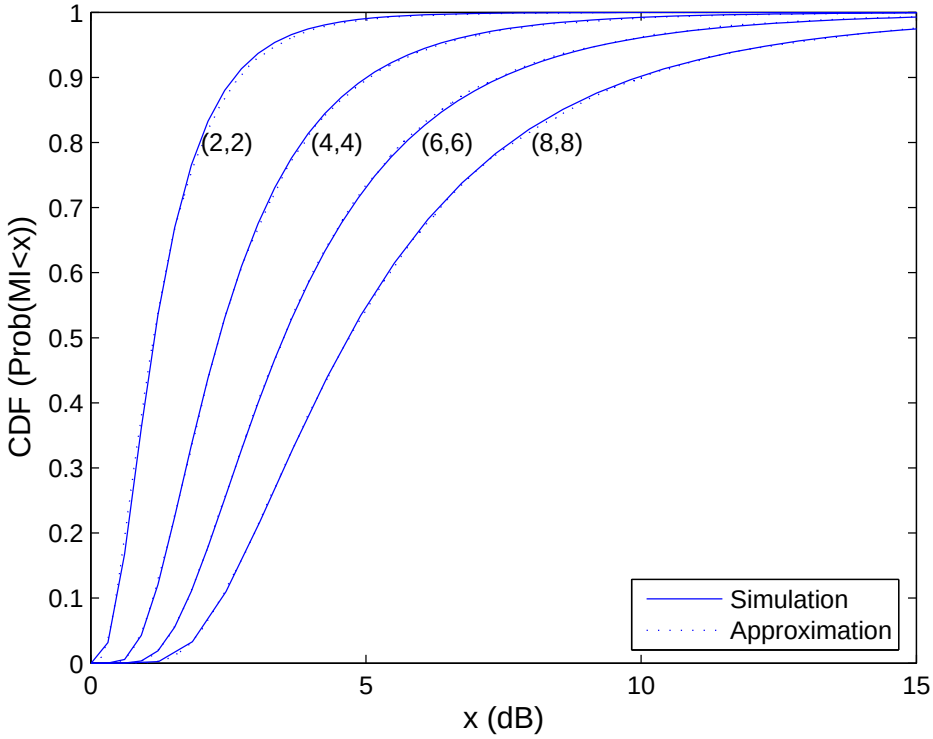

Figure 5.9 CDF of the MI for (2,2), (4,4) and (6,6) MIMO systems in a CMT channel with $r = 2$ and SNR = 0dB

Chapter 6

APPLICATIONS TO CELLULAR MIMO SYSTEMS

The applications to cellular MIMO systems have already been introduced in Section 3.4. In this chapter, the CMT model is applied to cellular MIMO systems and is extended to evaluate the mutual information and performance in Section 6.1 and 6.2, respectively. Note that the cellular MIMO scenario considered in this chapter is investigated in [32].

6.1 MUTUAL INFORMATION

The approach taken in Chapter 5 is to average the well-known results for an i.i.d. Rayleigh fading channel over a variable SNR. This is exactly the scenario considered in [32] where a cellular MIMO system is investigated and the system equation is written as

$$\mathbf{r} = \sqrt{\Gamma}\,\mathbf{H}\,\mathbf{s} + \mathbf{n} \tag{6.1}$$

In (6.1), $\mathbf{r}$, $\mathbf{H}$, $\mathbf{s}$ and $\mathbf{n}$ are defined in Section 2.2 and Γ is the SINR resulting from noise and inter-cellular interference. Note the equivalence to the system equation for a CMT channel which can be written

$$\begin{aligned} \mathbf{r} &= \mathbf{H}_{\mathrm{CMT}}\,\mathbf{s} + \mathbf{n} \\ &= \sqrt{\frac{S^2}{r-1}}\,\mathbf{H}\,\mathbf{s} + \mathbf{n} \end{aligned} \tag{6.2}$$

The distribution of Γ was simulated in [32] for various cellular scenarios, including the effects of lognormal shadowing, distance attenuation, cell size, frequency reuse, sectorization and random user locations. We consider a system consisting of 19 hexagonal cells shown in Figure 3.1. Each of the cells employs either 3, 6 or 12 sectors as shown in Figure 3.2. The scenarios considered in [32] are primarily defined by the number of sectors per cell and the frequency reuse. We consider 3, 6, or 12 sectors per cell, denoted S3, S6 and S12 and a reuse factor of 1 and 1/3, denoted F1 and F3 respectively. With F1, the same frequency is used in all sectors, whereas under F3, each cell users 3 disjoint frequency bands. Full details of the other parameters used, such as cell size, path loss exponent, etc., can be found in [32]. The 6 cellular scenarios considered can be abbreviated by S3F1, S3F3, S6F1, S6F3, S12F1 and S12F3.

For each of the 6 scenarios, we have replicated the results in [32] and have found that the distribution of Γ is well approximated by the scaling variable in the CMT model, namely a variable of the form, $\frac{\rho(r-1)}{S^2}$, a scaled inverse χ^2 variable. For increased accuracy in fitting we allow the variable S^2 to have fractional degrees of freedom. Using the method of moments, the first two moments of the χ^2 variables are chosen to match the first two moments of 1/SINR. Hence, we are able to quantify the behaviour of cellular MIMO systems in terms of ergodic MI and MI outage by a direct application of the results in Chapter 5.

6.1.1 MI Results

Sample results are given in Figure 6.1, which shows the ergodic MI for the 6 scenarios as computed via (5.12) and also from the cellular simulations. Stars represent the cellular simulations and circles denote the CMT approximation. Clearly, the analytical results are very accurate in all cases. Similarly, Figures 6.2 and 6.3 shows the cdf of the SINR

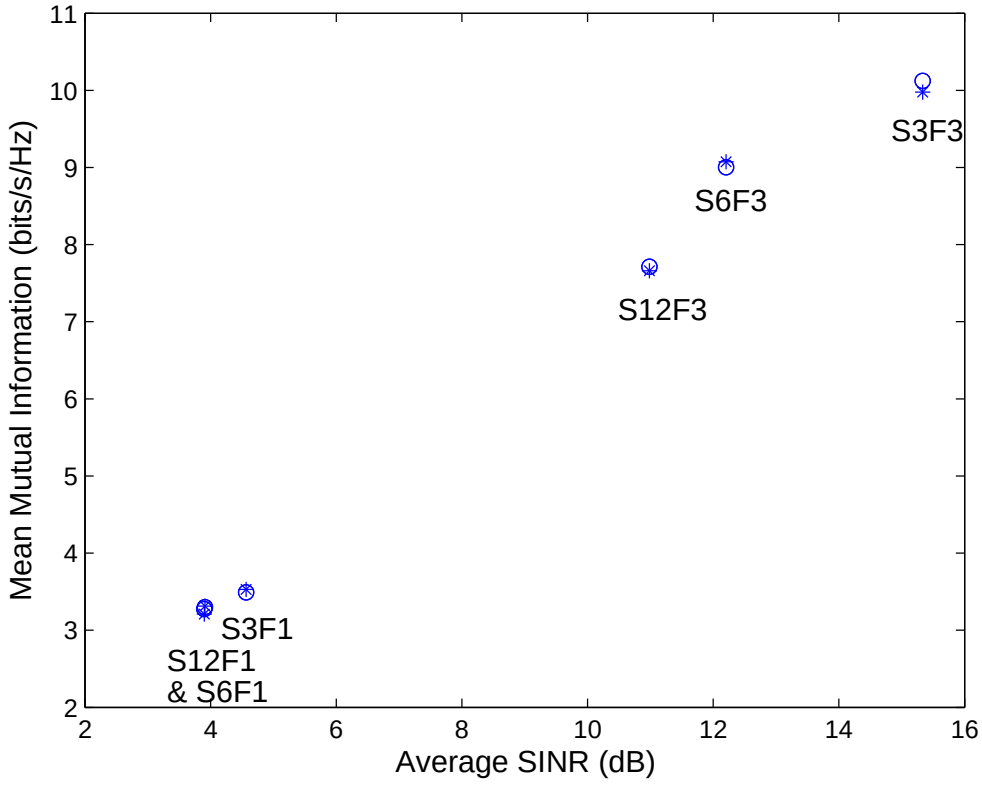

Figure 6.1 Ergodic MI vs average SINR for a (2,2) MIMO system and 6 cellular scenarios

for the 6 scenarios, using simulated cellular data and the approximate CMT model. It is observed that the CMT curves are reasonably good approximations to the cellular results. The CMT cdfs for the F1 case are more accurate than the cdfs for the F3 case.

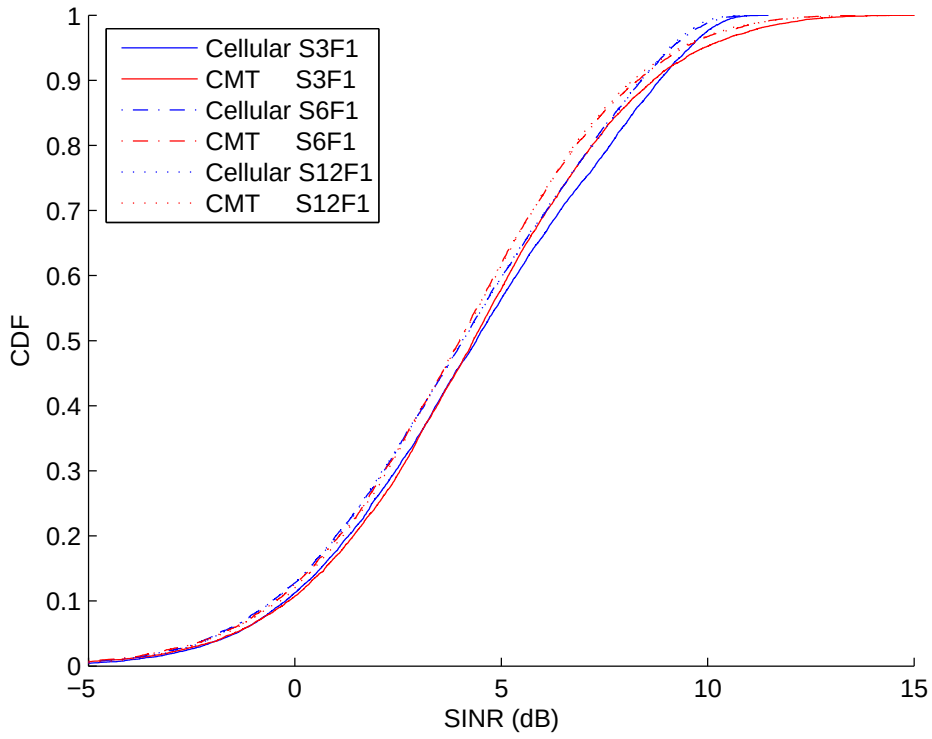

Figure 6.2 CDFs of the SINR for the S3F1, S6F1 and S12F1 cellular scenarios

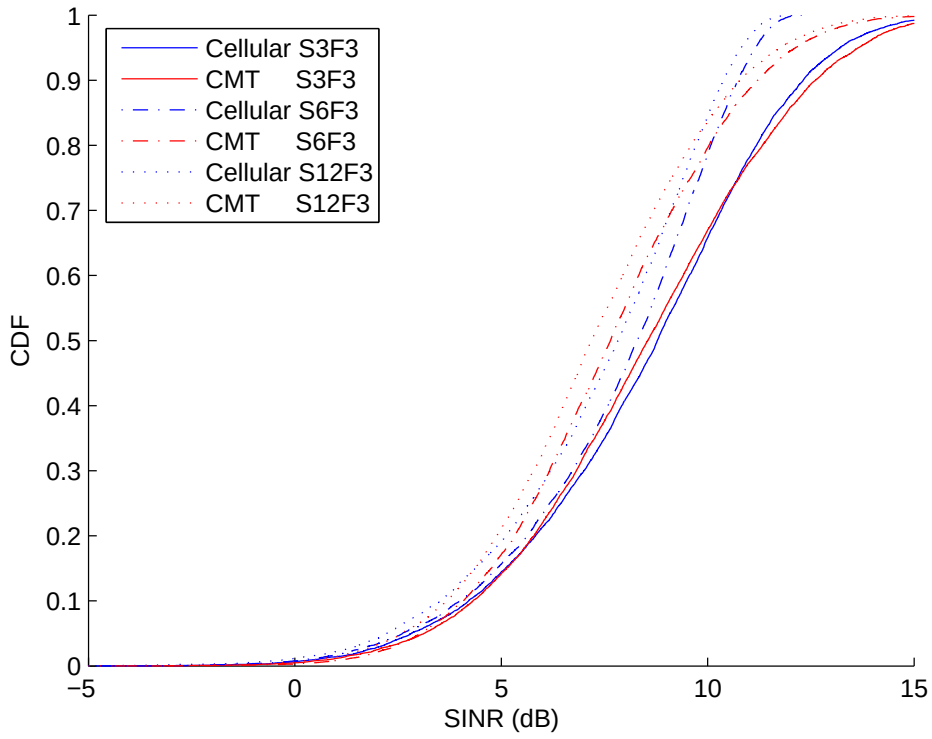

Figure 6.3 CDFs of the SINR for the S3F3, S6F3 and S12F3 cellular scenarios

6.2 SYSTEM PERFORMANCE

The CMT model can be considered as a classic Rayleigh fading channel with variable SNR. This makes a wide range of results available. For example, consider a MIMO receiver with outage probability $P_{\text{out}}(\text{SNR})$ and bit error rate, $P_{\text{e}}(\text{SNR})$ in an i.i.d. Rayleigh channel. Both metrics are functions of the SNR and we obtain the corresponding results for the CMT channel by averaging the classical results over the inverse χ^2 scaling variable. Hence, we have:

$$P_{\text{out,CMT}}(\text{SNR}) = E\left(P_{\text{out}}(\text{SNR})\right) \tag{6.3}$$

and

$$P_{\text{e,CMT}}(\text{SNR}) = E\left(P_{\text{e}}(\text{SNR})\right) \tag{6.4}$$

where $\text{SNR} = \frac{\rho(r-1)}{S^2}$, and the expectation is over the variable S^2.

6.2.1 Zero Forcing

In this section, we compare the outage probabilities for ZF receivers in both Rayleigh and SFCs. Firstly, consider an i.i.d. Rayleigh fading channel matrix, $\mathbf{H}$. With the ZF receiver assuming $n_R \geq n_T$, the signal estimate $\hat{\mathbf{s}}$ is defined in (2.25) and the SNR of the ZF receiver is given by

$$\text{SNR} = \frac{E|s_i|^2}{E|\tilde{n}_i|^2} \tag{6.5}$$

where $E|s_i|^2$ is the signal power and $E|\tilde{n}_i|^2 = \sigma_n^2$ is the noise power after receiver combining.

The covariance matrix of $\tilde{\mathbf{n}}$ is

$$\begin{aligned} E(\tilde{\mathbf{n}}\tilde{\mathbf{n}}^\dagger) &= E\left[(\mathbf{H}^\dagger\mathbf{H})^{-1}\mathbf{H}^\dagger\mathbf{n}\mathbf{n}^\dagger\mathbf{H}(\mathbf{H}^\dagger\mathbf{H})^{-1}\right] \\ &= \sigma_n^2(\mathbf{H}^\dagger\mathbf{H})^{-1} \end{aligned} \tag{6.6}$$

Hence,

$$E|\tilde{n}_i|^2 = \sigma_n^2\left[(\mathbf{H}^\dagger\mathbf{H})^{-1}\right]_{i,i} \tag{6.7}$$

Therefore,

$$\text{SNR} = \frac{E|s_i|^2}{\sigma_n^2\left[(\mathbf{H}^\dagger\mathbf{H})^{-1}\right]_{i,i}} \tag{6.8}$$

For the severely fading CMT channel in (5.1), the channel matrix $\mathbf{H}$ is replaced by $\mathbf{H}_{\text{CMT}}$ and we have

$$\begin{aligned} \tilde{\mathbf{r}} &= (\mathbf{H}_{\text{CMT}}^\dagger\mathbf{H}_{\text{CMT}})^{-1}\mathbf{H}_{\text{CMT}}^\dagger\,\mathbf{r} \\ &= \mathbf{s} + (\mathbf{H}_{\text{CMT}}^\dagger\mathbf{H}_{\text{CMT}})^{-1}\mathbf{H}_{\text{CMT}}^\dagger\,\mathbf{n} \\ &= \mathbf{s} + \tilde{\mathbf{n}} \end{aligned} \tag{6.9}$$

The covariance matrix of $\tilde{\mathbf{n}}$ now becomes

$$E(\tilde{\mathbf{n}}\tilde{\mathbf{n}}^\dagger) = \sigma_n^2(\mathbf{H}_{\text{CMT}}^\dagger\mathbf{H}_{\text{CMT}})^{-1} \tag{6.10}$$

and

$$E|\tilde{n}_i|^2 = \sigma_n^2\left[(\mathbf{H}_{\text{CMT}}^\dagger\mathbf{H}_{\text{CMT}})^{-1}\right]_{i,i} \tag{6.11}$$

We note that the CMT channel matrix $\mathbf{H}_{\text{CMT}}$ can be written in terms of the Rayleigh channel matrix as below.

$$\mathbf{H}_{\text{CMT}} = \frac{\mathbf{H}}{\sqrt{\frac{S^2}{r-1}}} \tag{6.12}$$

Hence, the SNR values can be written

$$\text{SNR}_{\text{Rayleigh}} = \frac{E|s_i|^2}{\sigma_n^2 \left[(\mathbf{H}^\dagger \mathbf{H})^{-1}\right]_{i,i}} \tag{6.13}$$

$$\text{SNR}_{\text{CMT}} = \frac{E|s_i|^2}{\sigma_n^2 \left[(\mathbf{H}^\dagger \mathbf{H})^{-1}\right]_{i,i}} \frac{(r-1)}{S^2} \tag{6.14}$$

From [91], we have the following distributional result for the diagonal entries of the inverse Wishart matrix:

$$\frac{2}{\left[(\mathbf{H}^\dagger \mathbf{H})^{-1}\right]_{i,i}} \sim \chi^2_{2r} \tag{6.15}$$

The scaling variable in the CMT model also has a χ^2 distribution:

$$2S^2 \sim \chi^2_{2r} \tag{6.16}$$

Note that these are standard χ^2 distributions, not the complex versions. Using (6.15) and (6.16), we can write

$$\text{SNR}_{\text{Rayleigh}} = \frac{E|s_i|^2}{\sigma_n^2} \times \frac{\chi^2_{2(n_R - n_T + 1)}}{2} \tag{6.17}$$

$$\text{SNR}_{\text{CMT}} = \frac{E|s_i|^2}{\sigma_n^2} \times \frac{(r-1)\chi^2_{2(n_R - n_T + 1)}}{\chi^2_{2r}} \tag{6.18}$$

Now we consider the outage probabilities given by the SNR cdfs

$$P(\text{SNR}_{\text{Rayleigh}} < x) = P\left(\chi^2_{2(n_R - n_T + 1)} < \frac{2\sigma_n^2 x}{E|s_i|^2}\right) \tag{6.19}$$

$$P(\text{SNR}_{\text{CMT}} < x) = P\left(\frac{\chi^2_{2(n_R - n_T + 1)}}{\chi^2_{2r}} < \frac{\sigma_n^2 x}{(r-1)E|s_i|^2}\right) \tag{6.20}$$

The probability in (6.19) is simply the cdf a χ^2 variable [98] and is given by

$$P(\text{SNR}_{\text{Rayleigh}} < x) = \frac{\gamma(v/2, x/2)}{\Gamma(v/2)} \tag{6.21}$$

where $v = 2(n_R - n_T + 1)$ and $\gamma(r, x)$ is the incomplete gamma function [99].

To compute the outage probability in the CMT case we note that $\frac{\chi^2_{v_1}/v_1}{\chi^2_{v_2}/v_2}$ is an F_{v_1,v_2} variable. Hence, the cdf for CMT case can be written

$$P(\mathrm{SNR}_{\mathrm{CMT}} < x) = P\left(F_{2(n_R-n_T+1),2r} < \frac{rx\sigma_n^2}{(r-1)E|s_i|^2 2(n_R-n_T+1)}\right) \tag{6.22}$$

The cdf of the F variable [98] can be written in terms of the incomplete beta function giving

$$P(\mathrm{SNR}_{\mathrm{CMT}} < x) = I_{\frac{v_1 x}{v_1 x+v_2}}\left(\frac{v_1}{2}, \frac{v_2}{2}\right) \tag{6.23}$$

where $v_1 = 2(n_R - n_T + 1)$, $v_2 = 2r$ and $I(\cdot,\cdot)$ is the incomplete beta function [99].

For the most interesting special case when $n_R = n_T$, define $\frac{E|s_i|^2}{\sigma_n^2} = \rho_0$ and the results are particularly simple.

$$\begin{aligned} P(\mathrm{SNR}_{\mathrm{Rayleigh}} < x) &= P\left(\chi^2_2 < \frac{2x\sigma_n^2}{E|s_i|^2}\right) \\ &= P\left(\chi^2_2 < \frac{2x}{\rho_0}\right) \\ &= 1 - \exp(-\frac{x}{\rho_0}) \end{aligned} \tag{6.24}$$

$$\begin{aligned} P(\mathrm{SNR}_{\mathrm{CMT}} < x) &= P\left(F_{2,2r} < \frac{rx\sigma_n^2}{(r-1)E|s_i|^2}\right) \\ &= P\left(F_{2,2r} < \frac{rx}{(r-1)\rho_0}\right) \\ &= 1 - \frac{1}{\left(1+\frac{x}{(r-1)\rho_0}\right)^r} \end{aligned} \tag{6.25}$$

ZF Results

In Figure 6.4, we plot the outage probability as a function of SNR for a ZF receiver in a (2,2) MIMO system with the Rayleigh and CMT case when $r = 40$. From the figure, it shows that the CMT results match the Rayleigh case almost perfectly.

Results for a ZF receiver in (2,2), (3,3), (4,4), (8,8), (2,4) and (2,8) MIMO systems for

a ZF receiver are shown in Figures 6.5–6.10, respectively. It is observed that the CMT curves become more closely spaced and approach the Rayleigh case as r increases.

For the special cases when $n_T = n_R$, the outage probability is computed via (6.25) and Figures 6.5–6.8 shows exactly the same results. The reason is that (6.25) does not depend on the system size (n_T, n_R), whereas for non-symmetric systems (6.22) does depend on the system size. Hence, when $n_T = n_R$ the system size has no effect on the outage probability.

A comparison of Figures 6.5, 6.9 and 6.10 has shown that increasing numbers of receive antennas leads to better performance, although the curves are spread out as the number of receiving antenna increases. For example, when SNR = -10 dB, the outage probabilities of the CMT case ($r = 1.1$) and the Rayleigh case ($r = 40$) for a (2,2) system are approximately 10^{-1} and 10^{-2}. However, for a (2,8) system, the outage probability of the CMT case is reduced to 10^{-4}, whereas the outage probability of the Rayleigh case is reduced to 10^{-8}. Hence, the extra receive antennas help the Rayleigh case much more than the CMT case. This difference is very large, being of several orders of magnitude.

6.2.2 Minimum Mean Squared Error

The SINR calculations for MMSE receivers are considerably more complex [100]. However, we can directly use previous results for the MIMO case with interferers by viewing a (n_T, n_R) MIMO system as a SIMO system with n_R receive antennas and $n_T - 1$ equal power interferers. Note that these results are for independent Rayleigh fading channels. From [100], the outage probability for such a system with a fixed SNR is given by

$$P(Z < z) = 1 - R(z) \tag{6.26}$$

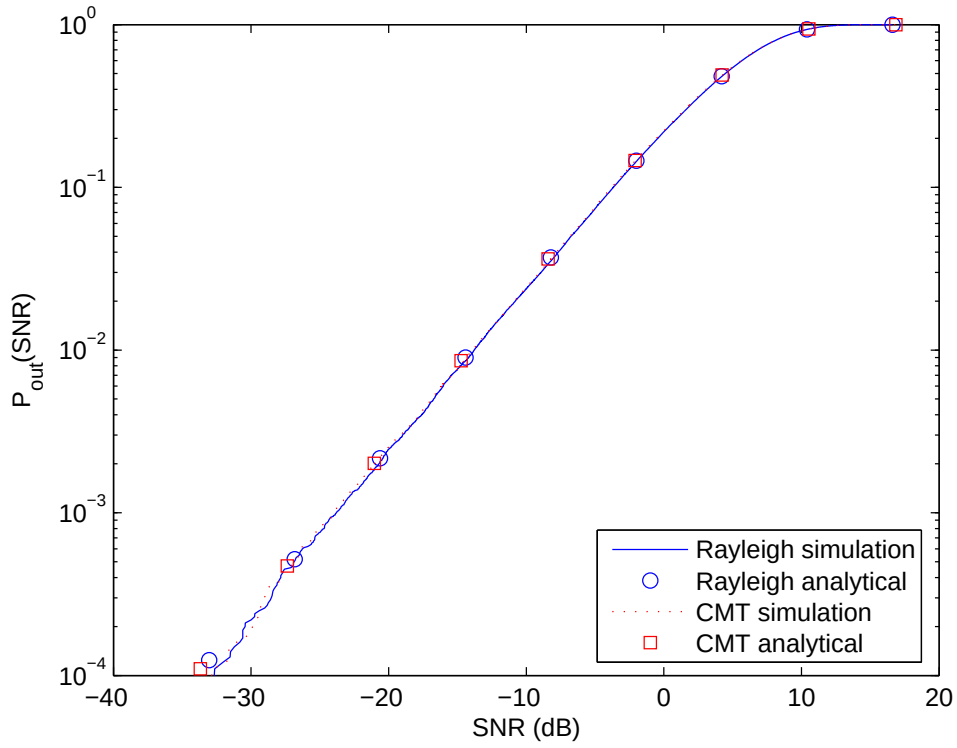

Figure 6.4 Outage probability vs SNR for a ZF receiver in a (2,2) MIMO system with the Rayleigh and CMT models when $r = 40$

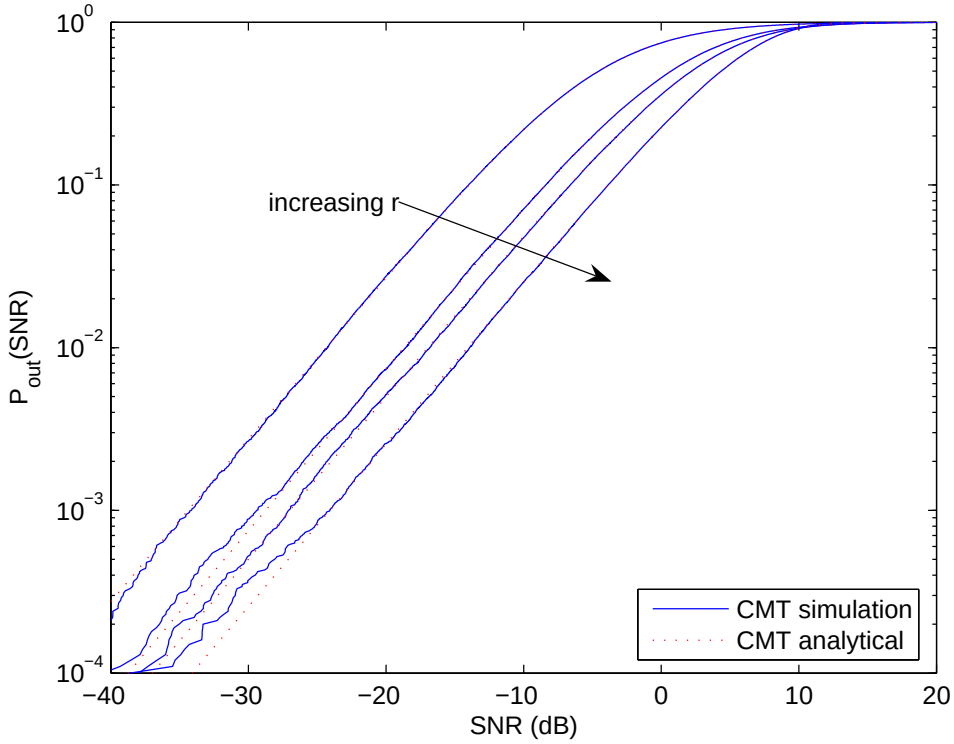

Figure 6.5 Outage probability vs SNR for a ZF receiver in a (2,2) MIMO system when $r = 1.1$, 1.5, 2, 40

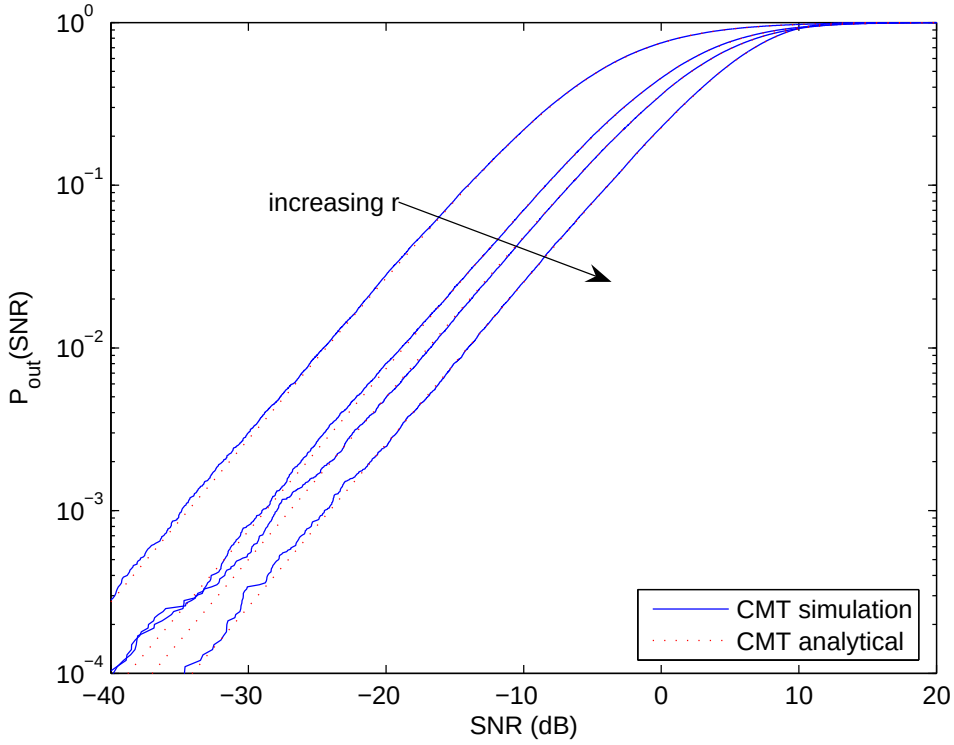

Figure 6.6 Outage probability vs SNR for a ZF receiver in a (3,3) MIMO system when $r = 1.1$, 1.5, 2, 40

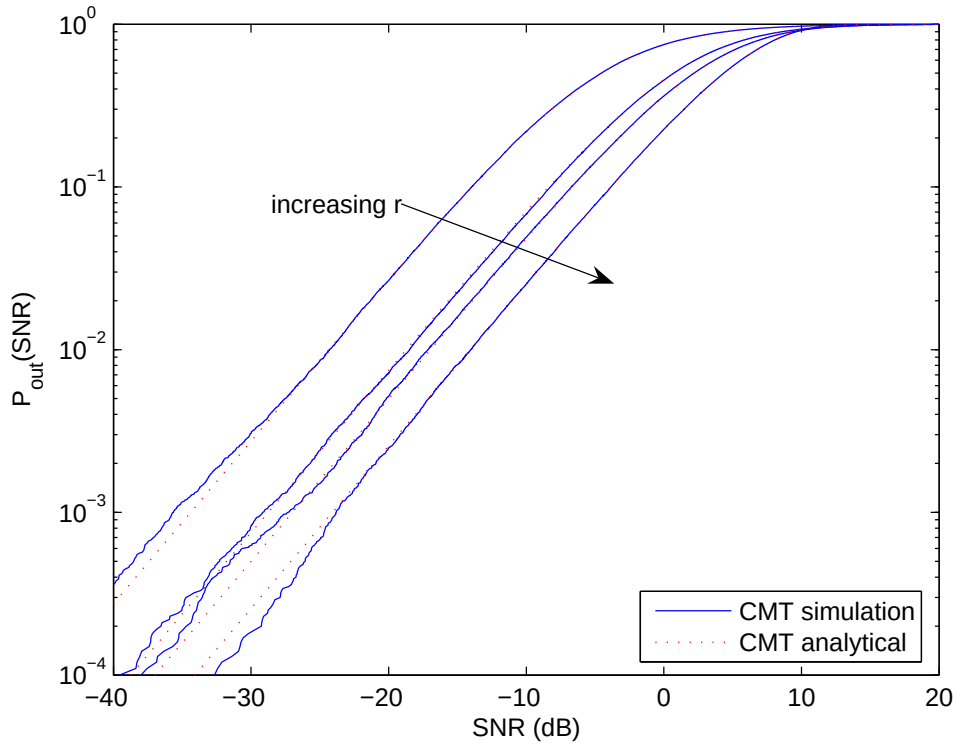

Figure 6.7 Outage probability vs SNR for a ZF receiver in a (4,4) MIMO system when $r = 1.1$, 1.5, 2, 40

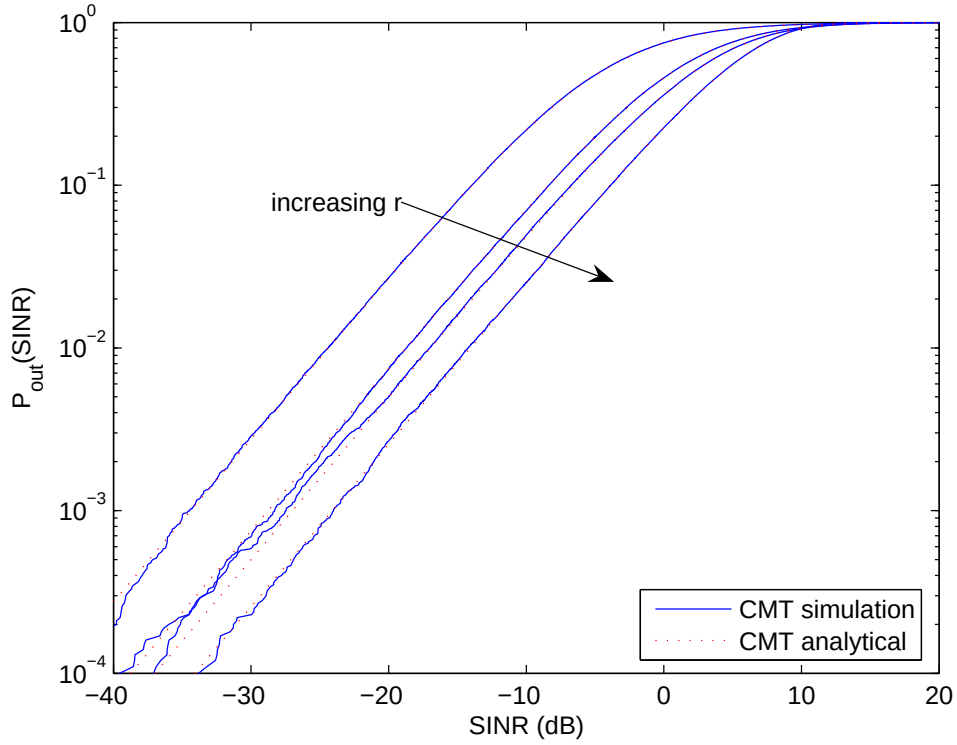

Figure 6.8 Outage probability vs SNR for a ZF receiver in a (8,8) MIMO system when $r = 1.1$, 1.5, 2, 40

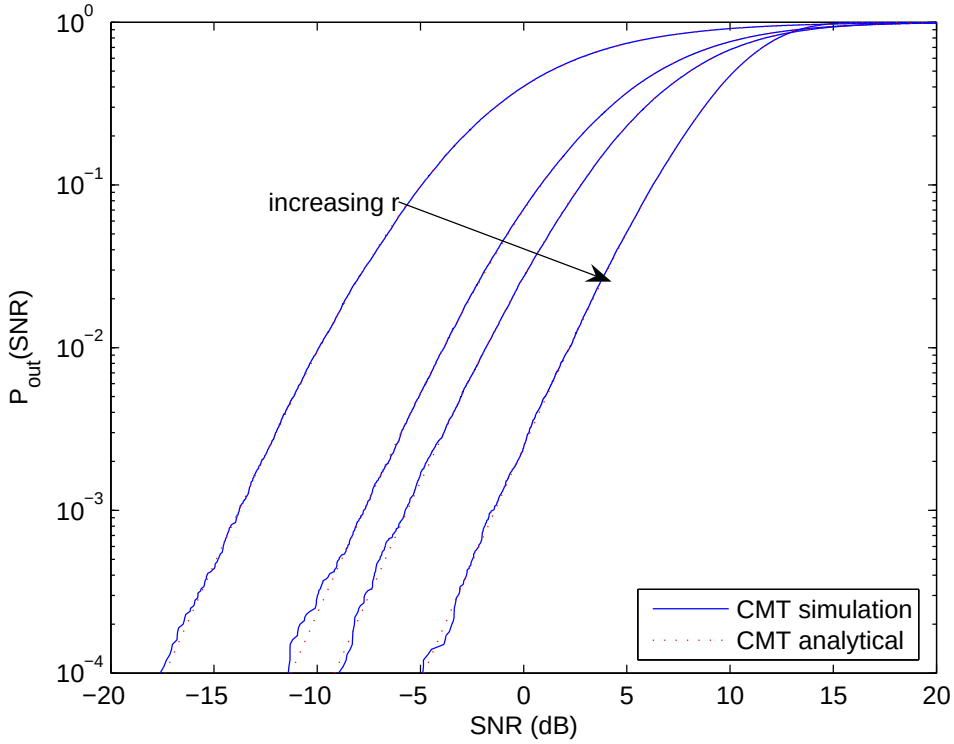

Figure 6.9 Outage probability vs SNR for a ZF receiver in a (2,4) MIMO system when $r = 1.1$, 1.5, 2, 40

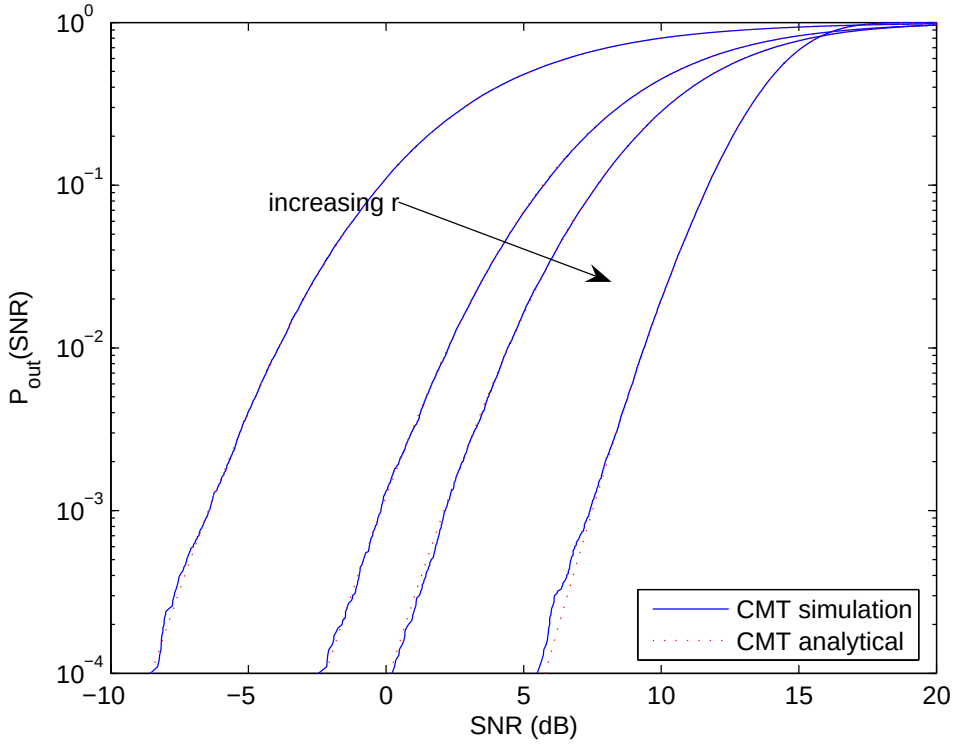

Figure 6.10 Outage probability vs SNR for a ZF receiver in a (2,8) MIMO system when $r = 1.1$, 1.5, 2, 40

where $R(z)$ is the link reliability and is given by

$$R(z) = \exp\left(-\frac{z}{\gamma}\right) \sum_{m=1}^{n_R} \frac{A_m(z)}{(m-1)!} \left(\frac{z}{\gamma}\right)^{n_R-1} \tag{6.27}$$

In (6.27), γ is the average SNR and $A_m(z)$ is given by

$$A_m(z) = \begin{cases} 1, & n_R \geq n_T - 1 + m \\ \frac{1+\sum_{i=1}^{n_R-m} C_i z^i}{\prod_{n=1}^{n_T-1}(1+\Gamma_n z)}, & n_R < n_T - 1 + m \end{cases} \tag{6.28}$$

where Γ_n is the power of the n^{th} interferer. Since all interferers are self-interferers which are normalized to one, we have

$$\Gamma_1 = \Gamma_2 = \ldots = \Gamma_{n_T-1} = 1 \tag{6.29}$$

In (6.28), C_i is the coefficient of z^i in $\prod_{n=1}^{n_T-1}(1+\Gamma_n z)$, and can be derived as follows

$$\prod_{n=1}^{n_T-1}(1+\Gamma_n z) = 1 + \sum_{i=1}^{n_T-1} C_i z^i \tag{6.30}$$

$$(1+z)^{n_T-1} = 1 + \sum_{i=1}^{n_T-1} C_i z^i \tag{6.31}$$

$$\sum_{i=0}^{n_T-1} \binom{n_T-1}{i} z^i = 1 + \sum_{i=1}^{n_T-1} C_i z^i \tag{6.32}$$

$$C_i = \binom{n_T-1}{i} \tag{6.33}$$

Hence, we can rewrite (6.27) as

$$A_m(z) = \begin{cases} 1, & n_R \geq n_T - 1 + m \\ \frac{1+\sum_{i=1}^{n_R-m} \binom{n_T-1}{i} z^i}{(1+z)^{n_T-1}}, & n_R < n_T - 1 + m \end{cases} \tag{6.34}$$

Hence, for a fixed SNR, the outage probability for a MIMO system in a Rayleigh fading channel is given by (6.26), (6.27) and (6.34). For the CMT channel the SNR is random

and we can write

$$P(outage) = \int_0^\infty P(Z < z|\gamma) f(\gamma) d\gamma \tag{6.35}$$

where $\gamma = \frac{\alpha}{S^2}$, $\alpha = \frac{(r-1)}{\sigma_n^2}$ and S^2 has pdf $f_X(x) = \frac{x^{r-1}\exp(-x)}{\Gamma(r)}$. Hence,

$$\begin{aligned} P(outage) &= \int_0^\infty \left(1 - \sum_{m=1}^{n_R} \frac{A_m(z) z^{m-1}}{(m-1)} \left(\frac{1}{\gamma}\right)^{m-1} \exp\left(-\frac{z}{\gamma}\right)\right) f(\gamma) d\gamma \\ &= 1 - \sum_{m=1}^{n_R} \frac{A_m(z) z^{m-1}}{(m-1)} \int_0^\infty \left(\frac{1}{\gamma}\right)^{m-1} \exp\left(-\frac{z}{\gamma}\right) f(\gamma) d\gamma \\ &= 1 - \sum_{m=1}^{n_R} \frac{A_m(z) z^{m-1}}{(m-1)} \int_0^\infty \left(\frac{1}{\alpha}\right)^{m-1} \exp\left(-\frac{zx}{\alpha}\right) f_X(x) dx \\ &= 1 - \sum_{m=1}^{n_R} \frac{A_m(z) z^{m-1}}{(m-1)} \int_0^\infty \frac{x^{x(m+r)-2}\exp(-x(z/\alpha+1))}{\Gamma(r)\alpha^{m-1}} dx \end{aligned} \tag{6.36}$$

The integrals in (6.36) are straight forward and are given by the following results.

$$\int_0^\infty x^{\alpha-1}\exp(-cx)dx = \int_0^\infty \left(\frac{u}{c}\right)^{\alpha-1}\exp(-u)\frac{du}{c} = c^{\frac{1}{\alpha}}\Gamma(\alpha) \tag{6.37}$$

Hence, we have the final result

$$P(outage) = 1 - \sum_{m=1}^{n_R} \frac{A_m(z) z^{m-1}}{(m-1)} \frac{\Gamma(m+r-1)}{\Gamma(r)(1+\frac{z}{\alpha})^{m+r-1}\alpha^{m-1}} \tag{6.38}$$

MMSE Results

In Figures 6.11–6.16, the outage probability is computed based on (6.38) for a MMSE receiver in (2,2), (3,3), (4,4), (8,8), (4,2) and (8,2) MIMO systems. Figures 6.11–6.14 allow a comparison of the effects of the system size. Clearly, the performance is aided by a larger system size, which helps the Rayleigh case more than the CMT case. The results in the figures show the same features as in the case of ZF receivers. However, the performance of the MMSE receiver is much better than the ZF receiver.

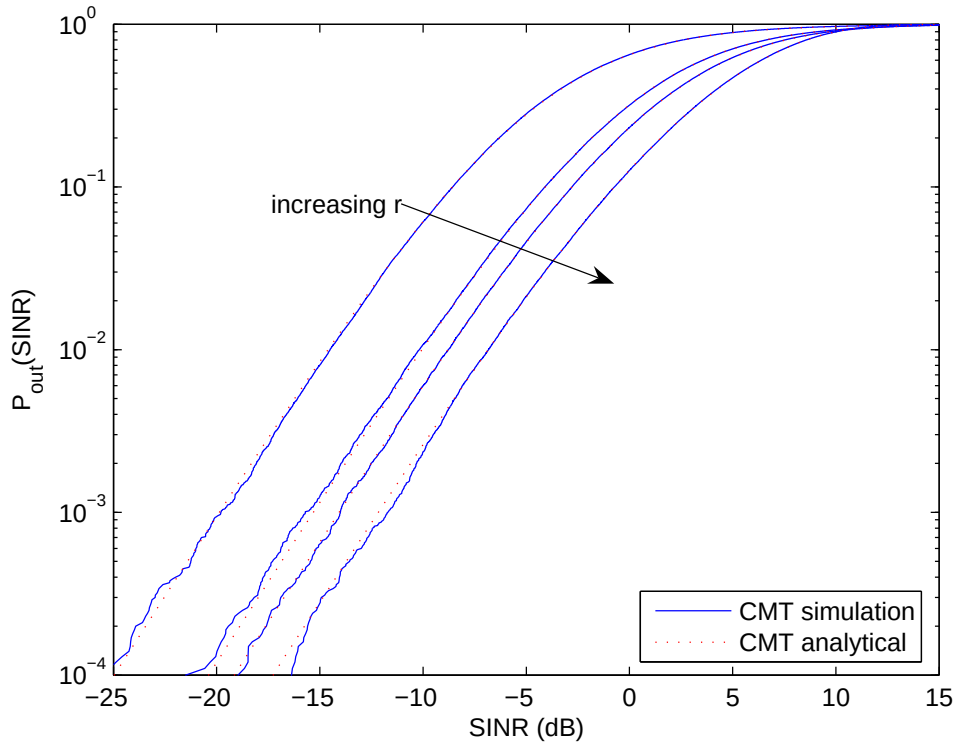

Figure 6.11 Outage probability vs SNR for a MMSE receiver in a (2,2) MIMO system when $r =$ 1.1, 1.5, 2, 40

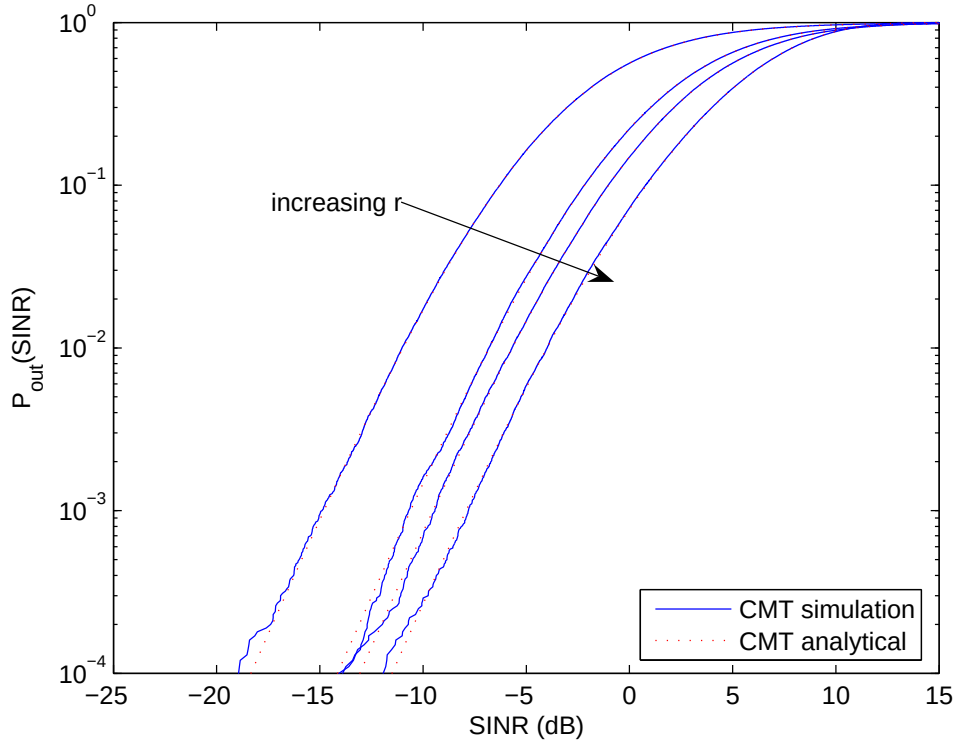

Figure 6.12 Outage probability vs SNR for a MMSE receiver in a (3,3) MIMO system when $r =$ 1.1, 1.5, 2, 40

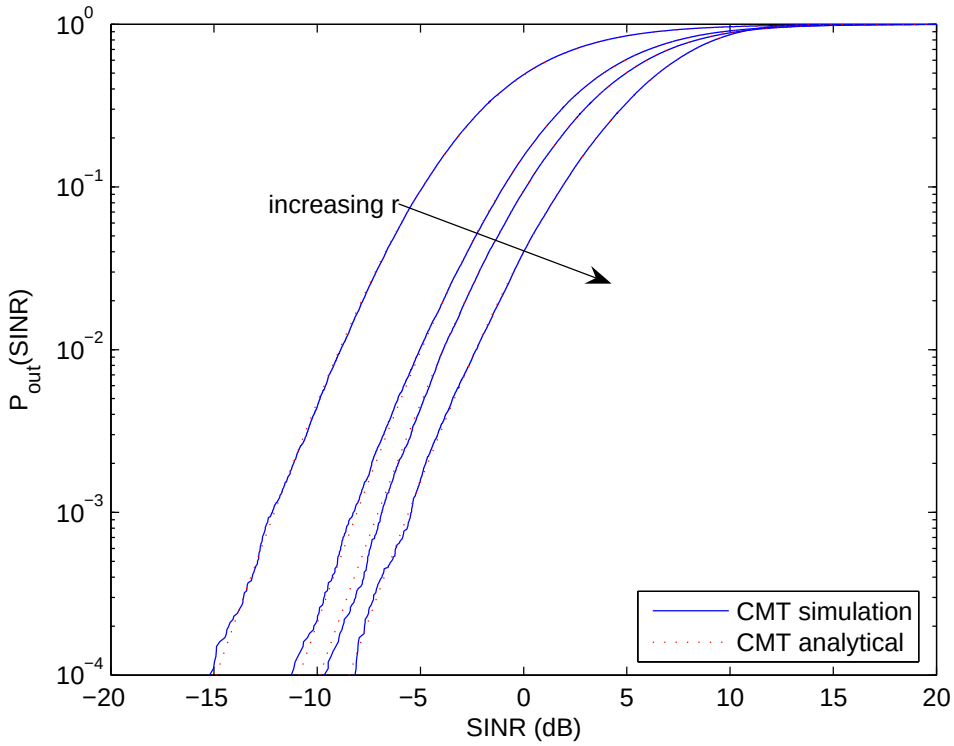

Figure 6.13 Outage probability vs SNR for a MMSE receiver in a (4,4) MIMO system when r = 1.1, 1.5, 2, 40

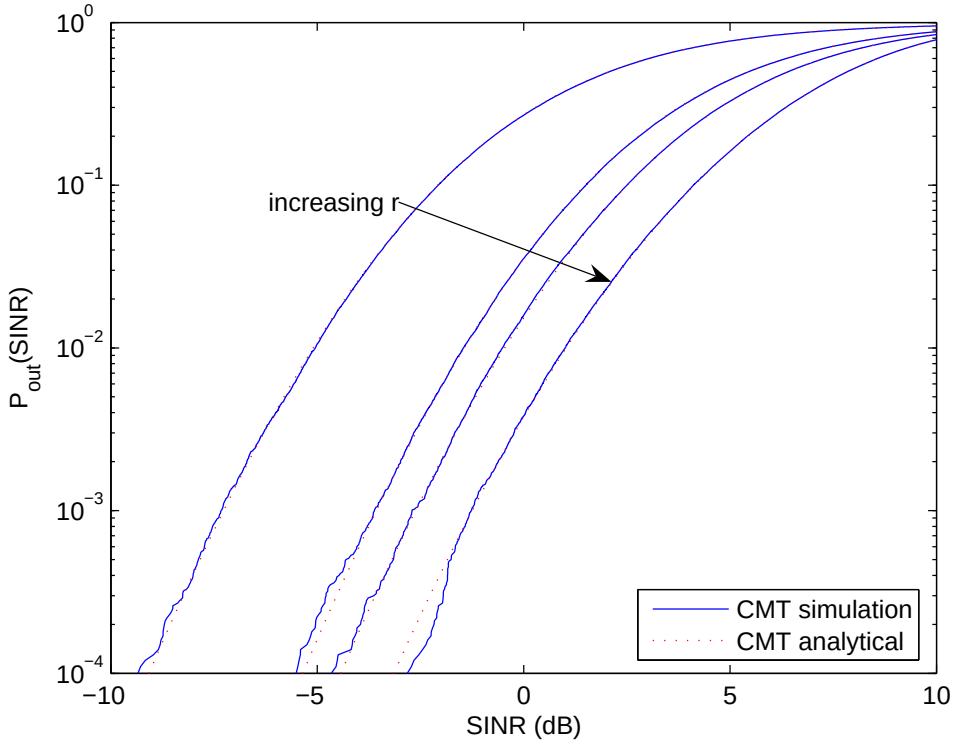

Figure 6.14 Outage probability vs SNR for a MMSE receiver in a (8,8) MIMO system when r = 1.1, 1.5, 2, 40

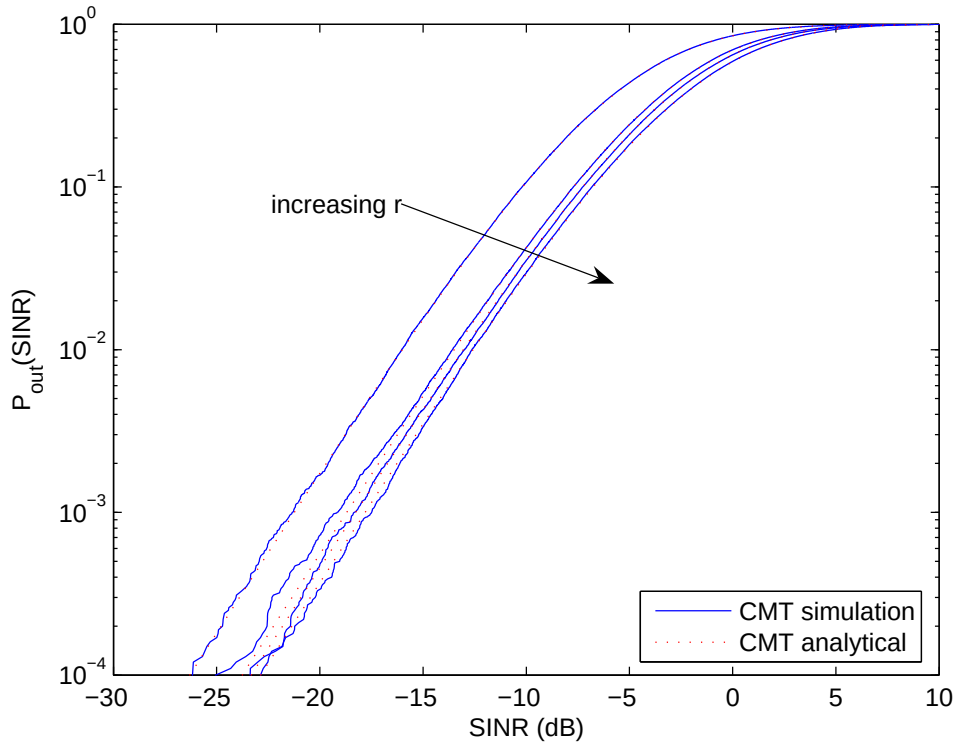

Figure 6.15 Outage probability vs SNR for a MMSE receiver in a (4,2) MIMO system when $r =$ 1.1, 1.5, 2, 40

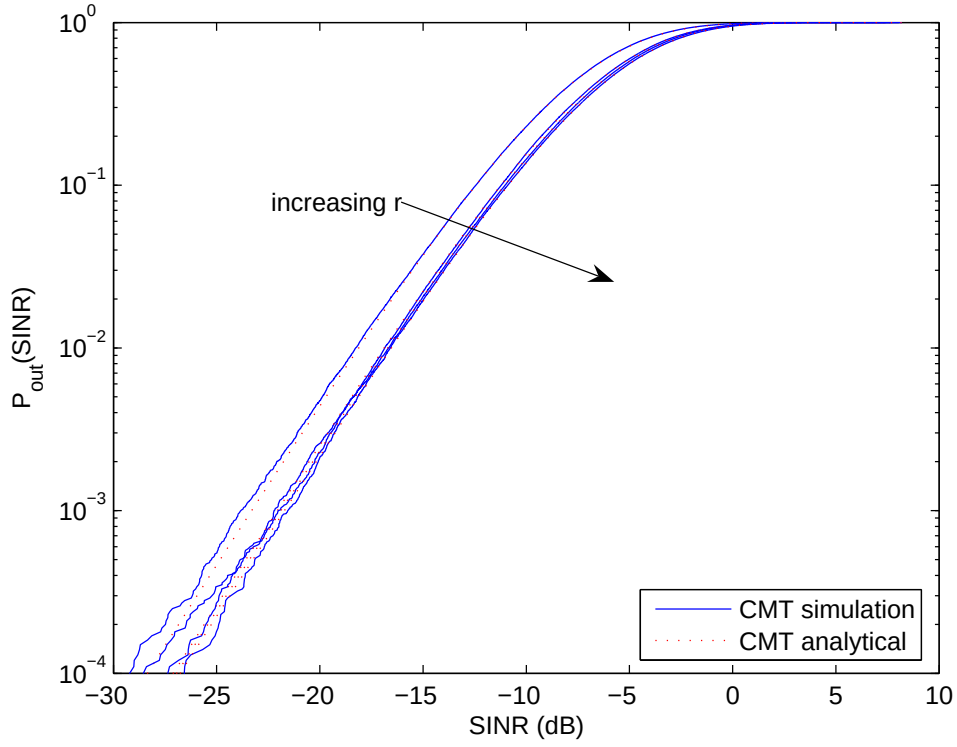

Figure 6.16 Outage probability vs SNR for a MMSE receiver in a (8,2) MIMO system when $r =$ 1.1, 1.5, 2, 40

Chapter 7

CONCLUSIONS AND FUTURE WORK

In this chapter, we draw conclusions based on the work presented in this thesis and summarize the major achievements and contributions. Some suggestions for future work are also presented at the end of the chapter.

7.1 CONCLUSIONS

Typically, MIMO channel models for flat fading are well-known, while severely fading MIMO channels (where the fading is more severe than Rayleigh fading) have received little attention and are of interest in their own right. Such scenarios arise in many applications: wireless sensors, RF tagging, land-mobile, indoor-mobile and ionospheric radio links in addition to cellular MIMO and UWB MIMO systems.

In this thesis, we have considered MIMO channels where the fading is more severe than Rayleigh fading. We have shown that the coefficient of variation of the channel amplitudes is a good predictor of the link mutual information for a variety of models. We have proposed a novel channel model for severely fading channels based on the complex multivariate t distribution. Furthermore, the model has extended to evaluate the performance of cellular MIMO links.

Results show that the CV is indeed a key metric for measuring the fading severity and we have derived the CV for a range of amplitude distributions in Chapter 4. These

are shown in Table 4.3. We have shown that for a fixed CV, the ergodic MI of a MIMO channel is relatively insensitive to the exact type of amplitude distribution. This conclusion is especially valid when the fading is not too severe or at high SNR. As the CV is varied, it is shown that the MI is more sensitive to values in the region $\mathrm{CV} > \mathrm{CV}_{\mathrm{Rayleigh}}$ than to smaller CV values, $\mathrm{CV} < \mathrm{CV}_{\mathrm{Rayleigh}}$. Moreover, the BER performance is affected negatively by increasing CV. It is observed that the Nakagami model is particularly sensitive to the CV and suffers a very large degradation in BER performance when the CV is large. We have shown a potential problem with the use of the Nakagami distribution as a model for SFC. Unlike the CMT model, the Rayleigh and the Ricean, the Nakagami distribution has a pdf with a peak at zero for large CV values. This does not match other commonly used amplitude distributions and is the reason for the massive BER degradation as the CV is increased.

In Chapter 5, we have proposed a novel model which is simple and analytically tractable, based on the complex multivariate t distribution. For this model, exact ergodic MI results are derived as well as approximations to the MI outage. The results indicated that for degree of freedom, r, greater than 30, the CMT model approximates the classic Rayleigh model. However, as r decreases, the CV increases, therefore the use of the CMT satisfies the requirement that $\mathrm{CV} > \mathrm{CV}_{\mathrm{Rayleigh}}$.

In Chapter 6, the CMT model is applied to cellular MIMO systems and we evaluated the mutual information of cellular MIMO and the performance of MIMO receivers using ZF and MMSE. The MI results for the 6 cellular scenarios, i.e. S3F1, S3F3, S6F1, S6F3, S12F1 and S12F3, have shown that the CMT model fits simulated cellular scenarios very well. Furthermore, the model has obvious extensions to MIMO performance analysis through the simple approach of averaging well-known i.i.d. Rayleigh fading results over

the inverse χ^2 scaling variables.

7.2 FUTURE WORK

Although this thesis has given valuable insights in severely fading MIMO channels, there are many more issues that can be extended for further research.

- The analytical results of the CMT model are compared with simulations in Chapter 5. To verify this model, an obvious extension is to see if the CMT model agrees with real measurements for severely fading channels.

- The scaling variable $\frac{1}{S^2}$ is used to fit the cellular data. However, alternative scaling variables could be considered for the cellular MIMO scenario to improve the fit.

- For the cellular MIMO scenario, another extension is to model the scaling variable with measured cellular data.

- The performance of different detection techniques is also of interest. We could study more complex receivers, such as MIMO-SVD and MIMO-beamformers.

- In this thesis, we assumed that all the MIMO channels experience i.i.d. fading. However, it will be interesting to observe the effects of correlated severely fading channels on both MI and performance.

REFERENCES

[1] (2007, Feb.) 2006 Hengchun earthquake - disruption in communications. [Online]. Available: http://en.wikipedia.org/wiki/2006_Hengchun_earthquake

[2] P. K. Bondyopadhyay, "The first application of array antenna," in *Proc. IEEE Phased Array Syst. Technol.*, Dana Point, CA, May 21–25, 2000, pp. 29–32.

[3] A. Goldsmith, *Wireless Communications*. Cambridge, UK: Cambridge University Press, 2005.

[4] T. S. Rappaport, *Wireless Communications: Principles and Practice*, 2nd ed. Upper Saddle River, NJ: Prentice Hall PTR, 2002.

[5] W. Lee, *Wireless and Cellular Telecommunications*, 3rd ed. New York, NY: McGraw-Hill, 2006.

[6] K. Biesecker, "The promise of broadband wireless," *IEEE IT Prof.*, vol. 2, no. 6, pp. 31–39, Nov./Dec. 2000.

[7] J. E. Padgett, "Overview of wireless personal communications," *IEEE Commun. Mag.*, vol. 33, no. 1, pp. 28–41, Jan. 1995.

[8] T. S. Rappaport, "Wireless personal communications: trends and challenges," *IEEE Antennas Propagat. Mag.*, vol. 33, no. 5, pp. 19–29, Oct. 1991.

[9] K. Basu and H. Lee, "Challenge of universal mobility and wireless internet," in *Proc. IEEE Wireless Commun. Networking Conf. (WCNC'00)*, vol. 3, Chicago, IL, Sept. 23-28, 2000, pp. 1563–1568.

[10] H. J. Bessai, *MIMO Signals and Systems*. New York, NY: Springer, 2005.

[11] A. J. Paulraj, D. A. Gore, R. U. Nabar, and H. Bölcskei, "An overview of MIMO communications - a key to gigabit wireless," *Proc. IEEE*, vol. 92, no. 2, pp. 198–218, Feb. 2004.

[12] D. Gesbert, M. Shafi, D. S. Shiu, P. J. Smith, and A. Naguib, "From theory to practice: An overview of MIMO space-time coded wireless systems," *IEEE J. Select. Areas Commun.*, vol. 21, no. 3, pp. 281–302, Apr. 2003.

[13] A. Goldsmith, S. A. Jafar, N. Jindal, and S. Vishwanath, "Capacity limits of MIMO channels," *IEEE J. Select. Areas Commun.*, vol. 21, no. 5, pp. 684–702, June 2003.

[14] R. U. N. Ö. Oyman, H. Bölcskei, and A. J. Paulraj, "Characterizing the statistical properties of mutual information in MIMO channels," *IEEE Trans. Signal Processing*, vol. 51, no. 11, pp. 2784–2795, Nov. 2003.

[15] C. E. Shannon, "A mathematical theory of communication," *Bell Syst. Tech. J.*, vol. 27, pp. 379–423 and 623–656, July/Oct. 1948.

[16] G. J. Foschini and M. J. Gans, "On limits of wireless communications in a fading environment when using multiple antennas," *Wireless Pers. Commun.*, vol. 6, no. 3, pp. 311–335, Mar. 1998.

[17] G. J. Foschini, "Layered space-time architecture for wireless communication in a fading environment when using multielement antennas," *Bell Labs Tech. J.*, pp. 41–59, Autumn 1996.

[18] I. E. Telatar, "Capacity of multi-antenna Gaussian channels," *European Trans. Telecommun.*, vol. 10, no. 6, pp. 586–595, Nov./Dec. 1999.

[19] J. H. Winters, "On the capacity of radio communication systems with diversity in a Rayleigh fading environment," *IEEE J. Select. Areas Commun.*, vol. 5, no. 5, pp. 871–878, June 1987.

[20] G. G. Raleigh and J. M. Cioffi, "Spatio-temporal coding for wireless communication," *IEEE Trans. Commun.*, vol. 46, no. 3, pp. 357–366, Mar. 1998.

[21] C. N. Chuah, D. Tse, J. M. Kahn, and R. A. Valenzuela, "Capacity scaling in MIMO wireless systems under correlated fading," *IEEE Trans. Inform. Theory*, vol. 48, no. 3, pp. 637–650, Mar. 2002.

[22] K. Yu and B. Ottersten, "Models for MIMO propagation channels: A review," *J. Wireless Commun. and Mobile Comput.*, vol. 2, pp. 653–656, Oct. 2002.

[23] D. Gesbert, H. Bölcskei, and A. J. Paulraj, "Characterizing the statistical properties of mutual information in MIMO channels," *IEEE Trans. Commun.*, vol. 50, no. 12, pp. 1926–1934, Dec. 2002.

[24] S. Haykin and M. Moher, *Modern Wireless Communications.* Upper Saddle River, NJ: Pearson Prentice Hall, 2005.

[25] D. Tse and P. Viswanath, *Fundamentals of Wireless Communication.* Cambridge, UK: Cambridge University Press, 2005.

[26] A. J. Paulraj, R. Nabar, and D. Gore, *Introduction to Space-Time Wireless Communications*. Cambridge, UK: Cambridge University Press, 2003.

[27] N. C. Sagias, G. S. Tombras, and G. K. Karagiannidis, "New results for the Shannon channel capacity in generalized fading channels," *IEEE Commun. Lett.*, vol. 9, pp. 97–99, Feb. 2005.

[28] F. Zheng and T. Kaiser. (2006) On the channel capacity of multiantenna systems with Nakagami fading. Eurasip J. Applied Signal Processing. [Online]. Available: http://www.hindawi.com/GetArticle.aspx?doi=10.1155/ASP/2006/39436&e=cta

[29] D. Kim and M. A. Ingram, "Measurements of small-scale fading and path loss for long range RF tags," *IEEE Trans. Antennas Propagat.*, vol. 51, no. 8, pp. 1740–1749, Aug. 2003.

[30] J. Galbreath and J. Frolik, "Channel allocation strategies for wireless sensors statistically deployed in multipath environments," in *Proc. IEEE Int. Conf. Infom. Processing Sensor Networks (IPSN'06)*, Nashville, TN, Apr. 19–21, 2006, pp. 334–341.

[31] W. P. Siriwongpairat, W. Su, M. Olfat, and K. J. Liu, "Multiband-OFDM MIMO coding framework for UWB communication systems," *IEEE Trans. Signal Processing*, vol. 54, no. 1, pp. 214–224, Jan. 2006.

[32] H. Huang and R. A. Valenzuela, "Fundamental simulated performance of downlink fixed wireless cellular networks with multiple antennas," in *Proc. IEEE Int. Symp. Pers., Indoor and Mobile Radio Commun. (PIMRC05)*, Berlin, Germany, Sept. 11–14, 2005, pp. 161–165.

[33] S. H. Choi and P. J. Smith, "Severely fading MIMO channels: Models and mutual information," in *Proc. IEEE Int. Conf. Communications (ICC'07)*, Glasgow, UK, June 24–27, 2007.

[34] B. A. Bjerke and J. G. Proakis, "Multiple antenna diversity techniques for transmitting over fading channels," in *Proc. IEEE Wireless Commun. Networking Conf. (WCNC'99)*, vol. 3, New Orleans, LA, Sept. 21-24, 1999, pp. 1038–1042.

[35] M. K. Simon and M. Alouini, *Digital Communication over Fading Channels: Unified Approach to Performance Analysis.* New York, NY: John Wiley & Sons, 2000.

[36] H. B. James and P. I. Wells, "Some tropospheric scatter propagation measurements near the radio-horizon," *Proc. IRE*, vol. 43, no. 10, pp. 1336–1340, Oct. 1955.

[37] G. R. Sugar, "Some fading characteristics of regular VHF ionospheric propagation," *Proc. IRE*, vol. 43, no. 10, pp. 1432–1436, Oct. 1955.

[38] T. L. Staley, R. C. North, W. H. Ku, and J. R. Zeidler, "Performance of coherent MPSK on frequency selective slowly fading channels," in *Proc. IEEE Veh. Technol. Conf. (VTC'96)*, Atlanta, GA, Apr. 28–1, 1996, pp. 784–788.

[39] S. O. Rice, "Statistical properties of a sine wave plus random noise," *Bell Syst. Tech. J.*, vol. 27, pp. 109–157, Jan. 1948.

[40] K. A. Stewart, G. P. Labedz, and K. Sohrabi, "Wideband channel measuremens at 900 MHz," in *Proc. IEEE Veh. Technol. Conf. (VTC'95)*, Chicago, IL, July 25–28, 1995, pp. 236–240.

[41] R. J. C. Bultitude, S. A. Mahmoud, and W. A. Sullivan, "A comparison of indoor radio propagation characteristics at 910 MHz and 1.75 GHz," *IEEE J. Select. Areas Commun.*, vol. 7, no. 1, pp. 20–30, Jan. 1989.

[42] T. S. Rappaport and C. D. McGillem, "UHF fading in factories," *IEEE J. Select. Areas Commun.*, vol. 7, no. 1, pp. 40–48, Jan. 1989.

[43] G. H. Munro, "Scintillation of radio signals from satellites," *J. Geophys. Res.*, vol. 68, p. 1851, Apr. 1963.

[44] P. D. Shaft, "On the relationship between scintillation index and Rician fading," *IEEE Trans. Commun.*, vol. 22, no. 5, pp. 731–732, May 1974.

[45] M. Nakagami, "The m-distribution: a general formula of intensity distribution of rapid fading," in *Statistical Methods in Radio Wave Propagation*, W. C. Hoffman, Ed. New York, NY: Pergamon Press, 1960, pp. 3–34.

[46] H. Suzuki, "A statistical model for urban multipath propagation," *IEEE Trans. Commun.*, vol. 25, no. 7, pp. 673–680, July 1977.

[47] T. Aulin, "Characteristics of a digital mobile radio channel," *IEEE Trans. Veh. Technol.*, vol. 30, no. 2, pp. 45–53, May 1981.

[48] W. R. Braun and U. Dersch, "A physical mobile radio channel model," *IEEE Trans. Veh. Technol.*, vol. 40, no. 2, pp. 472–482, May 1991.

[49] A. U. Sheikh, M. Handforth, and M. Ardi, "Indoor mobile radio channel at 946 MHz: measurements and modeling," in *Proc. IEEE Veh. Technol. Conf. (VTC'93)*, Secaucus, NJ, May 18–20, 1993, pp. 73–76.

[50] E. J. Fremouw and H. F. Bates, "Worldwide behavior of average VHF-UHF scintillation," *Radio Sci.*, vol. 6, no. 10, pp. 863–869, Oct. 1971.

[51] H. E. Whitney, J. Aarons, R. S. Allen, and D. R. Seeman, "Estimation of the cumulative probability distribution function of ionospheric scintillations," *Radio Sci.*, vol. 7, pp. 1095–1104, Dec. 1972.

[52] E. J. Fremouw, R. C. Livingston, and D. A. Miller, "On the statistics of scintillating signals," *J. Atmos. Terr. Phys.*, vol. 42, pp. 717–731, Aug. 1980.

[53] P. K. Banerjee, R. S. Dabas, and B. M. Reddy, "C-band and L-band transionospheric scintillation experiment: some results for applications to satellite radio systems," *Radio Sci.*, vol. 27, no. 6, pp. 955–969, June 1992.

[54] H. Hashemi, "The indoor radio propagation channel," *Proc. IEEE*, vol. 81, no. 7, pp. 943–968, July 1993.

[55] N. S. Adwi *et al.*, "Coverage prediction for mobile radio systems operating in the 800/900 MHz frequency range," *IEEE Trans. Veh. Technol.*, vol. 37, no. 1, pp. 3–72, Feb. 1988.

[56] N. C. Sagias, D. A. Zogas, G. K. Karagiannidis, and G. S. Tombras, "Channel capacity and second order statistics in weibull fading," *IEEE Commun. Lett.*, vol. 8, no. 6, pp. 377–379, June 2004.

[57] W. Weibull, "A statistical distribution function of wide applicability," *AMSE Trans. J. Appl. Mech.*, vol. 18, no. 3, pp. 293–297, 1951.

[58] G. L. Turin, F. D. Clapp, T. L. Johnston, S. B. Fine, and D. Lavry, "A statistical model of urban multipath propagation," *IEEE Trans. Veh. Technol.*, vol. 21, no. 1, pp. 1–9, Feb. 1972.

[59] H. Hashemi, "Simulation of the urban radio propagation channel," *IEEE Trans. Veh. Technol.*, vol. 28, no. 3, pp. 213–225, Aug. 1979.

[60] T. S. Rappaport, S. Y. Seidel, and K. Takamizawa, "Statistical channel impulse response models for factory and open plan building radio communication system design," *IEEE Trans. Commun.*, vol. 39, no. 5, pp. 794–807, May 1991.

[61] P. Yegani and C. McGlilem, "A statistical model for the factory radio channel," *IEEE Trans. Commun.*, vol. 39, no. 10, pp. 1445–1454, Oct. 1991.

[62] H. Hashemi, "Impulse response modeling of indoor radio propagation channels," *IEEE J. Select. Areas Commun.*, vol. 11, no. 7, pp. 967–978, Sept. 1993.

[63] P. B. Rapajic and D. Popescu, "Information capacity of a random signature multiple-input multiple-output channel," *IEEE Trans. Commun.*, vol. 48, no. 8, pp. 1245–1248, Aug. 2000.

[64] Z. Wang and G. B. Giannakis, "Outage mutual information of space-time MIMO channels," *IEEE Trans. Inform. Theory*, vol. 50, no. 4, pp. 657–662, Apr. 2004.

[65] R. U. Nabar, "Signaling for general MIMO channels," Ph.D. dissertation, Standford University, Standford, CA, Feb. 2003.

[66] U. Charash, "A study of multipath reception with unknown delays," Ph.D. dissertation, University of California, Berkeley, CA, Jan. 1974.

[67] L. Li, Y.-D. Yao, and H. Li, "Transmit diversity and linear and decision-feedback equalizations for frequency-selective fading channels," *IEEE Trans. Veh. Technol.*, vol. 52, no. 5, pp. 1217–1231, Sept. 2003.

[68] Q. T. Zhang, "A decomposition technique for efficient generation of correlated Nakagami fading channels," *IEEE J. Select. Areas Commun.*, vol. 18, no. 11, pp. 2385–2392, Nov. 2000.

[69] K. W. Yip and T. S. Ng, "A simulation model for Nakagami-m fading channels $m < 1$," *IEEE Trans. Commun.*, vol. 48, no. 2, pp. 214–221, Feb. 2000.

[70] J. Luo and J. R. Zeidler, "A statistical simulation model for correlated Nakagami fading channels," in *Proc. IEEE Int. Conf. Commun. Technol. (ICCT'00)*, vol. 2, Beijing, China, Aug. 21–25, 2000, pp. 1680–1684.

[71] G. D. Durgin, T. S. Rappaport, and D. A. de Wolf, "New analytical models and probability density functions for fading in wireless communications," *IEEE Trans. Commun.*, vol. 50, pp. 1005–1015, June 2002.

[72] L. J. Greenstein, V. Erceg, Y. S. Yeh, and M. V. Clark, "A new path-gain/delay-spread propagation model for digital cellular channels," *IEEE Trans. Veh. Technol.*, vol. 46, no. 2, pp. 477–485, May 1997.

[73] V. Erceg, L. J. Greenstein, S. Y. Tjandra, S. R. Parkoff, A. Gupta, B. Kulic, A. A. Julius, and R. Bianchi, "An empirically based path loss model for wireless channels in suburban environments," *IEEE J. Select. Areas Commun.*, vol. 17, no. 7, pp. 1205–1211, July 1999.

[74] D. Cassioli, M. Z. Win, and A. F. Molisch, "The ultra-wide bandwidth indoor channel: from statistical model to simulations," *IEEE J. Select. Areas Commun.*, vol. 20, no. 6, pp. 1247–1257, Aug. 2002.

[75] A. F. Molisch, J. R. Foerster, and M. Pendergrass, "Channel models for ultrawideband personal area networks," *IEEE Trans. Wireless Commun.*, vol. 10, no. 6, pp. 14–21, Dec. 2003.

[76] H. Bai, H. Aerospace, and M. Atiquizzaman, "Error modeling scheme for fading channels in wireless communications: A survey," *IEEE Commun. Surveys & Tutorials*, vol. 5, no. 2, pp. 1740–1749, Fourth Quarter 2003.

[77] I. Oppermann, M. Hämäläinen, and J. Linatti, *UWB Theory and Applications*. Chichester, UK: John Wiley & Sons, 2004.

[78] R. Blum, J. Winters, and N. Sollenberger, "On the capacity of cellular systems with MIMO," *IEEE Commun. Lett.*, vol. 6, no. 6, pp. 242–244, June 2002.

[79] M. Z. Win and R. A. Scholtz, "Impulse radio: how it works," *IEEE Commun. Lett.*, vol. 2, no. 2, pp. 36–38, Feb. 1998.

[80] ——, "Ultra-wide bandwidth time-hopping spread-spectrum impulse radio for wireless-access communications," *IEEE Trans. Commun.*, vol. 48, no. 4, pp. 679–691, Apr. 2000.

[81] L. Fullerton, "UWB waveforms and coding for communications and radar," in *Proc. IEEE Telesystems Conf.*, Huntsville, AL, Mar. 26–27, 1991, pp. 139–141.

[82] K. Siwiak, "Ultra-wide band radio: introducing a new technology," in *Proc. IEEE Veh. Technol. Conf. (VTC'01)*, Huntsville, AL, May 6–9, 2001, pp. 1088–1093.

[83] N. Blefari-Melazzi, M. G. D. Benedetto, M. Gerla, H. Luediger, M. Z. Win, and P. Withington, "Guest editorial: ultra-wideband radio in multi-access wireless communication," *IEEE J. Select. Areas Commun.*, vol. 20, no. 9, pp. 1609–1611, Dec. 2002.

[84] R. J. Fontana, A. Ameti, E. Richley, L. Beard, and D. Guy, "Recent advances in ultra wideband communications systems," in *Proc. IEEE Conf. Ultra-wideband System and Technlogies*, Germantown, MD, May 21–23, 2002, pp. 129–133.

[85] "Revision of part 15 of the commission's rules regarding ultra-wideband transmission systems," Fed. Commun. Comm. Rep. (FCC), First Report and Order ET-Docket 98-153, Apr. 2002.

[86] R. Aiello and A. Batra, *Ultra Wideband Systems: Technologies and Applications.* Oxford, UK: Newnes, 2006.

[87] A. Saleh and R. Valenzuela, "A statistical model for indoor multipath propagation," *IEEE J. Select. Areas Commun.*, vol. 5, no. 2, pp. 128–137, Feb. 1987.

[88] V. H. MacDonald, "The cellular concept," *The Bell Syst. Tech. J.*, vol. 58, no. 1, pp. 15–43, Jan. 1979.

[89] S. Catreux, P. F. Driessen, and L. J. Greenstein, "Attainable throughput of an interference-limited multiple-input multiple-output (MIMO) cellular system," *IEEE Trans. Commun.*, vol. 49, no. 8, pp. 1307–1311, Aug. 2001.

[90] H. Dai, A. Molisch, and H. Poor, "Downlink capacity of interference-limited MIMO systems with joint detection," *IEEE Trans. Wireless Commun.*, vol. 3, no. 2, pp. 4422–4453, Mar. 2004.

[91] T. W. Anderson, *An Introduction to Multivariate Statistical Analysis*, 2nd ed. New York, NY: John Wiley & Sons, 1984.

[92] J. Wang, A. Dogandzic, and A. Nehorai, "Maximum likelihood estimation of compound-Gaussian clutter and target parameters," *IEEE Trans. Signal Processing*, vol. 54, no. 10, pp. 3884–3898, Oct. 2006.

[93] H. Shin and J. H. Lee, "On the capacity of MIMO wireless channels," *IEICE Trans. Commun.*, vol. E87-B, no. 3, pp. 671–677, Mar. 2004.

[94] P. S. Fader, B. G. S. Hardie, and K. L. Lee. (2005, Mar.) A note on implementing the Pareto/NBD model in MATLAB. pareto_nbd_MATLAB.pdf. [Online]. Available: http://brucehardie.com/notes/008/

[95] I. Gradshteyn and I. Ryzhik, Eds., *Tables of Integrals, Series, and Products*, forth ed. New York, NY: Academic Press, 1965.

[96] P. J. Smith and M. Shafi, "An approximate capacity distribution for MIMO systems," *IEEE Trans. Commun.*, vol. 52, no. 6, pp. 887–890, June 2004.

[97] A. M. Tulino and S. Verdu, "Asymptotic outage capacity of multiantenna channels," in *Proc. IEEE Int. Conf. Acoust., Speech, Signal Processing (ICAPSSP'05)*, Philadelphia, PA, Mar. 18–23, 2005, pp. 825–828.

[98] N. L. Johnson, S. Kotz, and N. Balakrishnan, Eds., *Continuous Univariate Distributions*, 2nd ed. New York, NY: John Wiley & Sons, 1994, vol. 1,2.

[99] M. Abramowitz and I. A. Stegun, Eds., *Handbook of Mathematical Functions with Formulas, Graphs, and Mathematical Tables*, 9th ed. New York, NY: Dover, 1964.

[100] H. Gao, P. J. Smith, and M. V. Clark, "Theoretical reliability of mmse linear diversity combining in Rayleigh-fading additive interference channels," *IEEE Trans. Commun.*, vol. 46, no. 5, pp. 666–672, May 1998.